Synthesis and Application of the Materials based on Multi-Responsive Polymers

Zur Erlangung des akademischen Grades einer

DOKTORIN DER NATURWISSENSCHAFTEN

(Dr. rer. nat.)

von der KIT-Fakultät für Chemie und Biowissenschaften

des Karlsruher Instituts für Technologie (KIT)

genehmigte

DISSERTATION

von

M.Sc. Wenyuan Dong

geboren in Henan, China

KIT-Dekan: Prof. Dr. Hans-Achim Wagenknecht

Referent: Prof. Dr. Patrick Théato

Korreferent: Prof. Dr. Pavel Levkin

Tag der mündlichen Prüfung: 2023.04.28

Die vorliegende Arbeit wurde vom April 2018 bis März 2023 unter Anleitung von Prof. Dr Patrick Théato am Karlsruher Institut für Technologie (KIT).

Erklärung

Ich versichere hiermit, dass ich diese Arbeit selbstständig angefertigt habe und keine anderen, als die angegebenen Quellen und Hinweise benutzt, sowie die wörtlich oder inhaltlich übernommenen Stellen als solche kenntlich gemacht und die Satzung des Karlsruher Instituts für Technologie (KIT) zur Sicherung guter wissenschaftlicher Praxis in der gültigen Fassung beachtet habe. Die elektronische Version der Arbeit stimmt mit der schriftlichen überein und die Abgabe und Archivierung der Primärdaten gemäß Abs. A (6) der Regeln zur Sicherung guter wissenschaftlicher Praxis des KIT beim Institut ist gesichert.

Ort, Datum, Unterschrift

Abstract

Stimuli-responsive polymers are materials that undergo physical or chemical transitions corresponding to environment changes such as light, temperature or pH level. The development of stimuli-responsive materials, has drawn a lot of attention in the past decades as they show promising properties for applications in healthcare, agriculture and environmental protection. One of the most extensively studied materials – especially for water purification – is poly(*N*-isopropylacrylamide) (PNIPAAm) as it exhibits temperature-responsive behavior in terms of reversible hydrophilic/hydrophobic transition at 32 ℃.

In the present work three different multi-responsive polymers based on PNIPAAm were developed and investigated.

First, two novel temperature-responsive water-purifying hydrogels where designed. Their combination with the photothermally active materials polydopamine (PDA) and graphene oxide (GO), allowed the conversion of light energy into heat when exposed to visible light irradiation. In the first approach the hydrogel was coated with PDA, whereas in the second approach the GO was incorporated into the hydrogel's structure. Following cooling and heating cycles with visible light irradiation enabled a sponge-like behavior, where in the swelling phase contaminated water is absorbed and during the deswelling phase only pure water is released. Both hydrogels have demonstrated good purifying capability as well as reusability in several purification cycles of oil-water combinations, dye-contaminated water and heavy metal-contaminated water.

After investigating dual responsive materials, the second project was aimed to develop a triple responsive system sensitive to light, temperature and oxygen. Therefore, a polymer-based host-guest complex system was designed: Here, PNIPAAm again acted as temperature-responsive polymer backbone with cyclodextrin (CD) end-groups as guest complex. As corresponding counterpart, a pentaflourostyrene polymer was functionalized with a light-responsive azobenzene

end-group. The host-guest interactions between CD and azobenzene can now be reversibly controlled through light induced *cis-trans* isomerization of the azobenzene. The reversible linkage of hydrophilic and hydrophobic polymers also induces phase separation and thereby self-assembly into supramolecular micelles in aqueous solution. Finally, the formation of these structures can be controlled threefold: through temperature with PNIPAAm, through light with the responsive CD-azobenzene host-guest complex and through oxygen associated with the pentafluorostyrene moieties. This work provides a new method for the synthesis of multi-responsive polymers, and this method is expected to be used in the future as a controlled drug delivery system.

Zusammenfassung

Stimulus-responsive Polymere sind Materialien, die physikalische oder chemische Übergänge aufgrund von Umgebungsveränderungen wie Licht, Temperatur oder pH-Wert durchlaufen. Die Entwicklung von stimuli-responsiven Materialien hat in den letzten Jahrzehnten viel Aufmerksamkeit auf sich gezogen, da sie vielversprechende Eigenschaften für Anwendungen in der Medizin, Landwirtschaft und Umweltschutz aufweisen. Eines der meist untersuchten Materialien – insbesondere für die Wasseraufreinigung – ist Poly(N-isopropylacrylamid) (PNIPAAm), da es bei 32 °C einen reversiblen, temperaturabhängigen Übergang zwischen hydrophilem und hydrophobem Verhalten aufweist.

In der vorliegenden Arbeit wurden drei verschiedene multifunktionelle Polymere auf Basis von PNIPAAm entwickelt und untersucht. Zunächst wurden zwei neue temperatur-responsive Hydrogele für die Wasseraufreinigung synthetisiert. Deren Kombination mit den photothermisch aktiven Materialien Polydopamin (PDA) und Graphenoxid (GO) ermöglicht die Umwandlung von Lichtenergie in Wärme bei Bestrahlung mit sichtbarem Licht. Im ersten Ansatz wurde das Hydrogel mit PDA beschichtet, während im zweiten Ansatz das GO in die Struktur des Hydrogels eingebunden wurde. Abkühlungs- und Aufheizzyklen unter sichtbarem Licht verursachen ein schwammartiges Verhalten, bei dem im Quellvorgang verunreinigtes Wasser absorbiert wird und während des Schrumpfens nur reines Wasser freigesetzt wird. Beide Hydrogele zeigen eine gute Reinigungsfähigkeit sowie Wiederverwendbarkeit bei Anwendung auf Öl-Wasser-Gemischen, verunreinigtem Wasser mit Farbstoffen und Schwermetallen - selbst bei Durchlaufen von mehreren Zyklen.

Nach der Untersuchung von dual-responsiven Materialien lag der Fokus des zweiten Projekts auf der Entwicklung eines dreifach-responsiven Systems, das auf Licht, Temperatur und Sauerstoff reagiert. Hierzu wurde ein polymerbasiertes

Wirt-Gast-Komplexsystem entworfen: PNIPAAm fungiert abermals als temperaturresponsives Polymer mit Cyclodextrin- (CD) Endgruppen als Gastkomplex. Als entsprechendes Gegenstück wurde ein Pentaflourostyrol-Polymer mit einem lichtempfindlichen Azobenzol-Endgruppe funktionalisiert. Die Wirt-Gast-Wechselwirkungen zwischen CD und Azobenzol können nun durch die lichtinduzierte cis-trans-Isomerisierung des Azobenzols reversibel kontrolliert werden. Die reversible Verknüpfung von hydrophilen und hydrophoben Polymeren führt zusätzlich zu einer Phasentrennung und damit einer Selbstorganisation in supramolekularen Mizellen in wässriger Lösung. Letztendlich kann die Bildung dieser Strukturen dreifach gesteuert werden: durch die Temperatur über PNIPAAm, durch Licht über den responsiven CD-Azobenzol-Wirt-Gast-Komplex und durch Sauerstoff, der mit den Pentafluorstyrol-Gruppen assoziiert ist. Diese Arbeit bietet somit eine neue Methode zur Synthese von multi-responsiven Polymeren und soll in Zukunft eine Plattform für kontrollierte Arzneimittelabgabesysteme bieten.

Content

List of Figures

List of Schemes

List of Tables

1. Introduction

Staudinger introduced the terms "polymer" and "long-chain macromolecule" for the first time in 1920. Polymer science has since come on the stage of human development.[1] Polymers are large molecules or macromolecules composed of multiple repeating subunits (monomers), which may be natural or man-made. Because of the higher molecular weight, their physicochemical properties differ significantly from those of small molecules. Natural polymers, such as cellulose, starch, proteins, natural rubber, and silk, have a long history of use by humans and play a major role in people's daily lives due to their low cost, wide availability, environmental friendliness, and improved biocompatibility. However, the properties of many natural polymers or polymer-based materials have obvious drawbacks, such as easy hydrolysis, poor temperature resistance and easy ageing.[2–5]

Consequently, chemical modification of natural polymers and chemical conditioning employing functionalized monomers were introduced in order to obtain polymers or polymeric materials with excellent properties (such as firmness, elasticity, viscosity, etc.).[6–8] In recent years, the concept of truly customizable polymeric materials is becoming a reality due to the better understanding of the structure-property relationship of polymers, the introduction of new polymerization techniques and the availability of new, low-cost monomers. Furthermore, there is a growing interest in the synthesis of stimulus-responsive polymers that exhibit 'intelligence behavior' in response to specific environmental stimuli.

1.1 Stimuli-Responsive Polymers

Stimulus-responsive polymers, also commonly referred to as 'smart materials', have attracted a great deal of interest over the past few decades.[9–14] These polymers are typically able to respond to changes in the external environment.[15–17] In general, the responsiveness of polymer can be considered as a chain of succeeding events. First,

the polymer receives an extrinsic signal (physical or chemical); then it undergoes a chemical reaction or a change in its physical properties; finally, this change is amplified into a macroscopically detectable signal, such as a change in color or shape, the aggregation or dissociation of particles, the release of the guest, etc.[18]

The development of stimulus-responsive polymers and human observation of the natural world are inextricably linked. Nature has provided humans with many examples of how to respond to external stimuli.[19] For instance, wax catchers have traps that close quickly and catch small insects when they break in. Dancing grasses dance to light and music. Sunflowers turn their heads and stems in response to the sun. Chameleons change the color of their skin in response to changes in the color of their surroundings.[20] Many vital components of living things adapt their structure and behavior in response to their surroundings on a much smaller scale.[21]

Thus, a large range of functional stimulus-responsive polymers have been developed by scientists. In general, stimulus-responsive polymers are also known as soft substances which can respond to signals like chemical, physical, or biological stimuli in either solid, solution, or gel states.[22] They can be categorized as follows depending on the stimulus type: (1) chemical stimulus, including redox reagents, gases, humidity, ionic strength, solvent polarity, pH, etc. They have already attracted a lot of attention in the field of materials;[23–28] (2) physical stimulus, such as electric and magnetic fields, temperature changes, optical radiation, mechanical stresses, etc., are significant and promising types of stimuli response systems;[29–37] and (3) biochemical stimulus, such as antigens, enzymes, ligands, or other biochemical agents.[22,38]

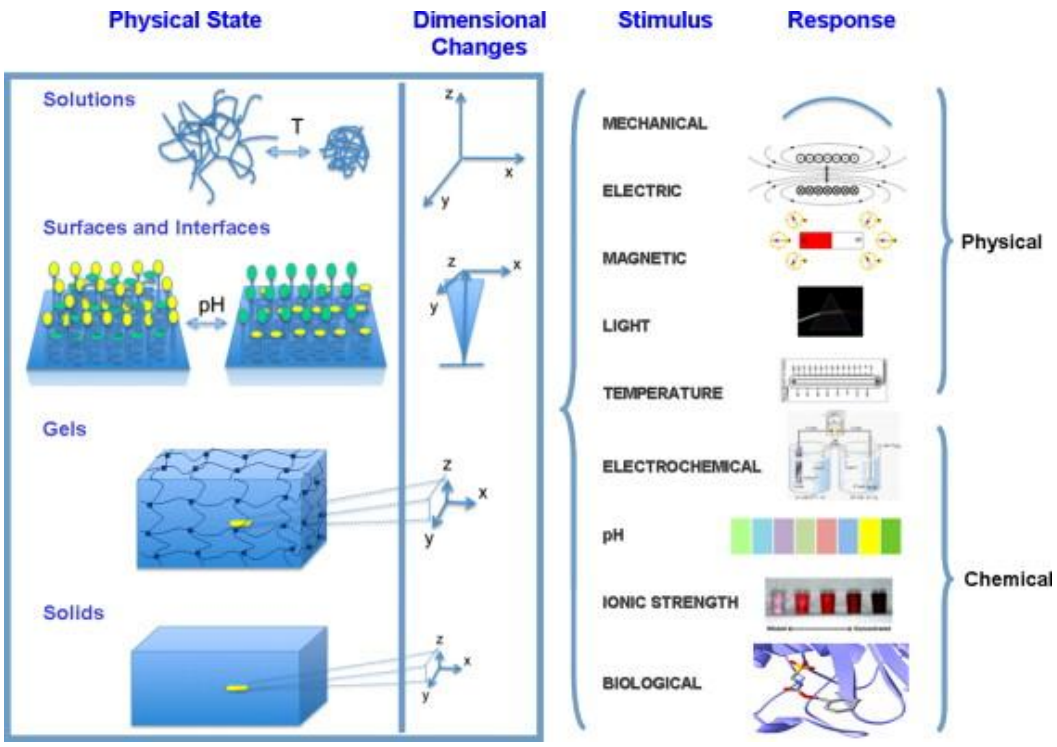

Figure 1.1 Schematic representation of dimensional changes in polymeric solutions, at surfaces and interfaces, in polymeric gels, and polymer solids resulting from physical or chemical stimuli. Reprinted with permission from Ref.[39], copyright (2010) Elsevier.

With the widespread use of responsive polymers in fields such as bio-nanotechnology, drug delivery and ecology, there is also an increasing interest in multi-responsive polymers that can produce more pronounced or detailed responses to stimuli from external stimuli, compared to single stimulus-responsive polymers.[40] Simultaneously, the development of synthetic techniques such as controlled polymerization and click chemistry has made it possible to design and synthesize polymers with multiple responsiveness. Inspired by nature, scientists have started to introduce a variety of functional groups into the same polymer to prepare a range of polymers with multiple responsiveness.[22,41,42] Polymers with multi-stimulus responsiveness stimulate a more significant or detailed response to external stimuli. New multi-responsive polymers can also be constructed by selecting the appropriate responsive groups according to practical requirements. This designability has enabled a wide range of materials with dual or multiple stimulus response capabilities being investigated.[22,43]

1.1.1. Stimuli Response to Physical Factors

1.1.1.1 Temperature-Responsive Polymers

Of the many physical response factors, temperature, as one of the most common environmental parameters, is not only easy to change and control, but also an important physiological indicator, making it one of the most widely used stimuli today.[30,44,45] In general, these polymers have a critical solubility temperature. Below this temperature, the polymers and the aqueous solution can be mixed in any ratio; above this temperature, the polymers transition from the hydrophilic dissolved state to the hydrophobic insoluble state and phase separation occurs, which is known as the lower critical solution temperature (LCST). Conversely, if a substance undergoes a transition from insoluble to dissolved only above a specific temperature, this temperature is known as the upper critical solution temperature (UCST).

A fundamental issue in the study of temperature sensitive polymers is the mechanism of their phase transition. Here, water-soluble polymers are used as an example. It is widely accepted that the equilibrium between hydrogen bonding and hydrophobic interactions in the polymer chain is what triggers the phase shift.[46,47] When the temperature is below LCST, water serves as a good solvent for the polymer and the interaction between the polymer and the solvent is greater than the interaction between the polymer molecules. The hydrophilic groups are bonded to the water molecules through hydrogen bonds and a solventized layer is formed around the macromolecular chains connected by hydrogen bonds. As the temperature increases, the hydrophobic groups become more bonded and some hydrogen bonds are broken. Then the solvent layer in the hydrophobic part of the macromolecular chain is destroyed, the solvent molecules separate from the polymer nematic, resulting in the polymer transitions from a loose nematic structure to a compact aggregate or collapsed sphere, and the polymer undergoes a phase transition. From a thermodynamic perspective, the dissolution process of LCST polymers is exothermic

due to the formation of hydrogen bonds, resulting in a negative value of ΔH. A highly ordered solvation layer made of water molecules forms at the same time, giving a negative value of ΔS. The free energy change of the dissolution process, $\Delta G=\Delta H-T\Delta S$, is $\Delta G<0$ at low temperatures due to the combined effect of enthalpy and entropy, but $\Delta G>0$ when the temperature increases, resulting in phase separation.[30,48]

Based on the response mechanism and the chemical functional groups that produce the change, a variety of temperature-responsive polymeric materials have been extensively developed by researchers (e.g., Tables 1.1 and 1.2). Currently, temperature-responsive polymers with LCST behavior are the most intensively and extensively investigated.[49–52] N-isopropylacrylamide (NIPAAm) is by far the most utilized and extensively researched monomer among the diverse that are employed to synthesize temperature-responsive polymers. NIPAAm and its polymer poly(N-isopropylacrylamide) (PNIPAAm) were studied by Scarpa in 1967, and he discovered that the LCST of PNIPAAm was around 32 °C.[53] As shown in Fig. 1.2, when the aqueous solution temperature reaches 32 ℃, PNIPAAm changes from linear to spherical (linear-spherical transformation). When the temperature of the aqueous solution is lower than 32 °C, PNIPAAm exhibits a linear chain water-soluble state; conversely, when the aqueous solution temperature is higher than 32 °C, PNIPAAm exhibits a hydrophobic spherical state. This is due to the fact that the monomer NIPAAm, which constitutes PNIPAAm, contains hydrophilic amide groups as well as hydrophobic isopropyl groups, and is subject to both hydrogen bonding and hydrophobic interactions in aqueous solution, resulting in a phase transition as the temperature changes.[54–56]

Table 1.1 Common polymers with LCST

Polymer	Abbreviation	LCST
Poly(*N*-isopropylacrylamide)[53]	PNIPAAm	32 ℃
Poly(*N*, N-diethyl acrylamide)[57]	PDEAM	33 ℃
Poly(ethylene glycol methacrylate)[58,59]	PEGMA	26~90 ℃
Poly(*N*-vinylcaprolactam)[60]	PNVCL	32 ℃
Poly(*N*-viny lisobutyramide)[61,62]	PNVIBA	39 ℃
Poly(2-isopropyl-2-oxazoline)[63]	PiPOx	36 ℃

Table 1.2 Common polymers with UCST

Polymer	Abbreviation	UCST
Poly(*N*-acryloyl glycinamide)[64,65]	PNAGA	22~23 ℃
Poly(methacrylamide)[66]	PMAAm	57 ℃
Poly(*N*-acryloyl asparagine amide)[67]	PNAAAM	4~28 ℃

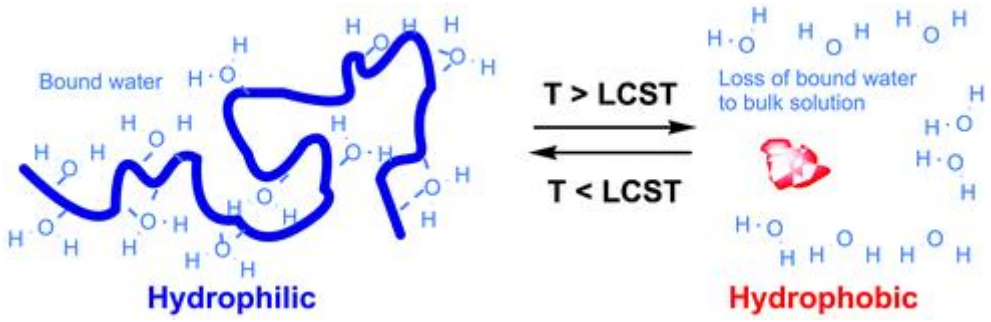

Figure 1.2 Schematic of PNIPAAm responses with temperature. Reprinted with permission from Ref.[56], copyright (2005) Royal Society of Chemistry

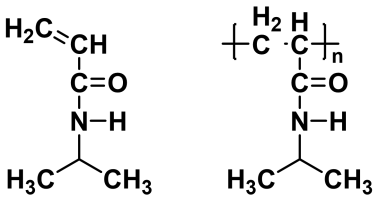

Figure 1.3 Structure of NIPAM and its polymer

LCST is influenced by parameters such as chain length, solvent, and copolymer type in addition to the structural composition of the polymer.[68–70] The introduction of hydrophilic or hydrophobic groups and chain segments into temperature-responsive polymers was found to significantly affect their LCST. Zhang *et al*. synthesized temperature-responsive block copolymer PEG-*b*-PNIPAAm and observed temperature-induced micelle formation behavior in aqueous solution. Additionally, they found that the addition of hydrophilic PEG blocks resulted in an elevated LCST of the copolymer compared to the PNIPAAm homopolymer.[71] Ksendzov *et al*. recently synthesized a number of *N*-isopropylacrylamide graft copolymers with polyesters (poly(d, l-lactide) and poly(-caprolactone)). It was discovered that as the ratio of polyester macromonomer with a hydrophobic butyl end group in a copolymer chain increased from 0 to 17 wt%, the LCST of the graft copolymers declined virtually linearly from 32.1 to 14 °C. For graft copolymers of N-isopropylacrylamide with polyesters bearing polar hydroxyl groups at the chain ends, much smaller variations in transition temperature were observed (from 32.1 to ~ 23 °C).[72]

The LCST of polymers are also influenced by the solvent. Many organic solvents, including acetone, tetrahydrofuran, butanone, methanol, ethanol, and dimethyl alum, can dissolve PNIPAAm without exhibiting LCST before the solvents reach their boiling points.[73] Theoretically, the addition of these solvents to the aqueous solution enhances the LCST as well as the solubility of PNIPAAm. In reality, PNIPAAm exhibits a reentrant behavior with a change in components in these mixed solvents since it is insoluble in the mixtures made up of both in a specific ratio.[31,73–87] For instance, the mixed solvent is the good solvent of PNIPAAm in the methanol-water mixed solvent system when the molar fraction of methanol X_m is less than 17 mol%;[80,81] when X_m is between 17-50 mol%, the methanol-water mixed solvent is changed from the good solvent of PNIPAAm to its bad solvent; when X_m is more than 50 mol%, the mixed solvent is its good solvent again. The systems of water/ethanol and water/dimethyl sulfoxide undergo a similar transformation.[82,83]

Liu *et al*. synthesized the novel thermosensitive star-shaped tetra-hydroxy-phenylporphyrin-cored (THPP) double hydrophilic poly(*N*-isopropylacrylamide)-block-poly(methylacrylamide glucose) block copolymers (THPP-(PNIPAAm-*b*-PMAGA)$_4$) via RAFT polymerization.[88] Notably, the LCST of the copolymer can be regulated by controlling the hydrophilic PMAGA content above the normal body temperature (37 °C). The copolymer can be neutralized into micelles in aqueous solution, encapsulate the anticancer medicine and then release it around the tumor cells when the ambient temperature is higher than the LCST of the copolymer.

Xu and coworkers developed a highly durable PNIPAAm-based loofah-shaped solar absorbing gel (LSAG) for solar water purification.[89] They first immersed the LSAG in contaminated water below LCST, and the gel absorbed large amounts of water and swelled while rejecting contaminants. The LSAG underwent a phase transition and changed from a hydrophilic to a hydrophobic state, rapidly releasing large amounts of pure liquid water. PNIPAAm provides an easy and green way for water purification.

1.1.1.2 Photo-Responsive Polymers

Due to its straightforward modulation mechanism and the reversibility of light-induced structural or functional group alterations, photo-responsiveness is becoming more and more significant. It is feasible to fabricate polymers with photosensitive capabilities by including photosensitive molecules in the molecular design.

Common photosensitive compounds are seen in Fig. 1.4, and there are three main changes in their molecular structures under irradiation of light: (A) azo-benzene molecules can change from *trans* to *cis* under the irradiation of ultraviolet light, and the molecular polarity increases;[90–92] (B) both leucocyanidin and spiro-pyranine dyes are capable of intra-ionic charge separation by ultraviolet irradiation, which increases the molecular polarity compared to the *cis*-transition of azobenzene molecules.[93–98] (C) cinnamic acid molecules are capable of producing dimers under specific light irradiation, which can be applied as cross-linking elements in polymers and have potential applications in morphological memory materials.[99–101]

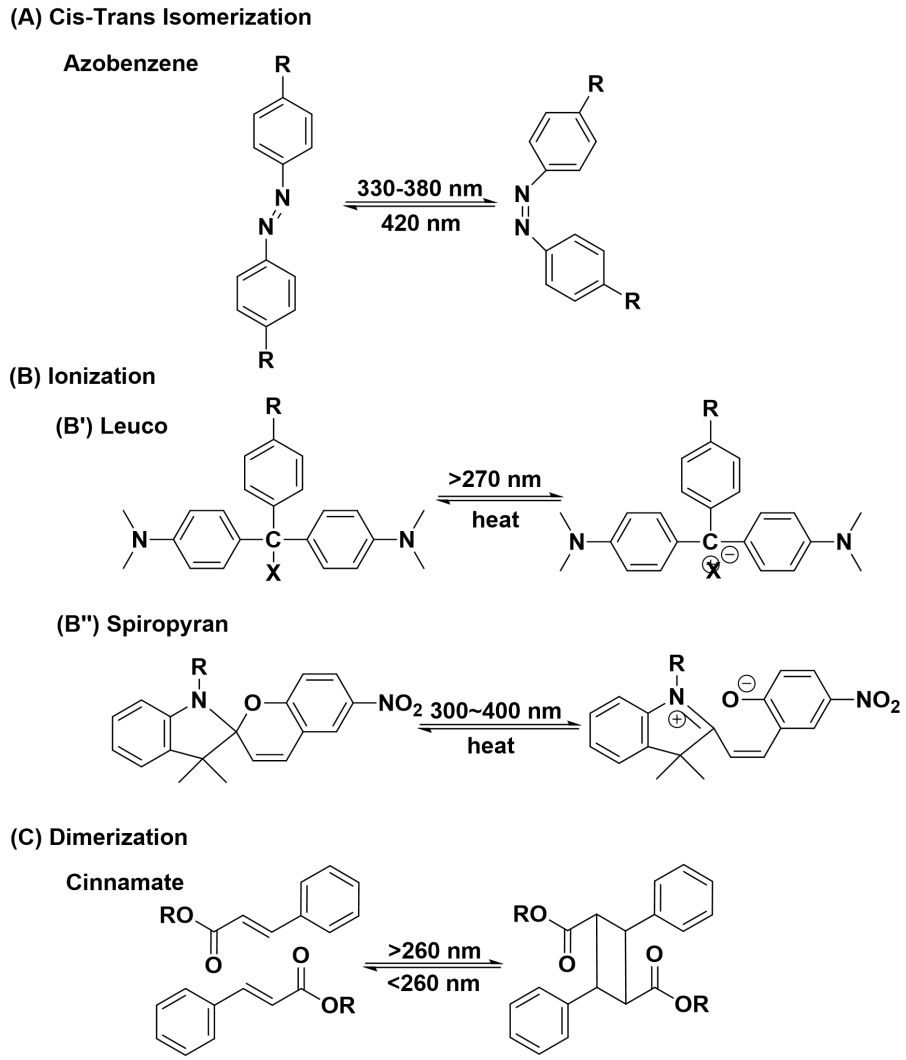

Figure 1.4 Examples of molecular structures of photo-responsive monomers: *cis–trans* isomer of azobenzene (A); ionization monomers (B) of leucos (B′) and spiropyran (B″); and dimerization monomer of cinnamate (C). Reprinted with permission from Ref.[39], copyright (2010) Elsevier.

Recently, a novel UV-reversible and reusable polymeric adhesive based on the photo-responsive properties of the α, β-unsaturated ester portion of the *p*-hydroxycinnamic acid structure has been developed.[102] This photosensitive adhesive's bonding strength can be optimized to 1.74 MPa, which is higher than the majority of UV-reversible adhesives currently listed in the literature. Through light conditioning, this polymer binder can be recycled, minimizing energy waste and environmental contamination.

1.1.1.3 Mechanical Force-Responsive Polymers

In recent years, the use of mechanical force-responsive polymers to study the stresses on macromolecules at the molecular level has received increasing attention. When subjected to external forces, responsive groups undergo covalent bond formation and breakage, resulting in mechanical force-responsive polymers.[103] Common mechanical forces include tension or pressure, fluid flow shear, ultrasonic waves, etc. From an energy standpoint, force-induced chemical change is analyzed as a process in which mechanical energy is transformed into chemical bonding energy, part of which is stored in the chemical bond and part of which is dissipated in other forms such as heat energy. In the opposite process, the release of stored chemical bond energy or tension energy, etc. is converted into mechanical energy, which is also investigated in mechanical force response.[104,105]

The most commonly employed mechanical force-responsive molecule is spiropyran (SP), whose C-O bond is ring-opened and cleaved under external force, and the spiro ring carbon atom changes from sp^3 hybridization to sp^2 hybridization, forming into merocyanine (MC).[106] As shown in Fig. 1.5, the conversion of SP to MC is reversible, where MC returns to SP under visible light irradiation.

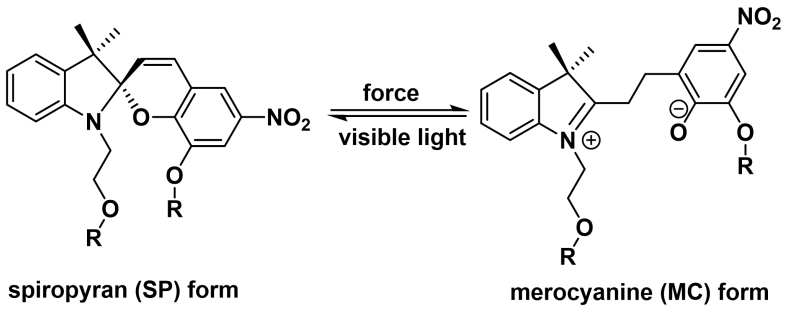

Figure 1.5 Chemical structure of the spiropyran (SP) mechanophore and its transformation into the merocyanine (MC) form. Reprinted with permission from Ref.[107], Copyright (2020) American Chemical Society

1.1.1.4 Electro-Responsive Polymers

Typical electro-responsive polymers are conducting polymers, such as polythiophene and sulfonated polystyrene, which can exhibit changes like shrinkage, swelling and bending under the modulation of an applied electric field.[108–111] Electro-responsive polymers can be divided into the following categories based on the response mechanism: electro-active polymers, ion-doped conducting polymers, and polymer composites/blends/coatings.[112]

Nasari *et al*. successfully prepared polypyrrole (PPy)-coated electrically resonant Poly(ε-caprolactone) (PCL)+ multi-walled carbon nanotubes (MWCNTs)/Poly(N-vinyl-2-pyrrolidone) (PVP) core-shell nanofibers, which were selected as carriers sensitive to electrical signals for loading the anticancer drug 5FU. In comparison to not applying an electric field, they discovered that the drug's rate of release can be increased in this way. This indicated that altering the electric field can be used to regulate the medication release from coated samples.[113]

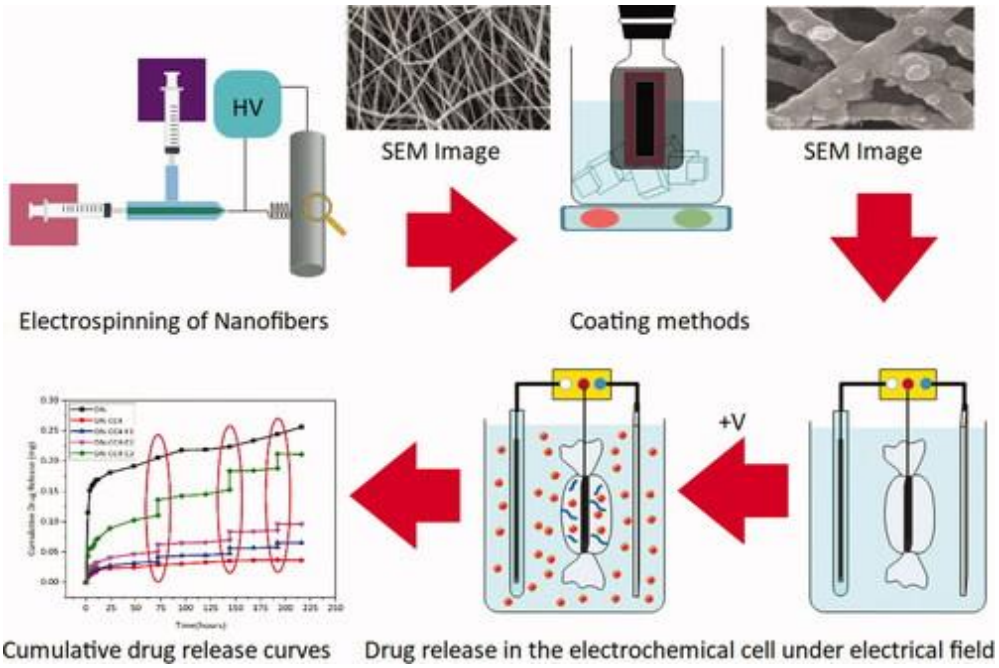

Figure 1.6 Electro-responsive polymers for controlled drug release. Reprinted with permission from Ref.[113], Copyright (2022) Taylor & Francis

1.1.2.Stimuli Response to Chemical Factors

1.1.2.1 pH-Responsive Polymers

Many biopolymers in nature can change their conformation and solubility in response to changes in the pH of ambient environment. pH-responsive polymers are of great practical value since different organisms have different pH values and many diseases occur with pH changes.[23,114–116] pH-responsive polymers generally contain easily ionized acid-base groups. When the external solution's acidity or alkalinity changes, these groups have the capacity to reversibly absorb or release protons. The reversible ionization/deionization transition endows the polymers with special features, such as precipitation or dissolution of polymer chains, shrinkage or swelling of polymer hydrogels, and hydrophobic transformation of the polymers' surface properties.[117]

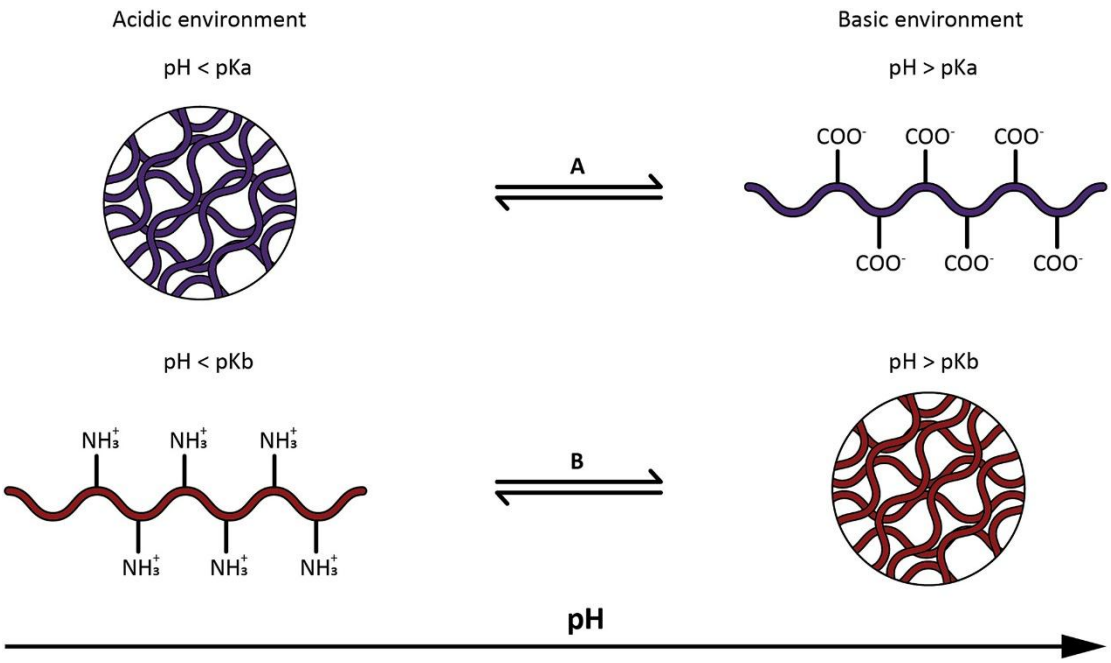

Figure 1.7 Polyacids (A) and polybases (B) polymeric chain state depending on the ionization degree. Reprinted with permission from Ref.[118], copyright (2021) John Wiley and Sons

Depending on the nature of the response group, pH-responsive polymers can be classified into two types: polyacids and polybases. As depicted in Fig. 1.7, polyacids

inflate when the medium pH > p*K*a, while polymeric chains collapse when pH < p*K*a. Conversely, polybases polymer chains collapse when pH > p*K*b and inflate when pH < p*K*b.[118]

The term "polyacid pH-responsive polymers" refers to those containing ionizable acid side groups along the polymer backbone, such as carboxylic acid (COOH), sulfonic acid (SO_3H), phosphonic acid (PO_3H_2), and boronic acid (H_3BO_3). Acrylate monomers containing phosphate groups are often employed to prepare functional hydrogels. pH-responsive polymers containing boronic acid groups are commonly used for the preparation of self-healing gels and glucose sensors.[117] The most prevalent polyacid pH-responsive polymers are listed in Fig. 1.8 and are categorized based on the characteristics of their functional groups. Zhang *et al*. prepared a new pH-responsive liquid marble based on 9,10-dihydroxystearic acid. This liquid marble has an effective pH-responsive behavior and can remain relatively stable in acidic solutions while decomposing immediately in alkaline solutions (pH > 7.5). They also found that the marbles decompose rapidly within 5 s after the addition of NH_3 gas, indicating that it can be utilized as a fast and convenient NH_3 detector.[119] A novel poly(acrylic acid)-based macroporous nanocomposite hydrogel was prepared and can be used as a pH-controlled swelling controlled release system to release amoxicillin.

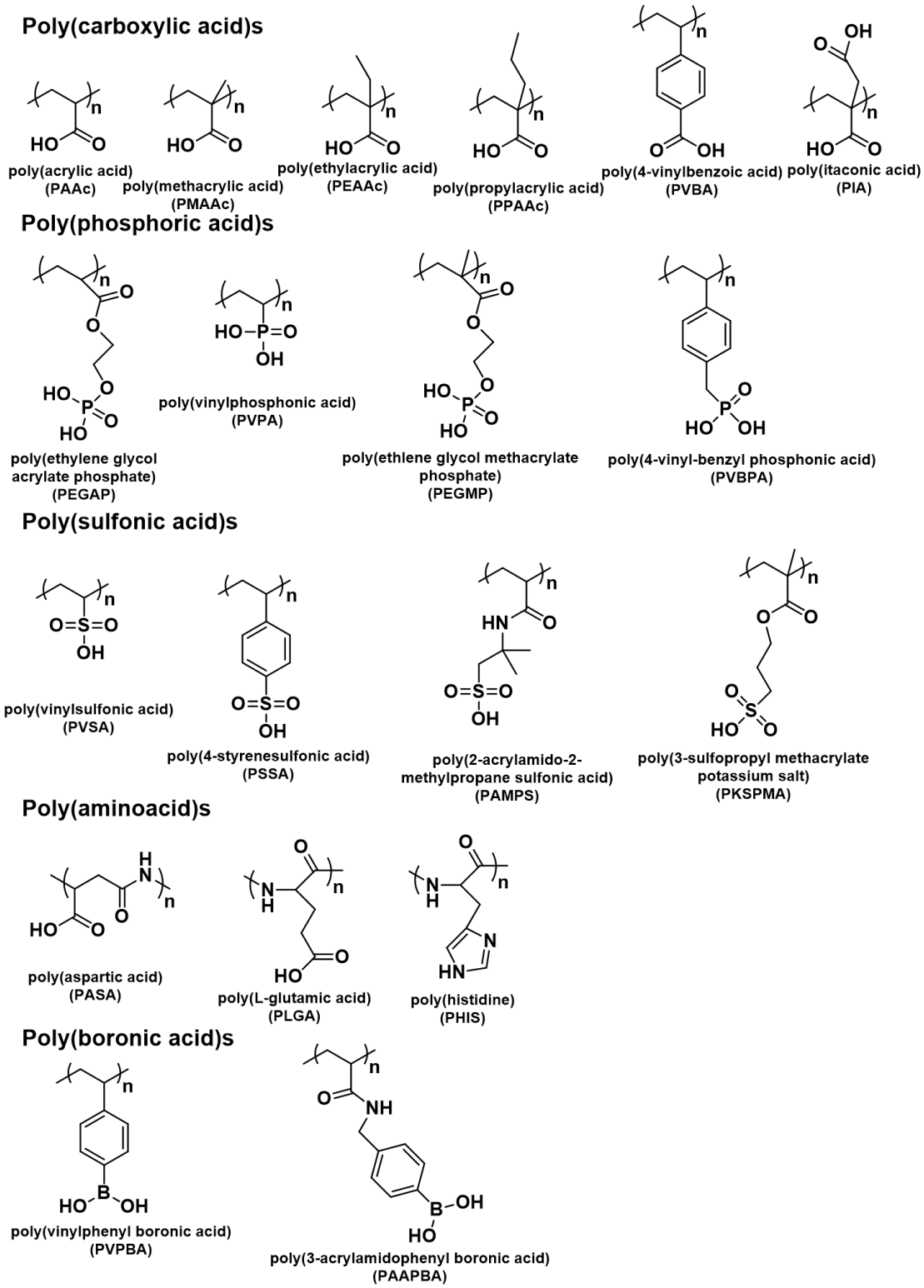

Figure 1.8 Chemical structures of polyacid pH-responsive polymers. Reprinted with permission from Ref.[117], copyright (2017) Royal Society of Chemistry

pH-responsive basic polymers typically have amine functional groups in the polymer's backbone or side chains. The chemical structures of the common

pH-responsive basic polymers are summarized in Fig. 1.9.

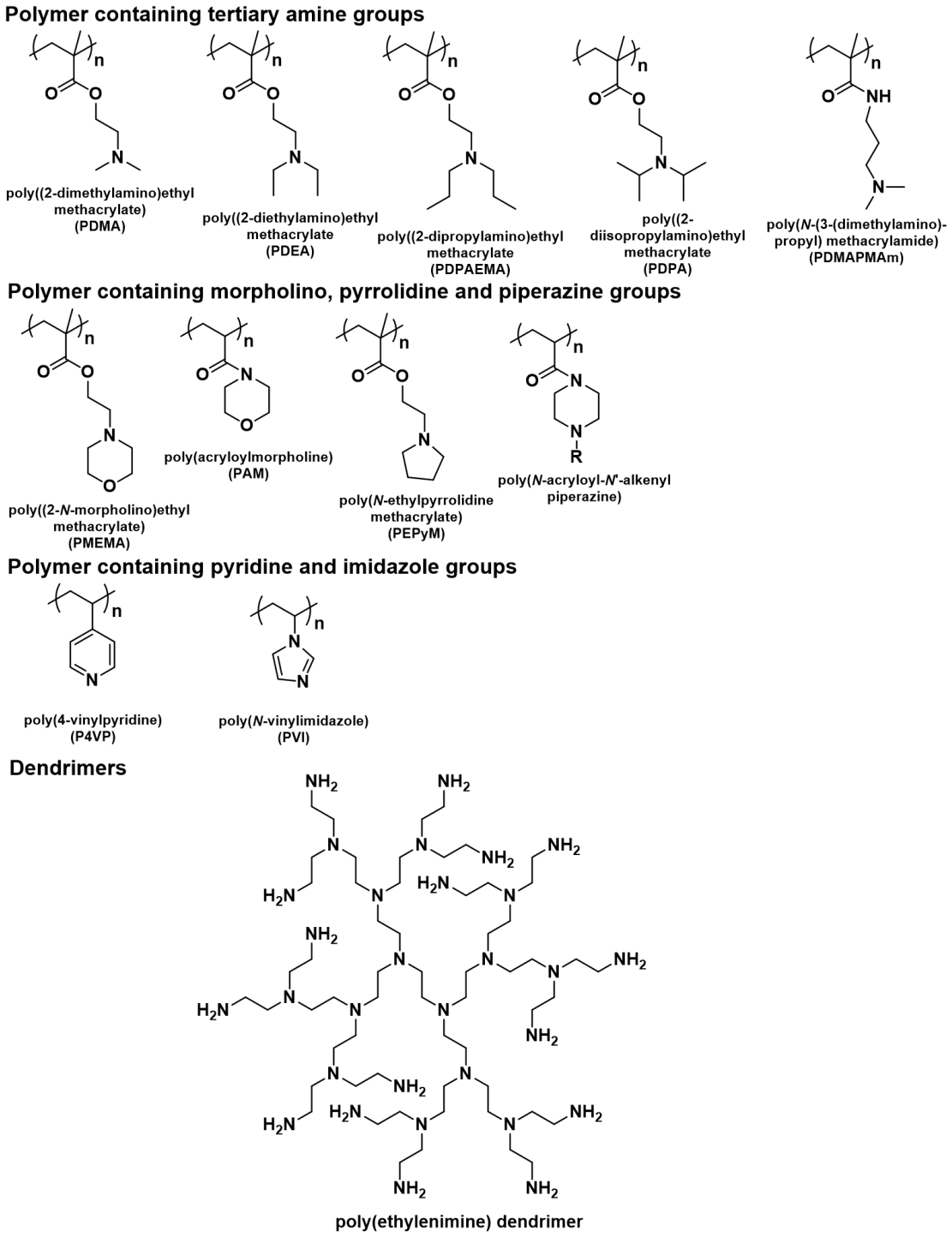

Figure 1.9 Chemical structures of polybase pH-responsive polymers. Reprinted with permission from Ref.[117], copyright (2017) Royal Society of Chemistry

1.1.2.1. Gas-Responsive Polymers

The aforementioned stimuli have some drawbacks in some aspects, such as the addition of acids and bases to the solution to adjust pH, which may introduce additional salts to contaminate the system and reduce the effective concentration of solutes in the solution;[120,121] temperature and light may affect biological tissues. gas stimuli are easy to add and remove during operation compared to other stimuli, therefore they are of great interest in practical applications.

Currently, gas irritants which are commonly investigated include carbon dioxide (CO_2),[122–125] oxygen (O_2), nitrous oxide (NO), hydrogen sulfide (H_2S), and sulfur dioxide (SO_2).

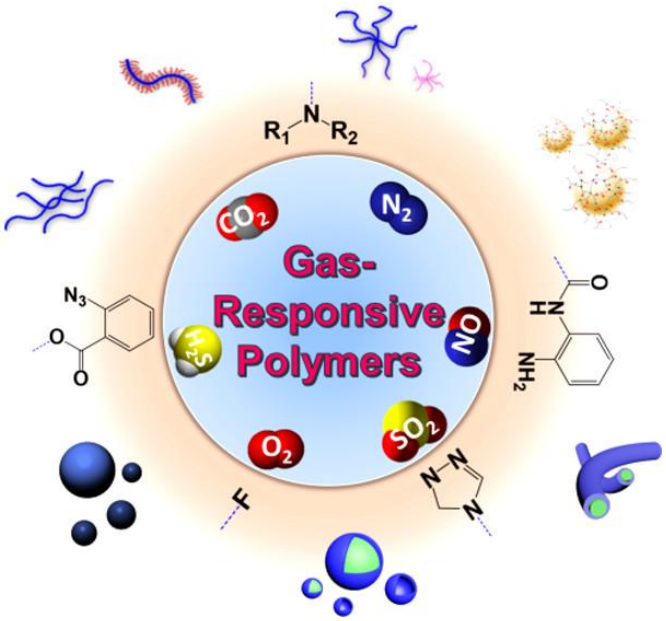

Figure 1.10 Summary of different gas-response functional groups. Reprinted with permission from Ref.[126], copyright (2017), American Chemical Society

CO_2, a mild, inexpensive and abundant gas, has become the most studied gas stimulus in the last decade. It can react with specific functional groups (such as amidine, guanidine, tertiary amine, imidazole, and carboxyl groups), causing a significant change in their hydrophilicity and polarity thus controlling the alteration of the

polymer. [126–129] Moreover, CO_2 has great reversibility and can be totally eliminated by washing with inert gases (such as argon, nitrogen, or air) under mild circumstances, making it free of accumulated chemical contamination.[126] Akoumy *et al*. synthesized yolk–shell nanoparticles consisting of a CO2-responsive crosslinked poly(*N*,*N*-diethylaminoethyl methacrylate) shell for the gas-controllable reduction. To change the permeability of the crosslinked polymer shell, manage the catalysis, and conveniently recycle the catalyst, CO_2 and N_2 were used as an uncontaminated stimulus.[130]

O_2, an important gas molecule that regulates physiological functions in the body, is very important for all living organisms on earth. Similar to CO_2, O_2 is another important gaseous stimulus. All of the O_2-responsive polymers currently described in the literature alter the hydrophilic/hydrophobic balance of the polymer through the reversible adsorption of O_2 by aliphatic or aromatic linked fluorine groups.[131–135] This is due to the special van der Waals interaction between the O_2 molecule and the C-F bond.[136] The first O_2-responsive polymer (pentafluorophenyl capped polyethylene glycol (PF-PEG-PF)) was reported by Choi *et al*.. When oxygen was applied, the LCST of the polymer increased from 24.5 to 26 °C. They also demonstrated that this LCST change is caused by van der Waals forces between the O_2 molecule and the C-F bond, as the fluorine in the polymer shifted in the ^{19}F NMR spectrum, while the proton of PEG is unchanged in the ^{1}H NMR spectrum.[136] Oxygen can also induce self-assembly of block polymers. Recently, Zhang *et al*. synthesized a diblock copolymer based on an O_2-responsive monomer (2,2,2-trifluoroethyl methacrylate (tFMA)) employing the RAFT polymerization method. This block copolymer can be stimulated by the conversion cycle of CO_2 and O_2 in aqueous solution, which leads to the formation and reversal of polymer micelles.[137]

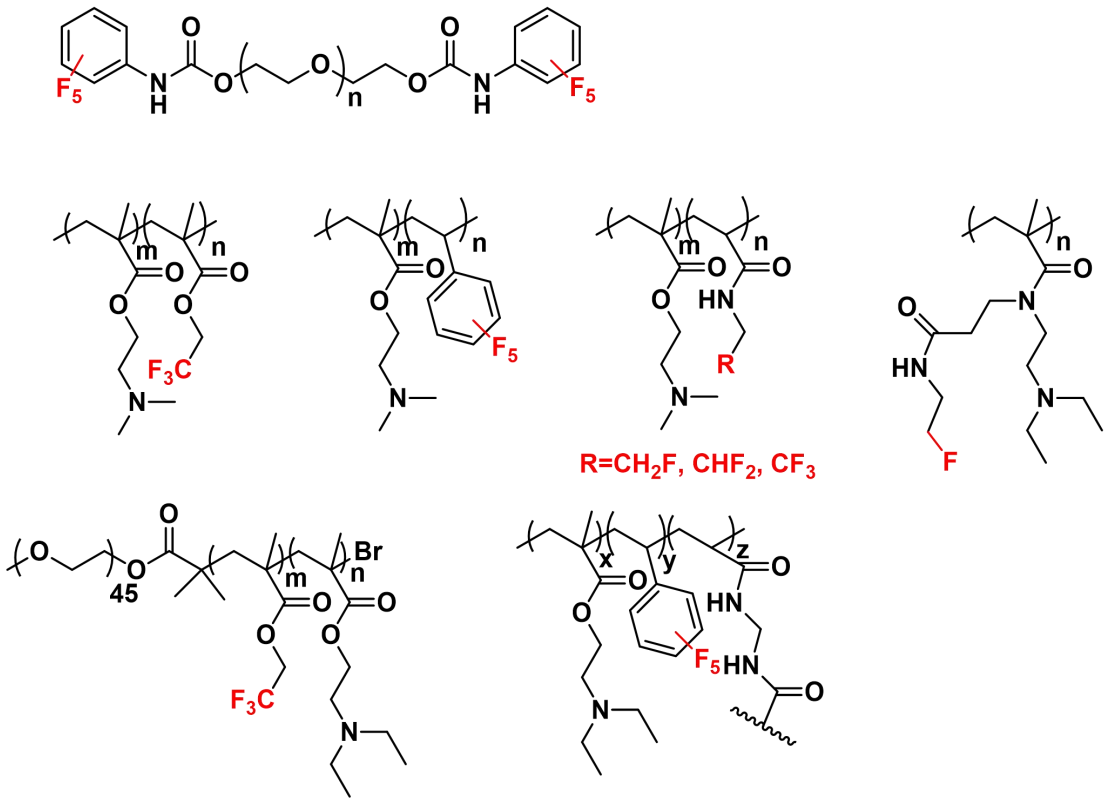

Figure 1.11 Summary of chemical structures of the reported O_2-responsive polymers. Reprinted with permission from Ref.[126], copyright (2017), American Chemical Society

NO is not only an important intermediate in the chemical industry, but also essential for mediating a variety of biological functions including angiogenesis, apoptosis, vasodilation, and immunological responses.[138] Currently, there are not many reports on NO-responsive polymers. The first nitric oxide responsive polymer was synthesized in 2014 by Hu *et al*. They first synthesized the novel NO-responsive monomers *N*-(2-aminophenyl) methacrylamide hydrochloride (NAPMA) and 2-(3-(2-aminophenyl)ureido)ethyl methacrylate hydrochloride (APUEMA) with *o*-phenylenediamine groups, and then prepared the temperature-sensitive copolymers P(NIPAM-co-NAPMA) and P(NIPAM-co-NAPMA). The NAPMA repeating units generates an amide-substituted benzotriazole intermediate when these copolymers are exposed to NO. This intermediate spontaneously hydrolyzes into a carboxylate portion, improving the copolymer's hydrophilicity. In contrast, the APUEMA monomer produces a urea-functionalized benzotriazole derivative which increased

hydrophobicity. This leads to NO-regulated copolymer LCST and induced nanoparticle self-assembly.[139]

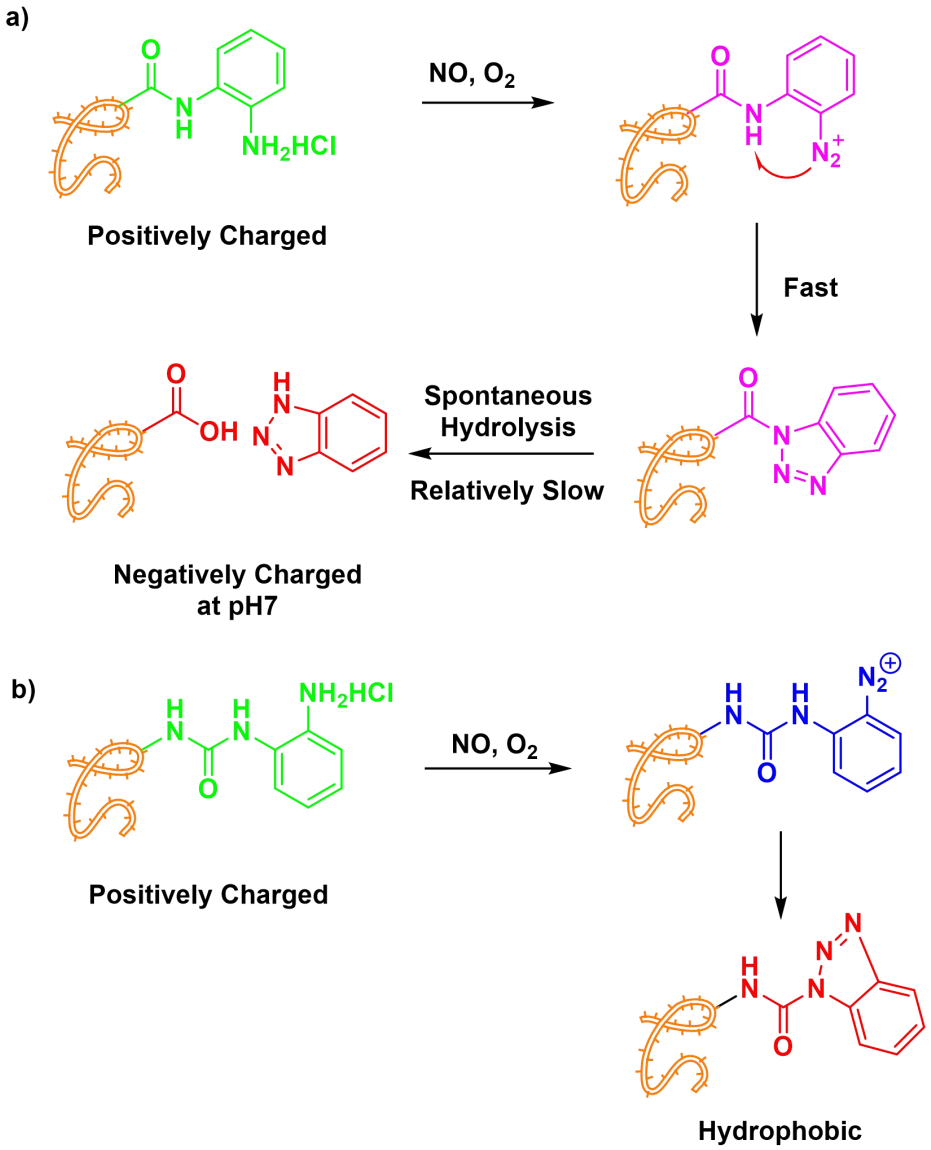

Figure 1.12 Schematic illustration of the proposed NO-triggered mechanisms of copolymers bearing NAPMA and APUEMA moieties. Reprinted with permission from Ref.[139], copyright (2014), John Wiley and Sons

SO_2 is a colorless, toxic gas with an irritating odor, mostly from industrial processes such as the combustion of fossil fuels. In 2016, Zhu *et al*. reported the first case of SO_2-induced phase transition in water-soluble polymer solutions. They prepared water-soluble α-helical random copolypeptides with pyridinium tetrafluoroborate

(PyBF$_4$) and oligoethylene glycol (OEG) pendants (PPLG-PyBF$_4$-r-OEG). The SO_2-induced reversible solution phase transition behavior was investigated by UV-visible spectroscopy and dynamic light scattering (DLS). The interaction between SO_2 and the triazole moieties was identified as the cause of this reversible phase transition by ^{1}H NMR analysis.[140]

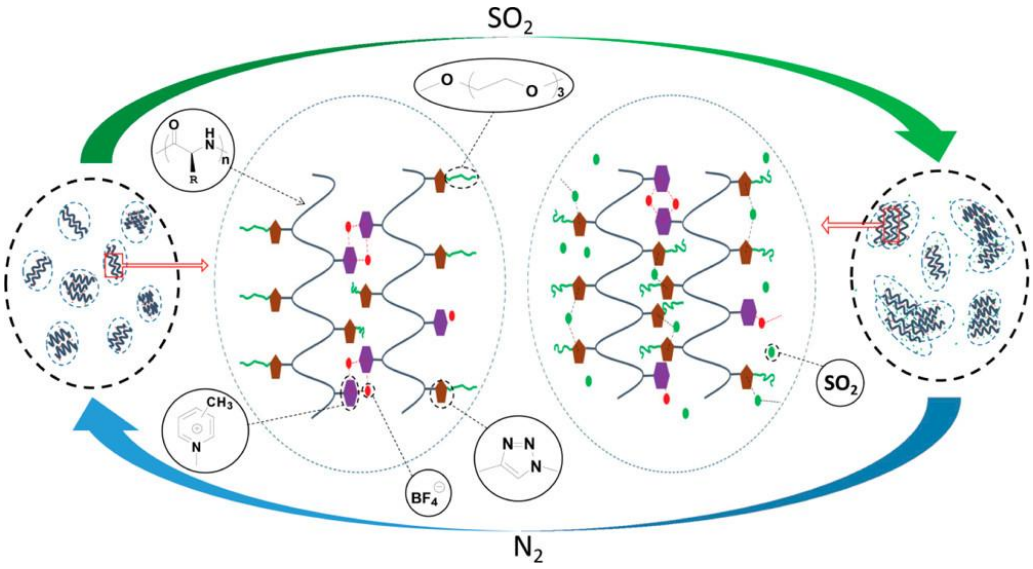

Figure 1.13 Proposed mechanism of SO_2-induced reversible solution phase transition. Reprinted with permission from Ref.[140], copyright (2016), American Chemical Society

1.1.2.2. Ion-Responsive Polymers

This kind of polymers exhibit an unusual rheological behavior due to the impact of Coulomb forces generated by species with opposite charges in the system. These changes result in the polymer becoming water soluble with the addition of the polyelectrolyte and the electron/electron interactions being shielded.[141] Consequently, altering the system's ion concentration can affect the length of the polymer chains, their solubility, and the interaction between the fluorescent chromophore and the polymer electrolyte.[141,142]

1.1.2.3. Oxidation-Responsive Polymers

Oxidation-responsive polymers are commonly employed in biomedical fields. Oxidation-responsive polymers can undergo drastic physical changes, such as solubilization or cross-linking, when they are stimulated.[143] Poly(propylene sulfide), selenium-based polymers, aryl oxalate- and phenylboronic ester-containing polymers are a few typical oxidation-responsive polymers.[144] A new drug delivery system for polymeric nanoparticles containing pinacol-type boronic esters and alkyne groups was reported. This system triggered the degradation of the self- immolative polymer in the presence of reactive oxygen species (ROS) resulting in the release of the drug.[145]

1.1.2.5 Reduction-Responsive Polymers

Reduction-responsive polymers can rapidly respond to differences in the concentration of reducing substances in specific physiological sites associated with pathology and are commonly employed as drug delivery systems for cancer cells. Polymers containing disulfide and diselenide bonds are the most popular reduction-responsive polymers.[146,147] Sun et al. discussed the effects of six chemical bonds: thioether bond, disulfide bond, selenoether bond, diselenide bond, carbon bond and carbon-carbon bond on reduction-responsive nanocomponents for drug delivery. The results revealed that diselenide bonds were second in sensitivity to reducing circumstances, after disulfide bonds. The carbon and carbon-carbon bonds were unresponsive to the reducing circumstances, as was expected, but the selenoether bond was more sensitive to hydrogen peroxide than the thioether bond.[148]

1.1.3. Stimuli Response to Biochemical Factors

Bio-responsive polymers are polymers that produce responsive behavior to specific macromolecules in the organism. The main biological substances that can induce stimulus responsiveness in polymers include: glucose, glutathione, enzymes, receptors,

metabolites produced by inflammation, etc.[149] In addition, the specificity of amino acid and enzyme responsiveness makes them more precise than stimulus responsiveness such as temperature and pH.[150]

Bio-responsive polymers are currently widely used in biomedical applications including drug delivery and biosensing since they can induce sol-gel conversion, self-assembly/self-dissociation, and structural reorganization of macromolecules.[151]

1.1.3.1. Enzyme-Responsive Polymers

Enzymes catalyze the conversion of specific molecules (called substrates) from one form to another, thus controlling almost all physiological activities that are essential for the maintenance of normal life activities.[125] Enzyme-responsive systems are particularly well suited for biomedical applications since enzyme catalysis generally occurs under mild conditions and does not require external conditions to trigger excellent biocompatibility.[152]

Recently, Wang *et al*. demonstrated the synthesis and application of an enzyme-responsive COF nanoinhibitor. The inhibitor has the capacity to effectively target and prevent the growth of bacteria during the treatment of wounds. It can accelerate the dissociation of the structural framework at the site of bacterial infection due to the cleavage of the azo bond by azo reductase, enabling the on-demand release of the loaded drug.[153]

1.1.3.2. Glucose-Responsive Polymers

Glucose-responsive polymers are polymers that respond to changes in the surrounding glucose concentration. Precisely designed glucose-responsive polymers are in great demand and have promising applications in the treatment of diabetes.[154] For example, the automatic regulation of quantitative release of insulin is a research area of great interest. Applications and mechanisms of glucose response are the two main areas for

studying glucose-responsive polymers. By response mechanism, they can be classified into three categories: glucose oxidase (GOx), lectins and phenylboronic acid (PBA) modified systems.

A novel hydrogel platform PEG-DA/PEI-PBA/insulin/CS-GA (PPIC) hydrogel platform was prepared. This hydrogel contains a unique glucose-sensitive phenylboronic acid (PBA) molecule. It not only has a remarkable biocompatibility, but also exhibits extraordinary antioxidant properties that effectively protect cells from oxidative damage. Also, PPIC hydrogel exhibits unique glucose-responsive insulin release properties, which can effectively regulate blood glucose levels.[155]

1.2 Stimuli-Responsive Hydrogels

In the 1960s, Wichterle and Lima synthesized the first cross-linked polyhydroxyethylene-acrylic acid (PHEMA) hydrogel that could be used as contact lens, thereby bringing hydrogels to the forefront of scientists' attention.[156] Hydrogels are cross-linked 3D network-structured hydrophilic polymer gels. In the hydrogel structure, the polymer network forms the "backbone", while a large amount of water is trapped in the pores or gaps to fill the space between the backbone.[157] Hydrogels are widely studied in materials science owing to their outstanding swelling properties, biocompatibility, and modifiability.[158–162] Conventional hydrogels have gradually evolved from static materials to smart materials, i.e. stimulus-responsive hydrogels, due to their single properties. Stimulus-responsive hydrogels are achieved by incorporating responsive groups into conventional hydrogels. They are capable of structural or property changes in specific response to external environmental changes (e.g., light, heat, chemicals, etc.).[163–165] Here the main focus is on temperature-responsive hydrogels.

1.2.1 Temperature-Responsive Hydrogels

Temperature-responsive hydrogels are a category of hydrogels composed of

temperature-responsive polymers that undergo volume shrinkage or expansion in response to temperature changes. They usually contain a specific ratio of hydrophilic and hydrophobic groups, and phase transition is achieved through reversible changes in hydrophilic/hydrophobic interactions or hydrogen bonding in the internal network.[166–168] When the external temperature increases or decreases to a specific critical value, the hydrogel undergoes a volumetric abrupt change, which can be up to tens of times. This behavior is defined as the bulk phase transition of the hydrogel, and the temperature is the bulk phase transition temperature.[169,170]

As a typical representative of temperature-responsive hydrogels, PNIPAAm hydrogels are of interest due to their LCST (32 ℃), which is the closest to human body temperature.[171] Koca *et al*. synthesized a novel thermo-responsive hydrogel from renewable resources BC/Poly(*N*-isopropylacrylamide) (PNIPAM) hydrogel, based on bacterial cellulose (BC) and castor oil (CO). The effect of CO on physical and thermal behaviors of the hydrogels was investigated. It's discovered that CO can enhance the temperature sensitivity of the hydrogels.[172] In addition, more efficient and rapid methods for the preparation of hydrogels have been reported. An efficient two-step polymerization method for the preparation of PNIPAAm hydrogels was reported by Liu *et al*. This method was achieved by freezing polymerization followed by thawing polymerization. This polymerization procedure took only 2 hours, which is a significant decrease in time compared to the 12 hours of conventional polymerization.[173]

1.2.2 Application of Temperature-Responsive Hydrogels

Due to the advantages of easy temperature control, temperature-responsive hydrogels are now widely used in drug delivery, sensors and water treatment.[163,174] In this section, the application in water treatment is mainly discussed.

Water is the most important resource for humans and other living beings. Providing a reliable source of clean and safe water is a major global challenge of the 21st

century.[175–177] However, due to the combined effect of population growth, freshwater resource pollution and climate change, the release of some harmful substances will cause water pollution, which not only negatively affect the species living in the water, but also the wider range of natural organisms, resulting in serious of health and environmental problems, the most prominent of which are dyes and organic pollutants. Hence, various methods have been developed to treat water pollution, such as chemical precipitation, ion exchange, adsorption, membrane separation, microbial, coagulation-flocculation, flotation, and electrochemical methods.[175,178,179]

The hydrophilic groups within the hydrogel structure, such as carboxyl (COOH), amide ($CONH_2$), amino (NH_2), sulfonic acid (SO_3H) and hydroxyl (OH), endow them with unique properties to adsorb and accommodate contaminants.[180] In addition, more functional groups can be modified during hydrogel synthesis to improve the ability of water treatment.[181,182] Therefore, temperature-responsive hydrogels have been drawing attention in water treatment.[183–186]

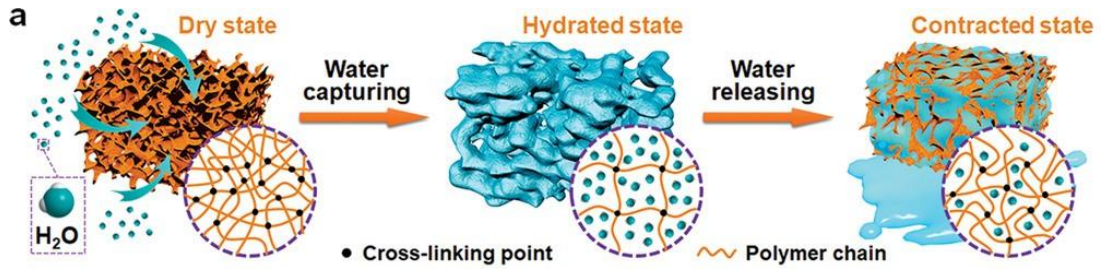

Figure 1.14 Schematic illustration of the atmospheric water harvesting process. Reprinted with permission from Ref.[183], copyright (2019) John Wiley and Sons

Zhao *et al*. Zhao et al. designed and prepared a super moisture-absorbent gel (SMAG) based on hygroscopic chloride-doped polypyrrole (PPy-Cl) and PNIPAAm. This hydrogel achieves atmospheric water harvesting through the adsorption of water molecules by hygroscopic PPy-Cl and subsequent contraction release of water by thermally responsive conversion of PNIPAAm. It is worth mentioning that the maximum daily water collection volume of the dry gel is ≈52.8 L and 19.2 L at 90%

and 60% ambient relative humidity, respectively.[183]

Temperature-responsive hydrogels can be used to purify polluted water in addition to collecting water from the atmosphere. Wei *et al*. synthesized a temperature-responsive hybrid hydrogel PNIPAM-co-PbrRP based on a reconstituted lead-binding peptide (PbrRP). The hydrogel exhibited high sensitivity and selectivity for lead ions. Also, it has been discovered that altering the temperature can influence the reversible capture and release of lead ions.[187]

2 Scope and Objective

The aim of this thesis is mainly to synthesize and prepare different stimulus-responsive polymers and hydrogels and to study their response mechanisms and applications.

Chapter 3 two photo-driven purification hydrogels based on the photothermal material PDA and GO, and the temperature-responsive polymer PNIPAAm will be prepared. The composition of the hydrogels will be studied by FT-IR. Subsequently, the kinetics of de- and re-swelling of hydrogels will be further investigated. The surface hydrophilicity of the hydrogels will be determined by the water contact angle. Afterwards, the purification capacity of hydrogels will be evaluated by purifying oil-water emulsions, dye-contaminated water, metal-contaminated water and microbially contaminated water. This work provides a new approach for hydrogels as emerging materials for water purification.

In Chapter 4, β-CD-PNIPAAm@PEG-FS-AZO complex will be designed and synthesized via host-guest interactions between β-CD and azobenzene. The guest polymer β-CD-terminated PNIPAAm (β-CD-PNIPAAm) will be synthesized by a combination of atom transfer radical polymerization (ATRP) and click reaction. In addition, PEG-FS-AZO with azobenzene capped end groups will be synthesized by ATRP and click reaction using PEG initiator and FS monomer. The host-guest complex will be confirmed by FT-IR, (2D NOESY)^{1}H NMR, etc. The obtained complexes will be triple responsive to light, oxygen and temperature. It can undergo reversible self-assembly and dissociation under alternating UV and visible light irradiation, oxygen influx/removal, and temperature increase/decrease.

3 Light-driven hydrogels for water purification based on Poly(*N*-isopropylacrylamide) (PNIPAAm)

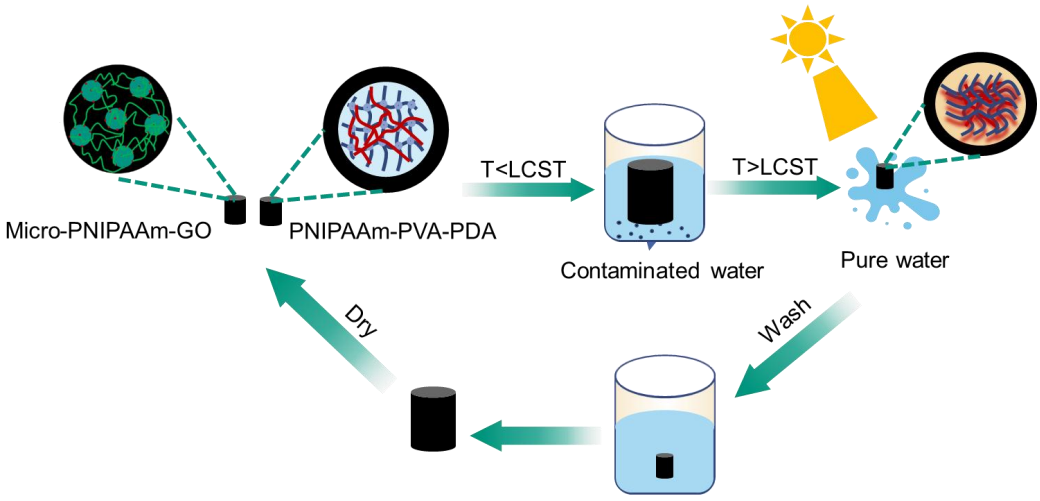

3.1 Strategy

In this chapter, two novel photo-driven absorption and release water purification hydrogels were designed and fabricated based on the water absorption and release cycle of puffer fish in danger. Specifically, Poly(*N*-isopropylacrylamide) (PNIPAAm) hydrogels can absorb and release water through a hydrophilic/hydrophobic transition at a lower critical solution temperature (LCST) (~32–34 °C), which is easy to reach.[188,189] Poly(vinyl alcohol) (PVA) is a water-soluble hydrophilic polymer which has been widely used as a biomaterial for drug delivery systems, sensors, and surgical repair due to its excellent mechanical properties, biocompatibility, and non-toxicity.[190] Pure PVA hydrogels are insensitive to environmental stimuli, and conventional PNIPAAm hydrogels respond relatively slowly. Therefore, the hydrogel prepared by cross-linking of PVA and PNIPAAm here has both the above advantages.[191] Dopamine belongs to a class of catecholamines with excellent biocompatibility that can spontaneously polymerize into polydopamine (PDA).[192] PDA is a kind of deep black solid which is insoluble in most solvents, exhibits broadband absorption from UV to visible light and high photothermal conversion efficiency.[193–195] Meanwhile, PDA is easy to coat almost all types of surfaces even PTFE and the coating provides good hydrophilicity, due to the catechol and aminoethyl units.[196–198] In addition, since the PDA coating still contains a variety of reactive functional groups (amino, catechol, *o*-quinone) after bonding, it can adsorb and remove pollutants in water to purify water. Graphene oxide (GO), a new type of carbon nanomaterial, exhibits strong hydrophilicity due to the presence of abundant surface functional groups.[199] Thus, GO can be easily dissolved in water and built into hydrogels using various forces like hydrogen bonding and van der Waals forces.[200,201] Graphene oxide also exhibits excellent photothermal effect, which is attributed to its large surface area and strong light absorption across the spectrum as well as high thermal and chemical stability.[202–204]

The preparation procedures for the two light-driven water purification hydrogels are

shown below, respectively. The first hydrogel was achieved by incorporating PVA into a conventional PNIPAAm network to obtain a PVA/PNIPAAm semi-IPN hydrogel and then depositing PDA on it. The second hydrogel was achieved by doping the micro crosslinked PNIPAAm hydrogel with graphene oxide. The principle of hydrogel water purification: when immersed in contaminated water, the hydrogel absorbed large amounts of clean water while repelling other contaminants such as microorganisms, oils, organic dyes and heavy metals. The swollen hydrogel was then exposed to light, and heated above the LCST of PNIPAAm by the photothermal conversion property of PDA and GO, resulting in a phase transition from the swollen hydrophilic state to the collapsed hydrophobic state. In this way, a large amount of clean water was released from the hydrogel. This purification mechanism can be used not only in the laboratory but also under sunlight, opening up a new paradigm of using renewable solar energy to produce clean water at high speed from polluted water sources.

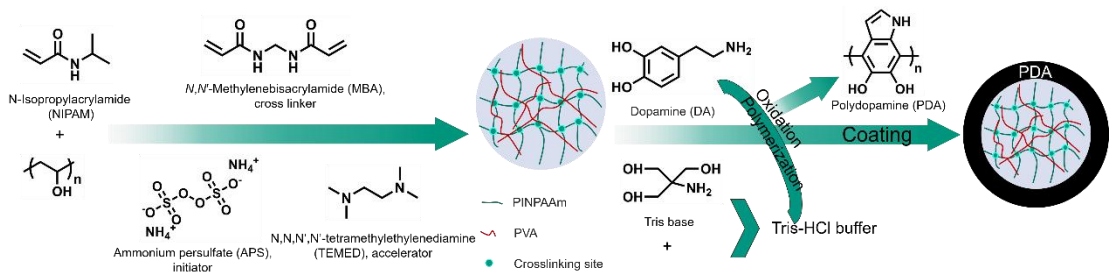

Scheme 3.1 Preparation process of the PNIPAAm-PVA-PDA hydrogel.

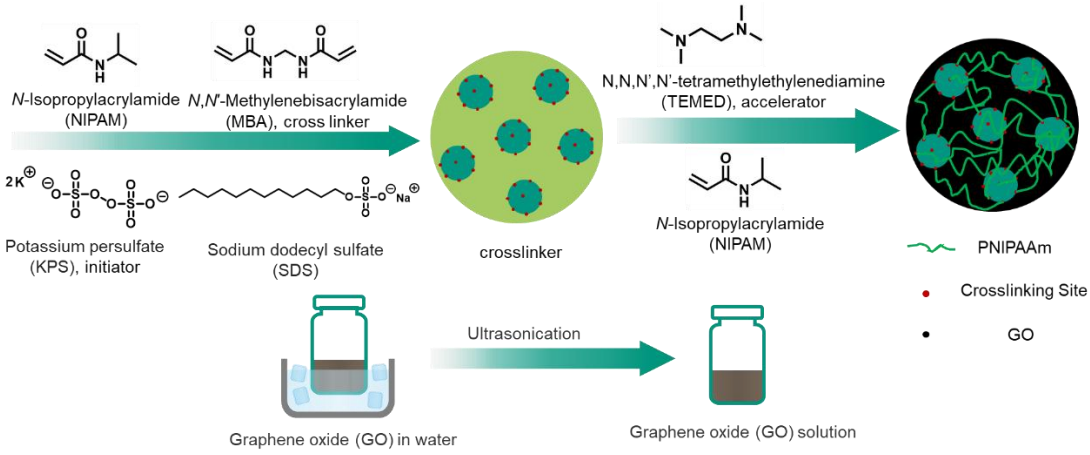

Scheme 3.2 Preparation process of the micro-PNIPAAm-GO hydrogel.

3.2 Results and Discussion

8 wt.% NIPAAm monomer solution was polymerized with *N*, *N*'-methylenebisacrylamide (MBA) and subsequently with 4 wt.% PVA solution (v:v, 1:1) to form a Interpenetrating polymer network (IPN) hydrogel in the presence of redox initiators Ammonium persulfate (APS) and N,N,N′,N′-Tetramethyl ethylenediamine (TEMED).[205] Afterwards, the formed hydrogel was immersed in dopamine tris-buffer solution (2 mg/mL) at room temperature resulting in the successful polymerization of PDA on the surface of the hydrogel, as evidenced by the darkening of the gel color (Figure 3.1).[206] The PDA content can be estimated to be around 10 mg by comparing the weight of the dried hydrogel before and after PDA coating. This kind of hydrogel has more excellent temperature responsiveness due to the presence of PVA.[191]

Conventional PNIPAAm gels cross-linked with MBA are brittle and cannot be reused repeatedly. In contrast, hydrogels prepared using PNIPAAm microgels as cross-linking agents exhibited better elasticity and mechanical stability than conventional hydrogels. First, microgel was prepared by precipitation polymerization of NIPAAm (90 mg) and MBA (5 mg) at 60 °C for 40 min, initiated by Potassium persulfate (KPS) in the presence of Sodium dodecyl sulfate (SDS) in water. 1 mL GO

solution (10 mg) was added into the cooled microgel. Afterwards, the NIPAAm monomer (0.56 g) was put into the above mixture and polymerized with MBA in the presence of redox initiators APS and TEMED to form a black hydrogel.[177,206] The Figure 3.2 demonstrates the successful incorporation of hydrogel.

Figure 3.1 Photograph of PNIPAAm-PVA hydrogel (left) and PNIPAAm-PVA-PDA hydrogel (right).

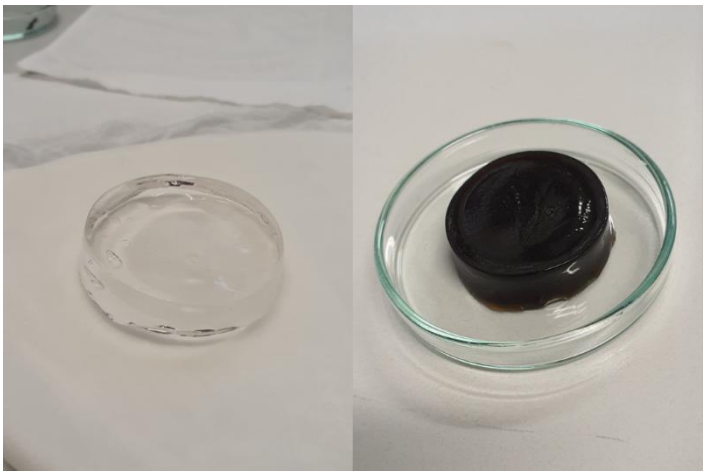

Figure 3.2 Photograph of micro-PNIPAAm hydrogel (left) and micro-PNIPAAm-GO hydrogel (right).

Figure 3.3 depicts the SEM images of PNIPAAm-PVA and PNIPAAm-PVA-PDA hydrogels. SEM showed that both hydrogels exhibit a high-porosity honeycomb structure, which provides a good structure for water transport through capillary flow. After coating with PDA, the hybrid gel retained an interconnected porous structure

with an average pore size of 10 µm. Higher magnification shows that PDA was indeed deposited as nanoparticles on top of the hydrogel structure (Figure 3.3 f).

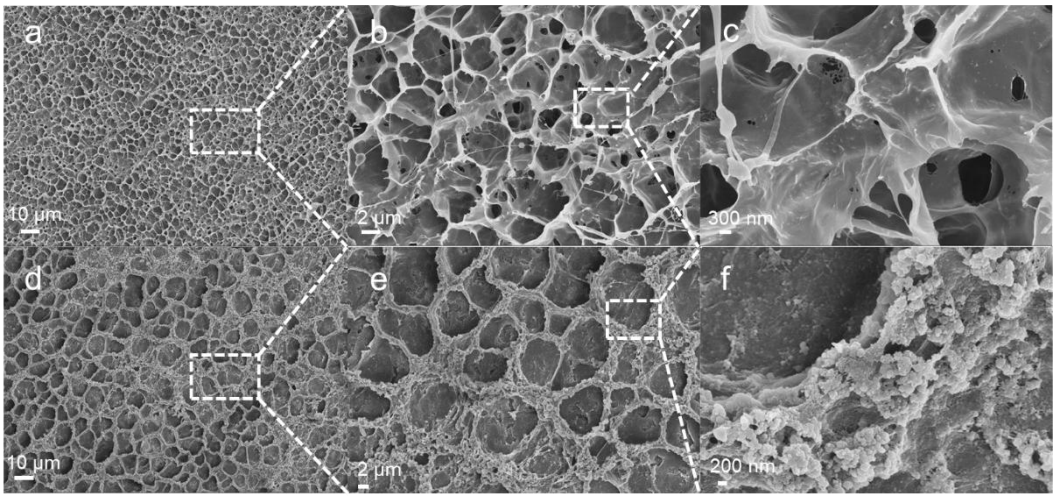

Figure 3.3 Scanning electron microscopy (SEM) images of PNIPAAm-PVA (a, b, c) and PNIPAAm-PVA-PDA (d, e, f) under different magnifications demonstrate macro porous architecture.

SEM images of GO, micro-PNIPAAm, and micro-PNIPAAm-GO hydrogels are shown in Figure 3.4. The SEM demonstrates that the morphology of GO is layered lamellar. Micro-PNIPAAm-GO exhibits a 3D network structure with an average pore size of roughly 10 µm. In contrast, micro-PNIPAAmb does not show such structure. It indicates that GO can lead to a porous network-like structure of the hydrogel. This structure offers favorable circumstances for water transportation. At higher magnifications, no obvious GO particles could be visible in the SEM pictures of the micro-PNIPAAm-GO hydrogel, and it is speculated that GO is uniformly distributed throughout the hydrogel network. This sustains the hydrogel's network structure and is also crucial for the subsequent conversion of light energy absorbed by GO into thermal energy to heat the whole hydrogel.

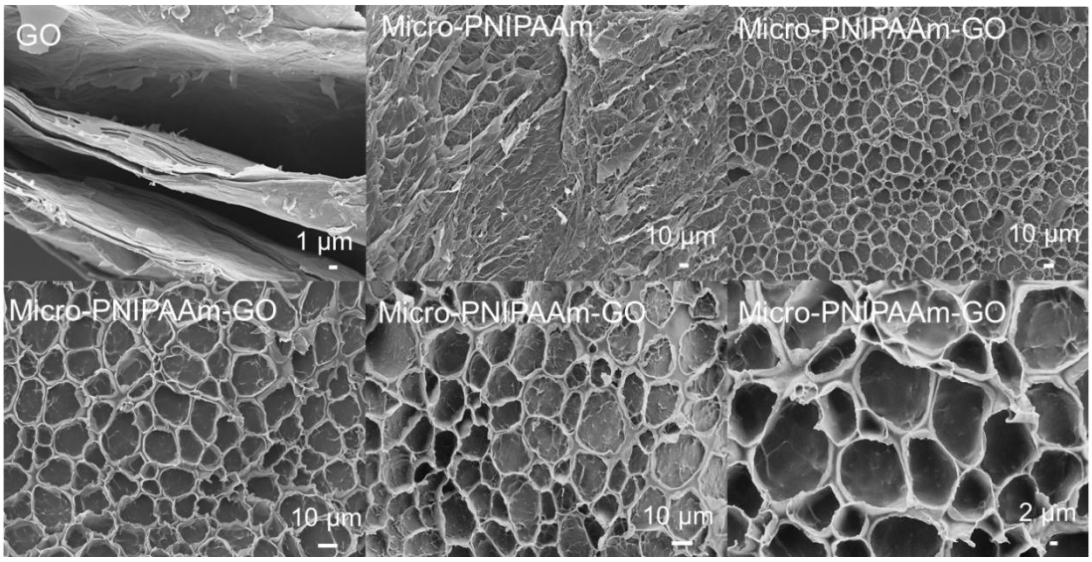

Figure 3.4 Scanning electron microscopy (SEM) images of GO, Micro-PNIPAAm, and Micro-PNIPAAm-GO under different magnifications demonstrate macroporous architecture.

The chemical composition of the both target hydrogels were confirmed by Fourier transform infrared spectroscopy (FTIR). As shown in the FTIR spectra (Figure 3.5), the broad absorption peak at ≈3300 cm^{-1} corresponds to the N-H stretching vibration of PNIPAAm and the O-H stretching vibration of the hydroxyl groups on PDA. The characteristic absorption bands of C-O stretching and N-H stretching of PNIPAAm appear at 1634 and 1529 cm^{-1}.[207] Taken together, these results strongly indicate the successful formation of the PNIPAAm-PVA-PDA hydrogel.

The large absorption peak at about 3300 cm^{-1}, which can be seen in Figure 3.6, is attributed to the N-H stretching vibration of PNIPAAm and the O-H stretching vibration of the hydroxyl groups of GO. The peak at 1730 cm^{-1} is attributed to the C=O stretching vibration in the COOH group. The peak at 1421 cm^{-1} comes from the bending vibration of the O–H group. The stretching peaks of the alkoxy C-O and epoxy C-O groups are located at 1048 and 1228 cm^{-1}, respectively. Overall, these observations clearly suggest that the micro-PNIPAAm-GO hydrogel was successfully formed.

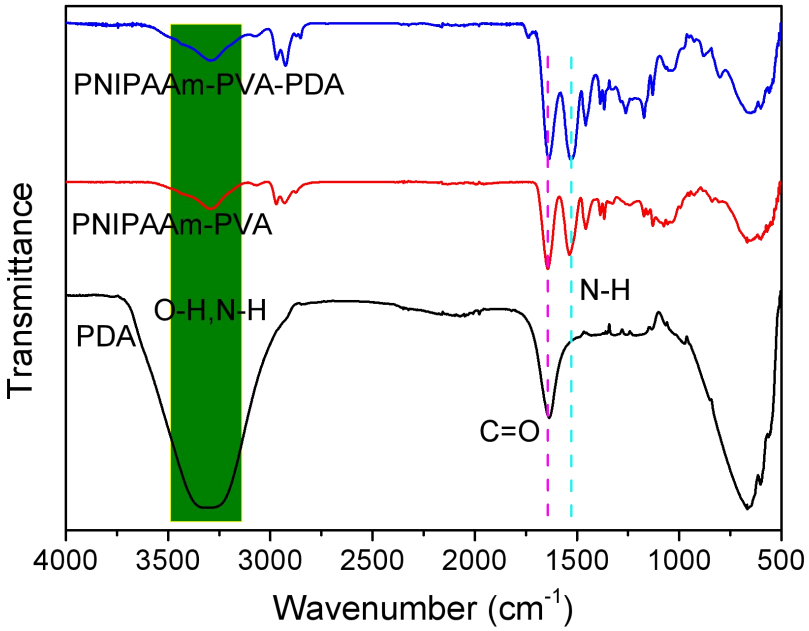

Figure 3.5 FTIR spectra of PDA, PNIPAAm-PVA hydrogel and PNIPAAm-PVA-PDA hydrogel.

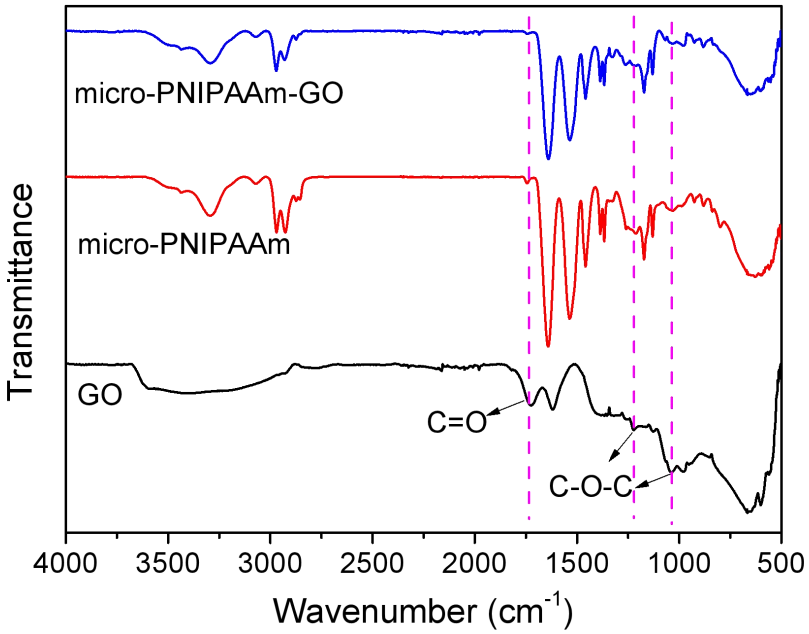

Figure 3.6 FTIR spectra of GO, micro-PNIPAAm hydrogel, micro-PNIPAAm-GO hydrogel.

The hydrophilic-hydrophobic transition of PNIPAAm at its LCST can trigger a phase

transition of the hydrogels, resulting in a rapid release of water. The LCST temperature of the hydrogels were confirmed by differential scanning calorimetry (DSC) in Figure 3.7. The LCST of PNIPAAm-PVA-PDA hydrogel and micro-PNIPAAm-GO hydrogel were determined by the endothermic peaks at ≈34 °C and ≈33 °C, respectively, which did not change much compared with the LCST of PNIPAAm. This demonstrates that the incorporation of PDA and GO do not affect the LCST of PNIPAAm. lower LCST is essential for the subsequent water purification.

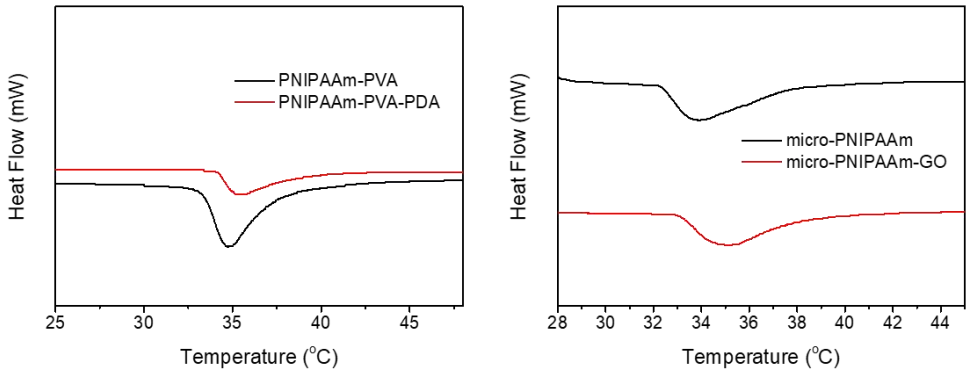

Figure 3.7 DSC thermogram of swollen PNIPAAm-PVA-PDA hydrogel (left) and swollen micro-PNIPAAm-GO hydrogel (right).

Low-temperature light-driven water release was assessed by near-infrared light. Under NIR irradiation (9 W, 850 nm), the surface temperature of PNIPAAm-PVA-PDA hydrogel increased with time and reached its LCST after 30 min of irradiation (Figure 3.8 top left). The final surface temperature is about 37 °C, which is 3 °C higher than its LCST. However, the surface temperature of PNIPAAm-PVA hydrogel can only reach about 25.7 °C, which is much lower than its LCST. The micro-PNIPAAm-GO hydrogel's surface temperature under NIR light increased over time and achieved its LCST after 40 minutes of exposure (Figure 3.10 bottom right). The final surface temperature is about 36°C, which is 3°C higher than the LCST of micro-PNIPAAm-GO hydrogel. In contrast, the surface temperature of micro-PNIPAAm hydrogel can only reach about 23.5 °C, which is much lower than

LCST (Figure 3.8 bottom left). Additionally, it indicates that PNIPAAm-PVA-PDA hydrogel has a faster temperature response than micro-PNIPAAm-GO due to PDA can execute photothermal conversion more quickly than GO. This comparison convincingly demonstrates the utility of PDA and GO as photothermal conversion materials, and both these hydrogels can be used to light-driven water release.

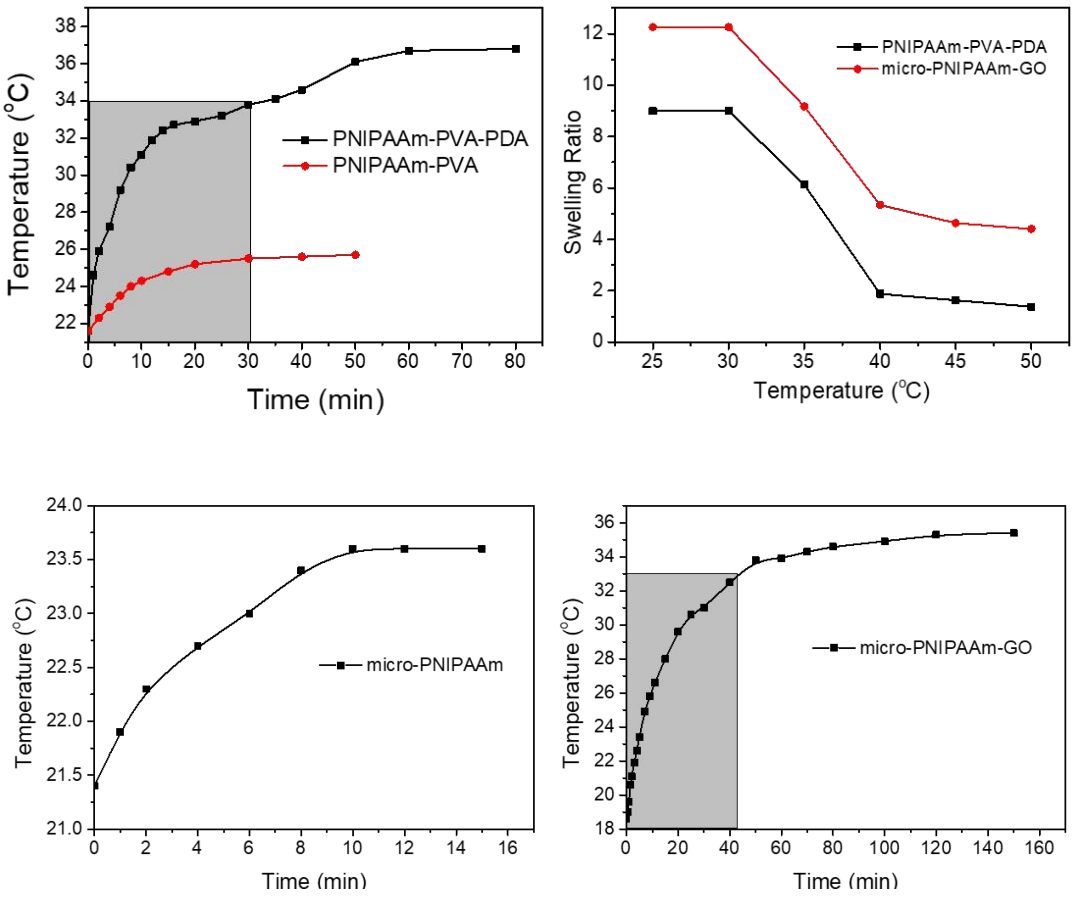

Figure 3.8 Surface temperature change of PNIPAAm-PVA-PDA and PNIPAAm-PVA hydrogels (top left), micro-PNIPAAm (bottom left) and micro-PNIPAAm-GO hydrogels (bottom right) overtime under NIR irradiation; equilibrium swelling ratio of PNIPAAm-PVA-PDA and micro-PNIPAAm-GO hydrogels over the temperature range from 25 to 50 °C (top right).

Figure 3.8 (top right) depicts the relationship between the hydrogels' swelling ratio (SR) and temperature over the range of 25 to 50 °C. Since PNIPAAm and PVA are both swellable and hydrophilic at temperatures below the LCST, the SR of both

hydrogels are higher at low temperatures. As the temperature rose above 30 °C, the hydrogels' SR rapidly decreased. According to the swelling ratio experiments, the phase transition temperature, also known as the LCST, is typically thought of as the temperature at which the SR rapidly declines (or an inflexion point occurs) and the degree of phase separation is at its highest. The LCST of PNIPAAm-PVA-PDA and micro-PNIPAAm-GO hydrogels are between 30 and 35 °C. The entire hydrogel system's phase separation is regulated by the temperature-responsive component PNIPAAm. The LCST of the hydrogels are unaffected by PDA and GO. In addition, micro-PNIPAAm-GO hydrogel exhibited a higher room temperature equilibrium swelling ratio compared to PNIPAAm-PVA-PDA, and both hydrogels were able to release about eight times their own weight of water. It indicates that the amount of water released by both hydrogels at above LCST is about the same.

The de-swelling kinetics of the hydrogels are shown in Figure 3.9 and 3.10. From Figure 3.9 we can find that the hydrogels respond quickly and can shrink to an equilibrium state in a very short time. The response speed decreased slightly after the surface was covered with PDA, losing 50 % of the water in two minutes compared to the PNIPAAm-PVA losing 50% of the water in about one minute. This may be due to the fact that PDA forms a thick and dense layer on the surface, which slows down the extrusion of water molecules and results in a slow response. Conversely, it can be seen from the re-swelling kinetics that the PDA layer greatly increases the re-swelling rate, from 50 % water uptake in 6 hours to 50 % water uptake in two hours.

It is obvious that the temperature response of the hydrogels is very fast from the change in the curve of the de-swelling kinetics. After GO incorporation, the response rate of the hydrogel increased compared to previous. 50% of the water was lost in about 40 minutes, while the micro PNIPAAm lost 50% of the water in about 90 minutes. This may be due to the 3D network structure formed by GO inside the hydrogel, which provides a conduit for the exclusion of water molecules, thus increasing the rate of water release and leading to an increase in the response rate. The

re-swelling kinetic curves show that GO also significantly accelerates the re-expansion rate, going from 50% water absorption at 6 hours to 50% water absorption at 2 hours. From the de-swelling kinetic curves, it can be seen that PNIPAAm-PVA-PDA hydrogel can release water more rapidly at 50 ℃ compared to micro-PNIPAAm-GO hydrogel. And this result is consistent with the above results of the surface temperature change of the hydrogels under NIR irradiation. The swelling behaviors of the hydrogels indicate that the hydrogels can rapidly release water above the LCST and re-swell intact and without rupture when immersed in water at ambient temperature. This also demonstrates the reusability of the hydrogels.

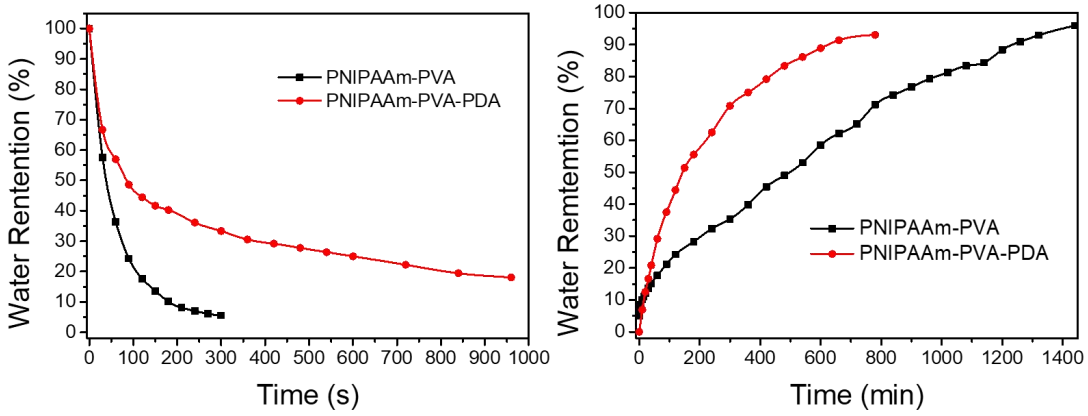

Figure 3.9 De-swelling kinetics of PNIPAAm-PVA and PNIPAAm-PVA-PDA hydrogels at 50 ℃ (left) and re-swelling kinetics at 25 ℃ (right).

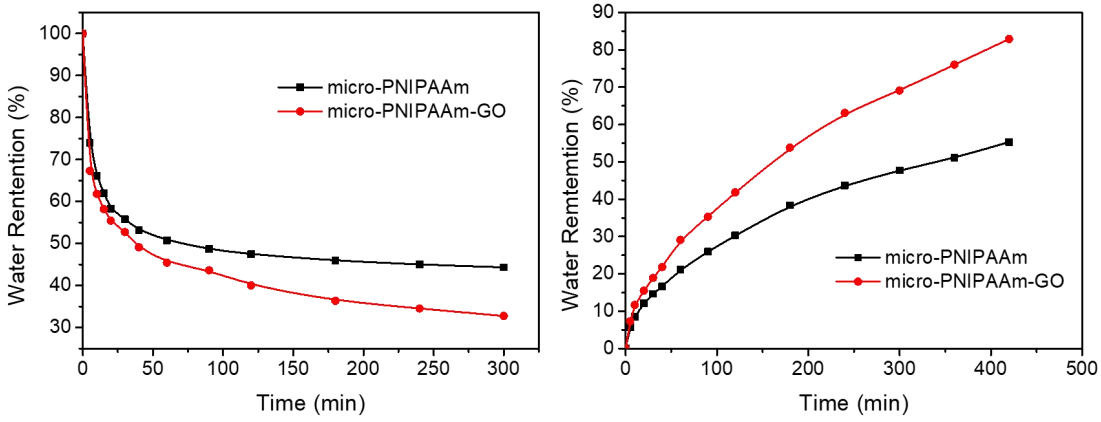

Figure 3.10 De-swelling kinetics of micro-PNIPAAm and micro-PNIPAAm-GO hydrogels at

50 ℃ (left) and re-swelling kinetics at 25 ℃ (right).

The effect of PDA and GO on the wetting properties of the hydrogels were investigated by recording the dynamic wetting behavior of water droplets at room temperature. As shown in Figure 3.11, when placed on PNIPAAm-PVA, the water droplets remained stable with a water contact angle less than 20º. In contrast, for PDA-modified PNIPAAm-PVA hydrogel, the water droplets immediately spread on the surface of the PNIPAAm-PVA hydrogel due to the hydrophilicity of polydopamine. As shown in Figure 3.12, the contact angle was both around 70º when drops of water were applied to the surface of micro-PNIPAAm and micro-PNIPAAm-GO hydrogels. However, after 20 s, the water contact angle on the micro-PNIPAAm-GO surface decreased to around 40º, and the water contact angle on the micro-PNIPAAm surface basically did not change significantly. It is speculated that it's due to the incorporation of hydrophilic GO and the formation of porous network structure. The water contact angles of the hydrogels containing GO are larger than those of the hydrogels containing PDA, which is attributed to the strongly hydrophilic PVA. Both hydrogels have outstanding hydrophilicity, which is necessary to promote water transport within the hydrogel and to repel hydrophobic impurities like oil, according to the results of the water contact angle tests.

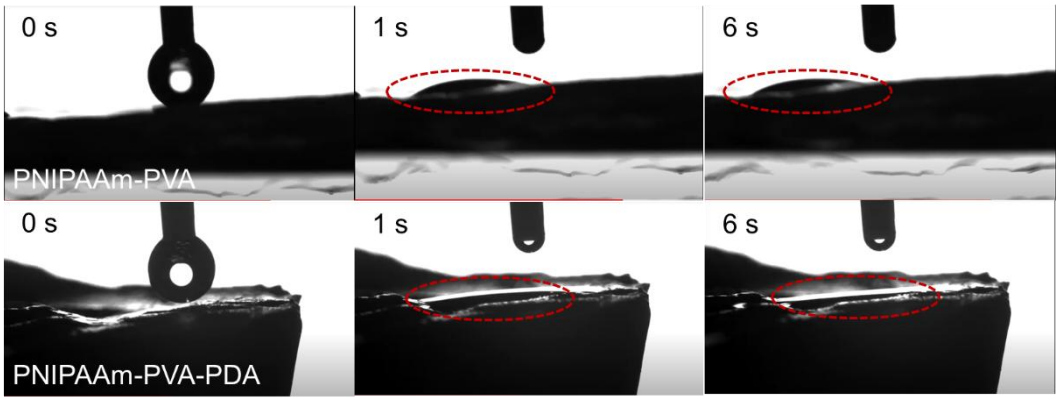

Figure 3.11 Dynamic wetting behaviors of a water droplet (≈20 μL) atop PNIPAAm-PVA and PNIPAAm-PVA-PDA at room temperature.

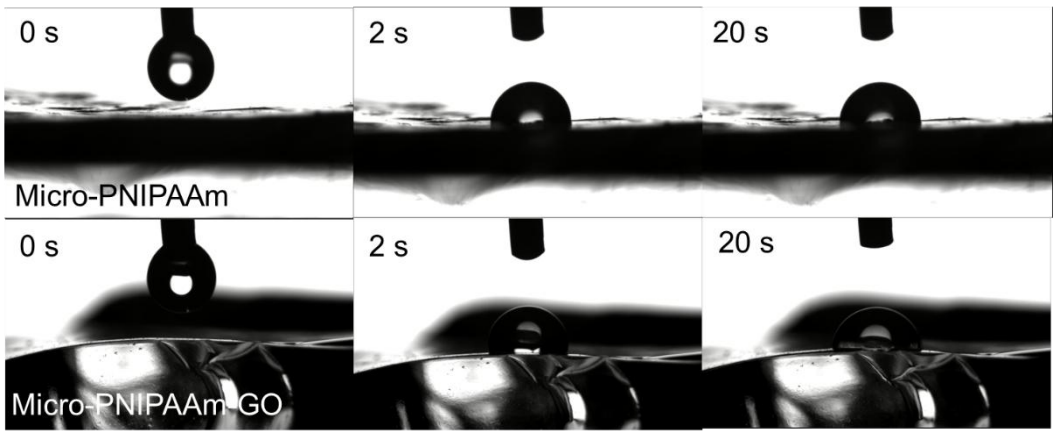

Figure 3.12 Dynamic wetting behaviors of a water droplet (≈20 μL) atop micro-PNIPAAm and micro-PNIPAAm-GO at room temperature.

An aqueous R6G solution was employed in this work as a wastewater model to evaluate the adsorption-desorption process and the reusability of the hydrogels. The procedure is as follows: First, the dried hydrogels were immersed in an aqueous R6G solution. After the hydrogels reached the equilibrium dissolved state, they were exposed to NIR irradiation to release water. The shrunk hydrogels after storage water release were washed with distilled water and ethanol as a desorbent for R6G. Then the swollen hydrogels were dried at a high temperature, and the resulting dried hydrogels were submerged in the dye solution for the subsequent adsorption-purification procedure. The original R6G solution showed a light pink color, while the purified solutions were colorless, which means that the dye were adsorbed into the hydrogels. Meanwhile, the water released from the hydrogels under NIR irradiation were clear and transparent without UV absorption, indicating that there was no any R6G present in the water. This demonstrates that the hydrogel has strong dye adsorption and pure water release capabilities. Figure 3.13 (right) and 3.14 (left) show the weight change of water produced by 10 adsorption-desorption cycles of the hydrogel. The weight of the resulting pure water did not change significantly in ten cycles, indicating the good reusability of the hydrogels. After 10th cycles, both the water released from the hydrogel and the adsorbed remaining dye solution were essentially free of UV absorption peaks of R6G, further confirming the high adsorption capacity and good

cycling stability of the hydrogel.

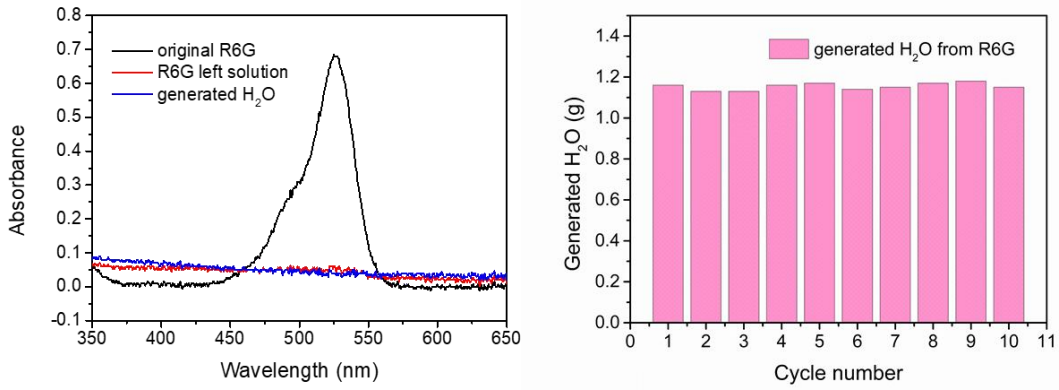

Figure 3.13 Adsorbed Dye Evaluation. UV-Vis adsorption of generated water from R6G solution (left) and Purification recyclability test of the PNIPAAm-PVA-PDA hydrogel (right).

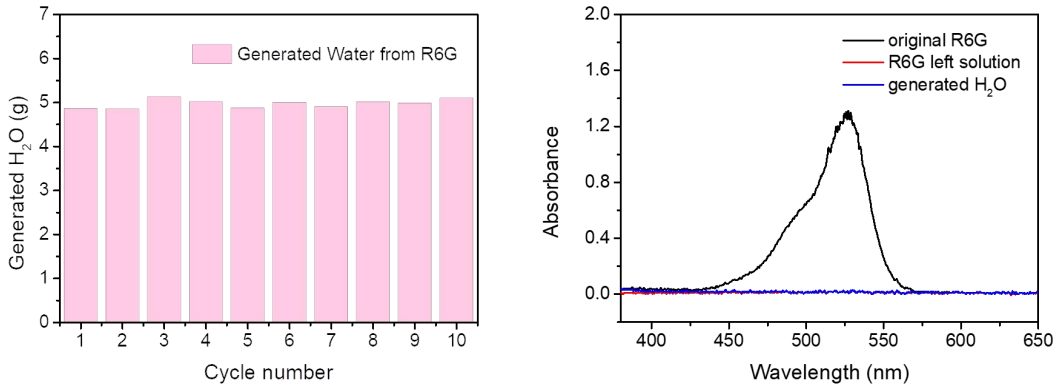

Figure 3.14 Adsorbed Dye Evaluation. Purification recyclability test of the micro-PNIPAAm-GO hydrogel (left) and UV-Vis adsorption of generated water from R6G solution (right).

Three different oil-in-water emulsions were used as test groups for the hydrogels' purification capabilities: petroleum ether, cyclohexane, and hexane. As shown in Figure 3.15, the original petrol ether-in-water emulsions were milky white. After purification, there was no sign of oil droplets and the liquids were clear and transparent. Microscopic pictures also confirmed this result. Before purification, the emulsions were full of small droplets with the diameter of less than 20 nm. And there were no small droplets after purification. The same method was used to verify the

other two oil-in-water emulsions, and clear purified water was also obtained. This indicates that the hydrogels are able to repeatedly purify polluted water and produce clean water from oil-in-water emulsions due to the hydrophilicity and anti-oil absorption.

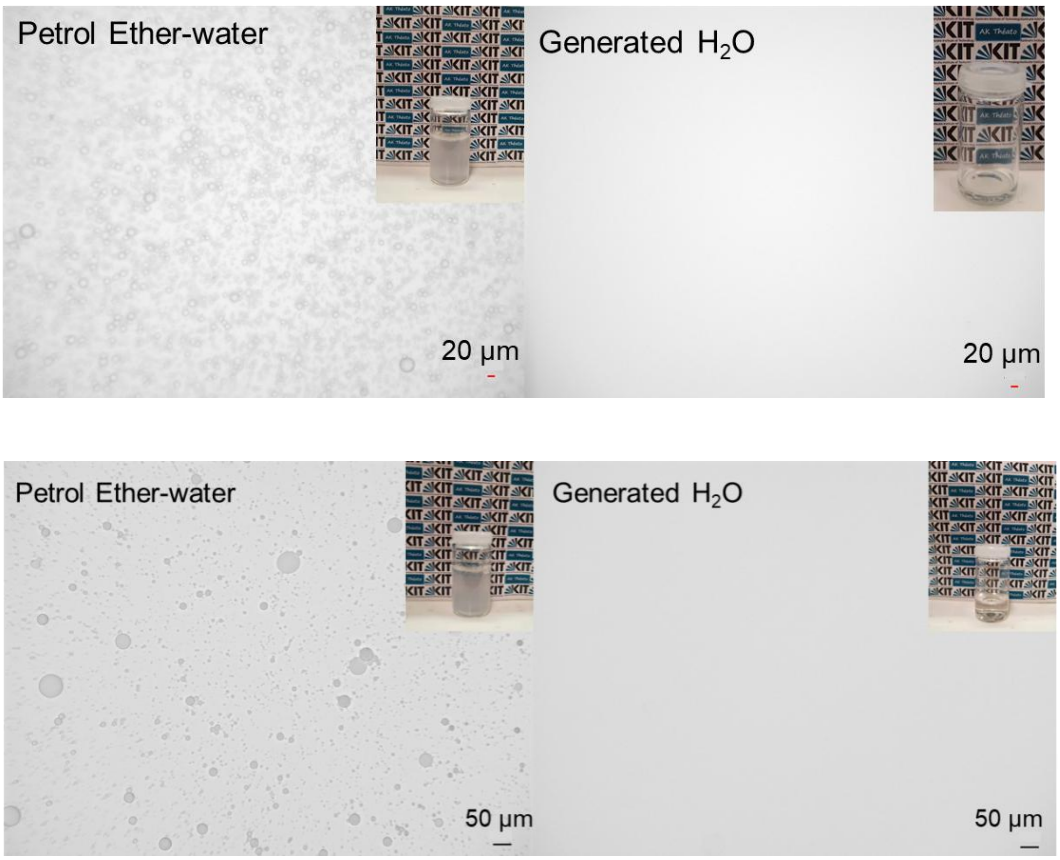

Figure 3.15 Microscopy photographs of SDS-stabilized petrol ether-in-water emulsions before and after treatment with PNIPAAm-PVA-PDA hydrogel (top) and micro-PNIPAAm-GO hydrogel (bottom).

The level of microorganisms is also one of the important criteria for evaluating the quality of water. The hydrogels were immersed to the 0.1 wt.% yeast solution to evaluate its capacity to purify microorganisms in water. The micrographs indicate that there were no microorganisms in the water generated by the hydrogels in contrast to the initial yeast solutions before purification, which had high concentration of yeast cells. This demonstrates that hydrogels can clean microbially contaminated water in addition to oil-water emulsions, which paves the way for expanding the potential uses

of the hydrogels.

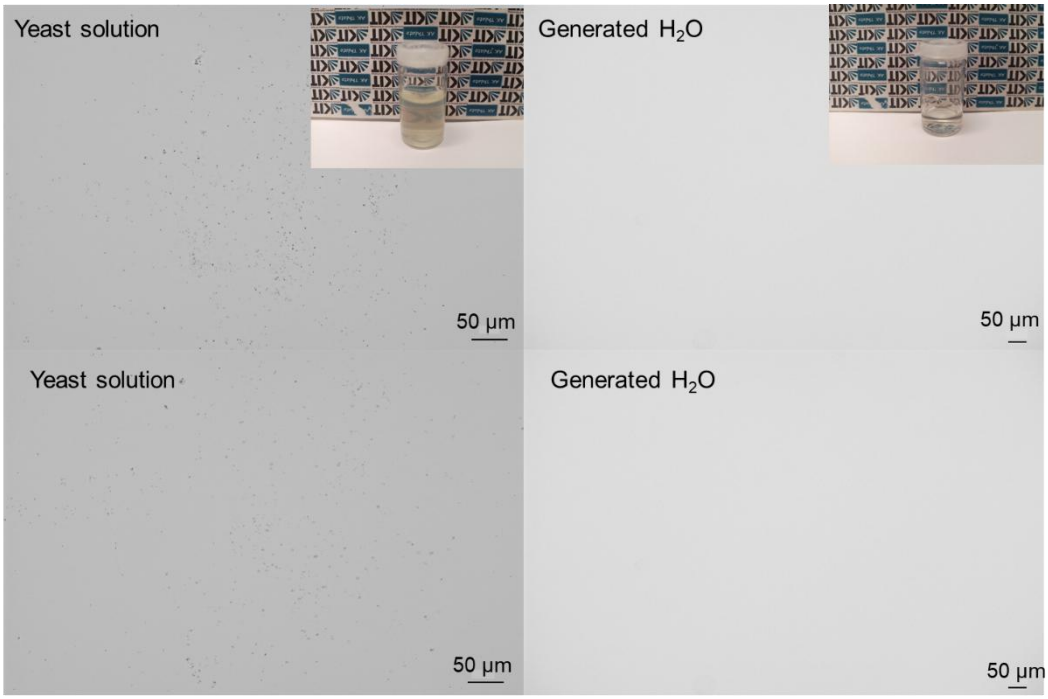

Figure 3.16 Digital and microscopy photographs of yeast solutions before and after treatment with PNIPAAm-PVA-PDA hydrogel (top) and micro-PNIPAAm-GO hydrogel (bottom).

Metal contaminants account for a significant portion of water pollution and are very difficult to remove. Two different metal contaminated waters were chosen as examples of hydrogel purification. The hydrogels purified water from two different metal contaminants, including Pb $(CH_3CO_2)_2 \cdot 3H_2O$ and Pd $(OAc)_2$. First, the hydrogels were immersed in an aqueous solution containing 0.0001 M Pb $(CH_3CO_2)_2 \cdot 3H_2O$ and Pd $(OAc)_2$, then left at room temperature until equilibrium was reached. The swollen hydrogels were subsequently exposed to NIR irradiation and the resulting water were collected. The concentration of heavy metal ions in the solution was measured using ICP-OES, as shown in Figure 3.17. The PNIPAAm-PVA-PDA hydrogel was able to reduce the Pd^{2+} concentration from 11.4 mg/Kg to 5.15 mg/Kg, a reduction of 54.8 %, while the ion concentration in the generated water was only 0.4 %. However, micro-PNIPAAm-GO hydrogel was only able to reduce the Pd^{2+} concentration from 12.3 mg/Kg to 10.7 mg/Kg, a reduction of 13 %, but the ion

concentration in the generated water was 16.7 %. On the contrary, both hydrogels were highly adsorptive for Pb^{2+}. The PNIPAAm-PVA-PDA hydrogel was shown to reduce the Pb^{2+} concentration from 18.4 mg/Kg to 0.895 mg/Kg, adsorbing 95 % of the Pb^{2+} in the aqueous solution, while the Pb^{2+} concentration in the generated water was below 0.1 %, which is below the detection limit of the instrument. Comparably, the micro-PNIPAAm-GO hydrogel was observed to reduce the Pb^{2+} concentration from 20.6 mg/Kg to 0.089 mg/Kg, adsorbing 99.6 % of the Pb^{2+} in the aqueous solution, while the concentration of Pb^{2+} in the generated water was below 0.3 %, which is also below the detection limit of the instrument. The higher adsorption capacity of hydrogels for Pb^{2+} may be due to the higher binding affinity of functional groups such as carboxyl, hydroxyl and amine groups in hydrogels, compared to Pd^{2+}. In addition, it can be seen from the above results that PNIPAAm-PVA-PDA hydrogel has higher adsorption for Pd^{2+} compared to micro-PNIPAAn-GO hydrogel, while micro-PNIPAAn-GO hydrogel has higher adsorption for Pb^{2+} than PNIPAAm-PVA-PDA hydrogel. This may be attributed to the difference of PDA and GO functional groups. More importantly, all the generated water has very low concentration of heavy metal ions.

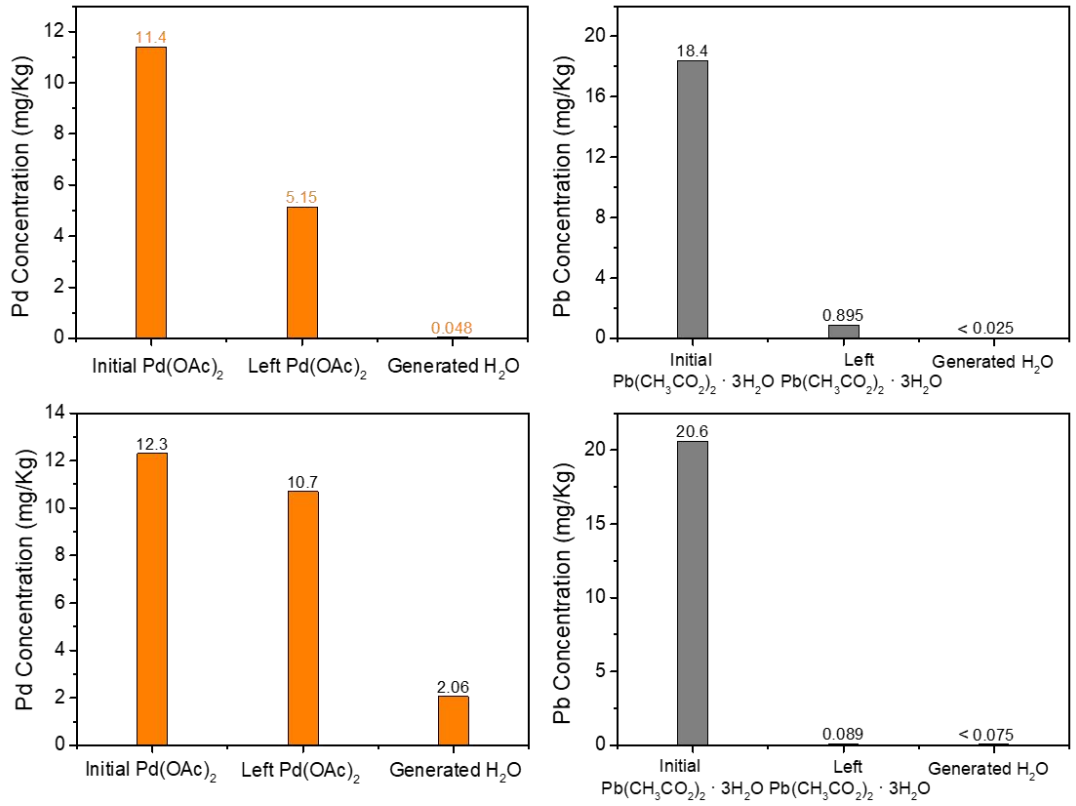

Figure 3.17 Concentrations of Pb^{2+} and Pd^{2+} in water purified by the PNIPAAm-PVA-PDA hydrogel (top) and micro-PNIPAAm-GO hydrogel (bottom).

To investigate the practical application of hydrogel in outdoor sunlight, the water release of the light-driven hydrogel under sunlight was performed. As shown in Figure 3.18, more than 90% of the water in the PNIPAAm-PVA-PDA hydrogel and about 60% of the water in the micro-PNIPAAm-GO hydrogel was released after placing the hydrogels under sunlight for half an hour. This indicates that the surface temperature of the hydrogels has reached the LCST and changed from the hydrophilic state to the hydrophobic state. PDA and GO show excellent photothermal conversion performance, and even the water release is faster due to the greater intensity of outdoor sunlight than the NIR light in the laboratory. Therefore, both hydrogels are potential materials that can be used for actual water purification.

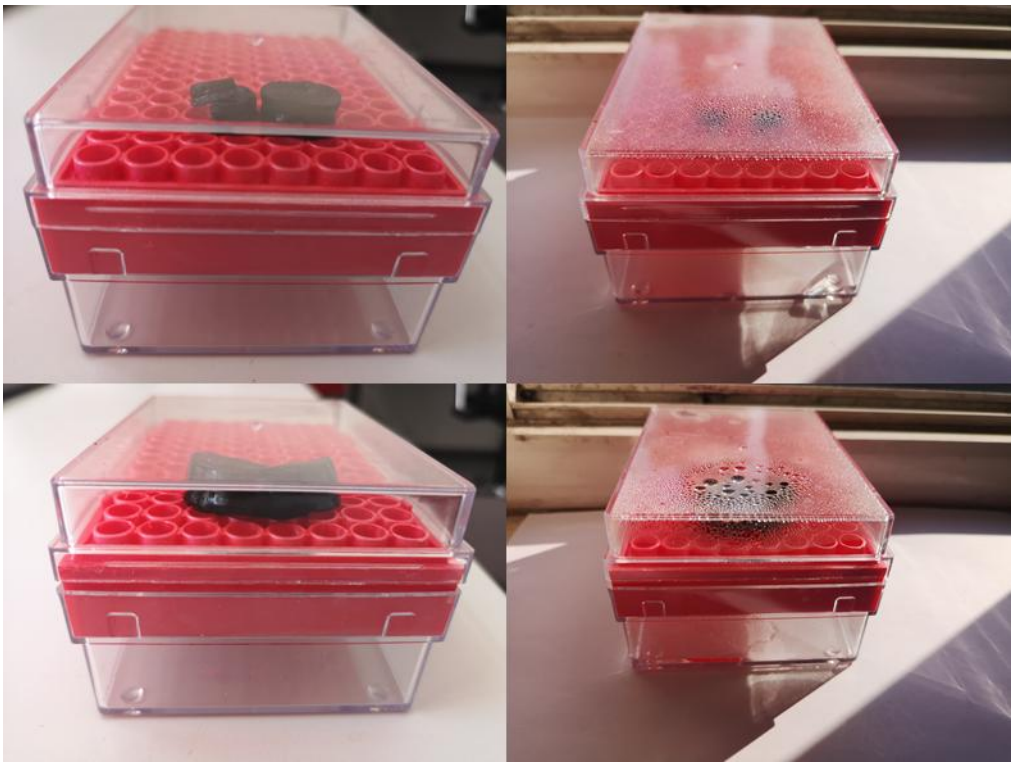

Figure 3.18 Natural sunlight-driven clean water generation. PNIPAAm-PVA-PDA (top) and micro-PNIPAAm-GO (bottom) hydrogels placed indoors without sunlight (left); PNIPAAm-PVA-PDA (top) and micro-PNIPAAm-GO (bottom) hydrogels placed in outdoor sunlight (right).

3.3 Conclusion

In summary, two novel light-driven purification hydrogels were prepared based on the photothermal material PDA and GO, PNIPAAm-PVA-PDA hydrogel and micro-PNIPAAm-GO hydrogel. Under NIR irradiation at 850 nm, the surface temperature of PNIPAAm-PVA-PDA hydrogel can rise to LCST within 30 min, much faster than that of micro-PNIPAAm-GO hydrogel within 40 min. The equilibrium swelling ratios show that both PNIPAAm-PVA-PDA and micro-PNIPAAm-GO hydrogels can generate eight times their own weight of water at above LCST. A series of contaminated water purification tests were then performed to demonstrate that the prepared hydrogels were all capable of obtaining clean water from oil-water contaminants, dye wastewater, heavy metal contaminated water and microbially

contaminated water. Both hydrogels have better adsorption for Pb^{2+} compared to Pd^{2+}. PNIPAAm-PVA-PDA hydrogel has higher adsorption for Pd^{2+} compared to micro-PNIPAAn-GO hydrogel, while micro-PNIPAAn-GO hydrogel has higher adsorption for Pb^{2+} than PNIPAAm-PVA-PDA hydrogel. All the generated water has very low concentration of heavy metal ions, especially the Pb^{2+} concentration is already below the minimum detection range of the instrument. This provides a new approach to the current water pollution problem that is more energy efficient, environmentally friendly and convenient.

4 Light, temperature and O_2 Stimuli-responsive polymer based on host-guest interaction

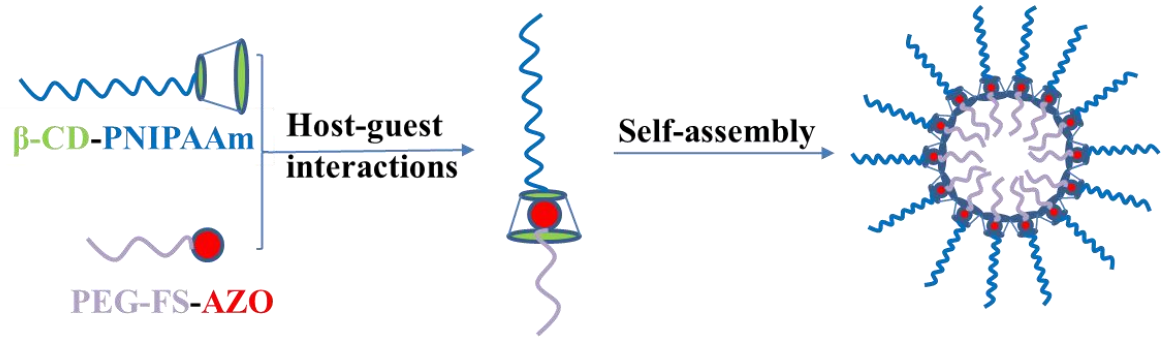

4.1 Strategy

Cyclodextrin (CD) and azobenzene (AZO) are typical systems that form complexes through host-guest interactions.[208] Since azobenzene undergoes reversible isomerization under UV and visible light, the formation and dissociation of the complexes can be controlled by light.[209] Poly(*N*-isopropylacrylamide) (PNIPAAm) is one of the well-known thermally responsive polymers that undergoes thermally induced reversible hydrophilic/hydrophobic phase transitions above the lower critical solubility temperature (LCST).[31] Pentafluorophenyl-capped poly(ethylene glycol) which is O_2-sensitive was very recently described by Jung et al. It was discovered that the solubility of the polymer in water was slightly improved by the interaction between oxygen and C-F bonds.[136]

Our target is to construct supramolecular polymers from host-guest inclusion polymers, *β*-cyclodextrin-poly(*N*-isopropylacrylamide)@poly(ethylene glycol)-pentafluorostyrene-azobenzene (*β*-CD-PNIPAAm@PEG-FS-AZO) based on the interaction between *β*-CDs and azobenzene groups. Atom transfer radical polymerization (ATRP) was used to produce the guest polymer PEG-FS-AZO as well as the host polymer *β*-CD-PNIPAAm. Herein, the hydrophobic FS forms the core of the supramolecular micelle and the hydrophilic PNIPAAm is used as the shell of the supramolecular micelle. FS can be converted from hydrophobic to hydrophilic after the exposure to oxygen; PNIPAAm changes from hydrophilic to hydrophobic with increasing temperature; Azobenzene is a typical photosensitive group that can undergo cis/trans conversion in the presence of light. Therefore, a polymer micelle with multiple responses to light, oxygen and temperature is prepared.

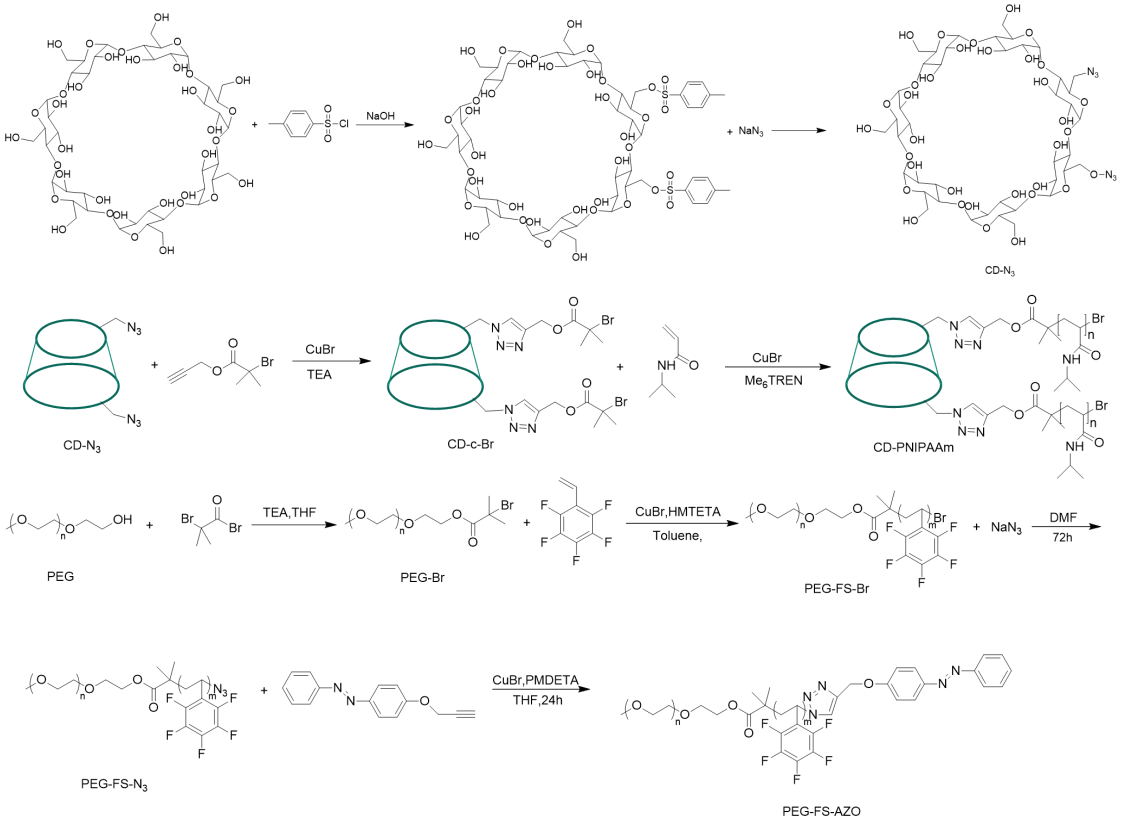

Scheme 4.1 Preparation Strategy Sketch Map of β-CD-PNIPAM@PEG-FS-AZO Supramolecular Polymers.

4.2 Results and Discussion

β-CD-PNIPAAm was synthesized as previously reported.[210] Scheme 4.1 depicts the reaction strategy for the synthesis of *β*-CD-PNIPAAm. Starting with the synthesis of monoazide-functionalized β-cyclodextrin (*β*-CD-N_3), then the ATRP-initiating moiety was introduced by a click reaction with 2-bromoisobutyryl propargyl ester (PBM). Afterwards, *β*-CD-functionalized initiator was used to initiate the ATRP of NIPAAm to produce the final polymer (*β*-CD-PNIPAAm).

The click reaction of *β*-CD-N_3 with the alkyne PBM was subsequently carried out, employing CuBr as catalyst. As shown by ^{1}H NMR spectra, the peak at 8.12 ppm proved the formation of the triazole ring and the product *β*-CD-PBM was successfully obtained (Figure 6.3.4). All characteristic peaks of *β*-CD-PBM can be assigned in the spectrum. As shown in the Figure 6.3.1, by calculating the integral area ratio of the

two peaks at 2.43 ppm and 4.76 ppm, it was demonstrated that about two -OH groups in the whole *β*-CD structure were involved in the reaction.

The obtained *β*-CD-functionalized initiator and NIPAAm monomer were subjected to ATRP to obtain the target polymer. During this ATRP reaction, the CATALYST system CuBr/Me_6TREN was employed, which allows polymerization at room temperature. In the ^{1}H NMR spectrum (Figure 4.1), the proton peak of -NH appears at 6.84-7.5 ppm, demonstrating the successful proceeding of ATRP. This result is also confirmed by the -CH_3 peak at 1.0 ppm and the -CH peak at 3.65-3.89 ppm. All characteristic peaks of the polymer have been attributed in the spectra. The degree of polymerization of the polymer was estimated by comparing the integrated area ratio of -CH_3 (0.7-1.09 ppm) of the repeating unit with the proton signal of the CD fraction (4.55 - 5.2 ppm) to be about 32. Thus, the experimental number average molecular weight ($M_{n,\ NMR}$) of *β*-CD- PNIPAAm is about 5000 g mol^{-1}. The values determined by GPC ($M_{n,\ GPC}$ = 4321 g mol^{-1}) and calculated from ^{1}H NMR spectra do not differ much, which shows good agreement. The host polymer *β*-CD-PNIPAAm showed a slightly wider molecular weight distribution in the result tested by GPC, with a Đ of 1.39. This is due to the difference in the number of -OH groups involved in the reaction in each *β*-CD, although on average two -OH groups are involved in the reaction. In conclusion, the experimental results showed that the host polymer was effectively purified and the polymerization process was well controlled.

The FT-IR spectra also demonstrate the successful preparation of the host polymer. As shown in the Figure 4.2, the absence of the characteristic absorption peak of azide at 2100 cm^{-1} indicates that the previous click reaction was complete. The absorption peak at 3290 cm^{-1} is attributed to -OH of *β*-CD. The characteristic absorption peak of -NH of PNIPAAm appears at 2967 cm^{-1}.

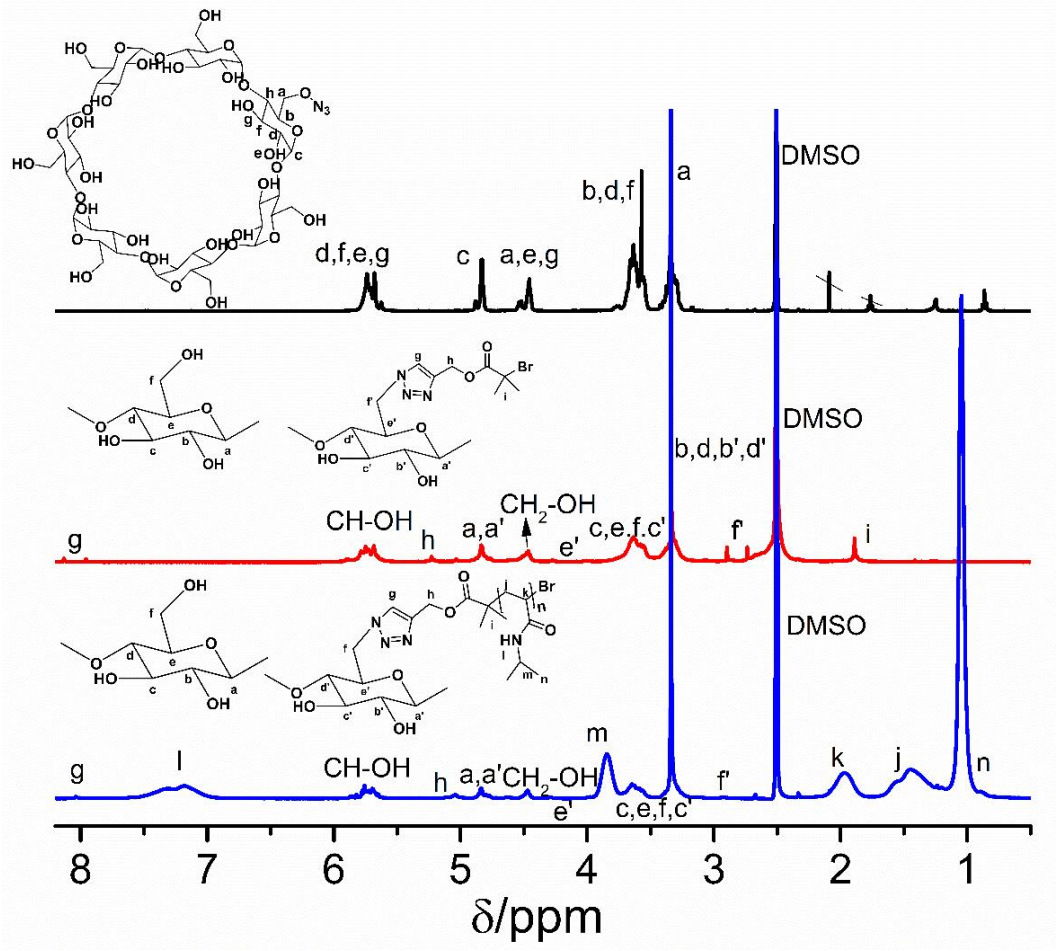

Figure 4.1 ^{1}H NMR spectra of *β*-CD-N_3 (top), *β*-CD-PBM (middle) and *β*-CD-PNIPAAm (bottom) recorded in DMSO-d_6.

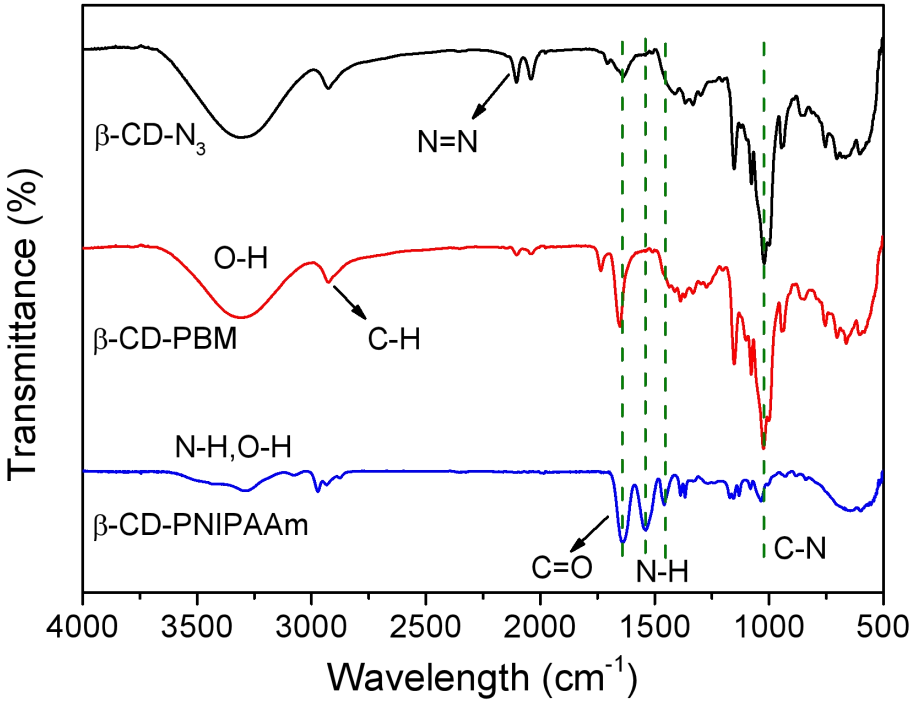

Figure 4.2 FT-IR spectra of β-CD-N3, β-CD-PBM and β-CD-PNIPAAm.

The guest polymer PEG-FS-AZO was synthesized with reference to a previous study.[208] The synthesis process is shown in the Scheme 5.1. The -CH_3 peak at 1.87 ppm and the -CH_2 peak at 3.67 ppm (Figure 6.3.6) indicate the successful preparation of the PEG-Br macromolecular initiator. Subsequently, the ATRP polymerization of FS monomer was initiated by the PEG-Br macromolecular initiator in the presence of HMTETA and CuBr as catalysts. As shown in the ^{1}H NMR spectra (Figure 6.3.7), the -CH, -CH_2 proton signal peaks of the FS repeating unit appeared at 2.16-2.46 ppm and 1.75-2.07 ppm, which indicated the successful obtaining of the target polymer PEG-FS-Br. This result was also confirmed by the ^{19}F NMR spectra. The characteristic peaks of pentafluorostyrene appeared at -137.8, -148.2, and -160.2 ppm, as shown in the Figure 6.3.8. The absorption peak at 1517 cm^{-1} in the IR spectrum is attributed to the aromatic C-F of FS repeating unit in the polymer.

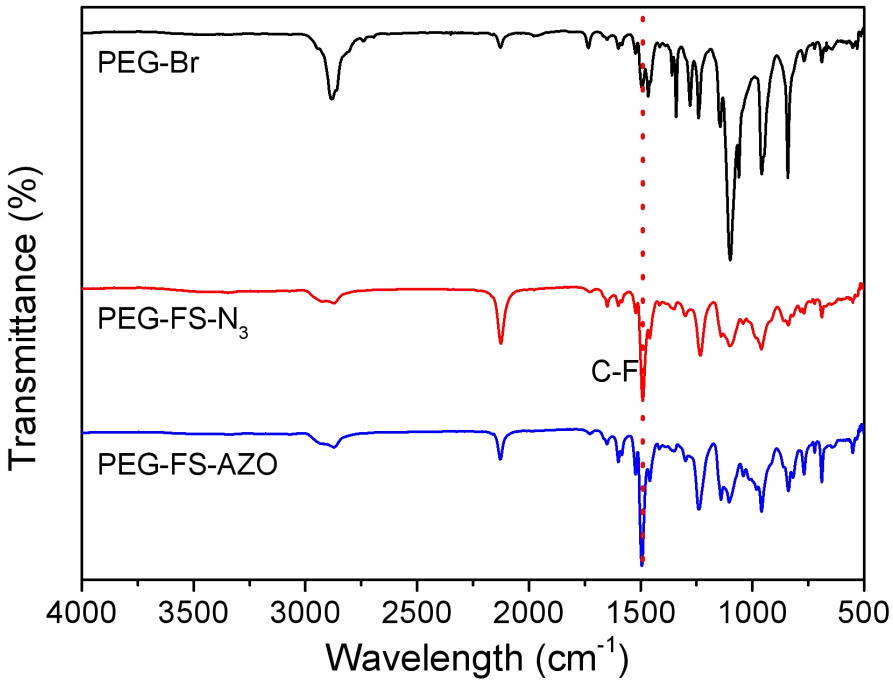

Figure 4.3 FT-IR spectra of PEG-Br, PEG-FA-N_3 and PEG-FS-AZO.

In a next step, a polymer end-group azide modification reaction was carried out. The appearance of azide characteristic peak around 2100 cm^{-1} in FT-IR (Figure 4.3) indicated the successful azide reaction between PEG-FS-Br and NaN_3.

Subsequently, the above obtained polymer with the azide end group and the terminal alkyne azobenzene underwent a click reaction. The synthesis of terminal alkynes of azobenzene is shown in Scheme 6.3.10. The proton signal of the terminal alkyne -CH appears at 2.48 ppm, and all other proton signals have been marked in the spectra for attribution, which proves the successful synthesis of alkyne-azobenzene. PMDETA and CuBr were used as catalysts in the click reaction. As shown in the ^1H NMR spectra, the new peaks appeared at 7.67-7.9 ppm and 7.28-7.5 ppm, corresponding to the H signals of azobenzene, indicated that the goal product PEG-FS-AZO was successfully obtained (Figure 4.4). The degree of polymerization of PEG-FS-Br was calculated to be around 32 by comparing the integration area ratio of the FS repeat unit -CH peak at 1.75-2.07 ppm to the -CH_3 peak at 2.29 ppm, giving the polymer an

experimental number average molecular weight ($M_{n,\ NMR}$) of roughly 9200 g mol^{-1}. However, the values determined by GPC is 12500 g mol^{-1}, which is a little higher than the $M_{n,\ NMR}$. This discrepancy is probably ascribed to the large hydrodynamic volumes of the guest polymer or the mass loss during preparation and post-treatment. It is encouraging to see that the PEG-FS-Br polymer has a nearly central distribution and a low Đ of 1.05.

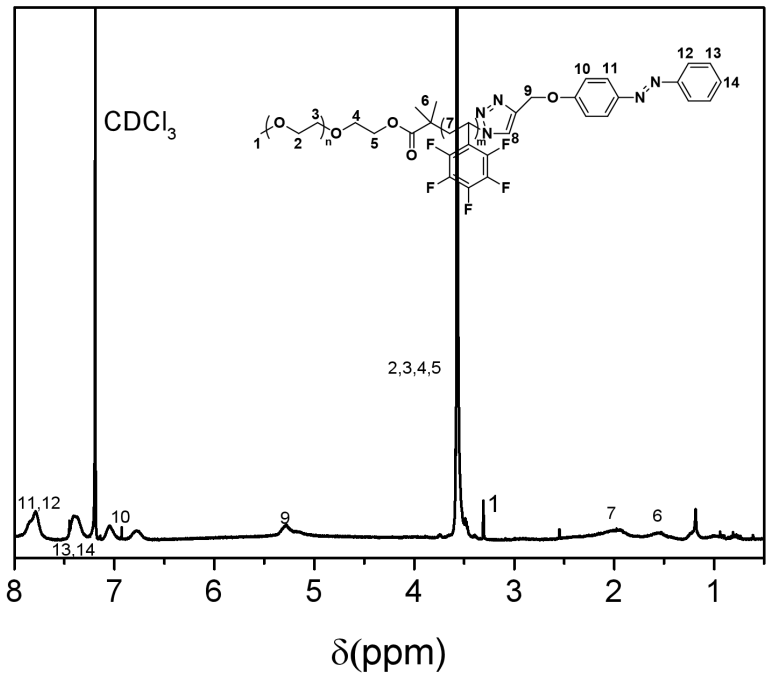

Figure 4.4 ^{1}H NMR spectra (400 MHz) of PEG-FS-AZO $CDCl_3$.

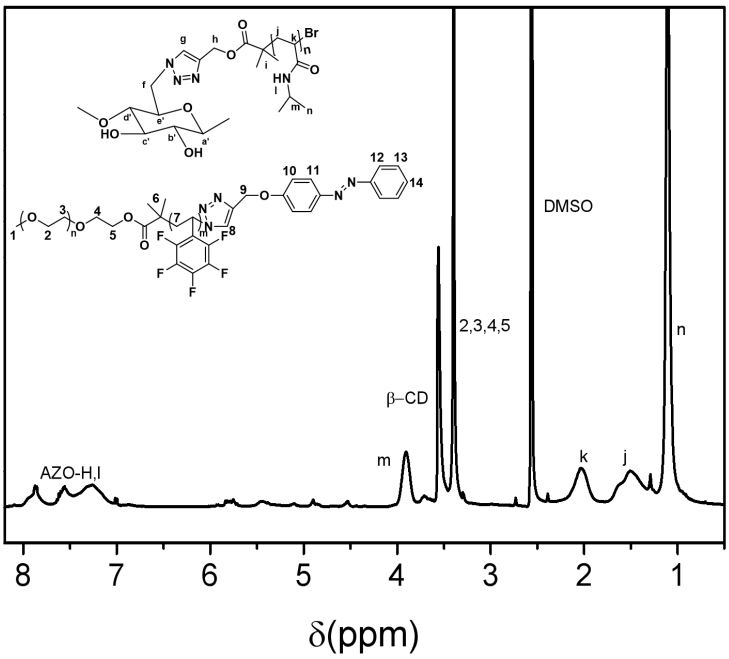

Figure 4.5 [1]H NMR spectra of *β*-CD-PNIPAAm@PEG-FS-AZO supramolecular micelles.

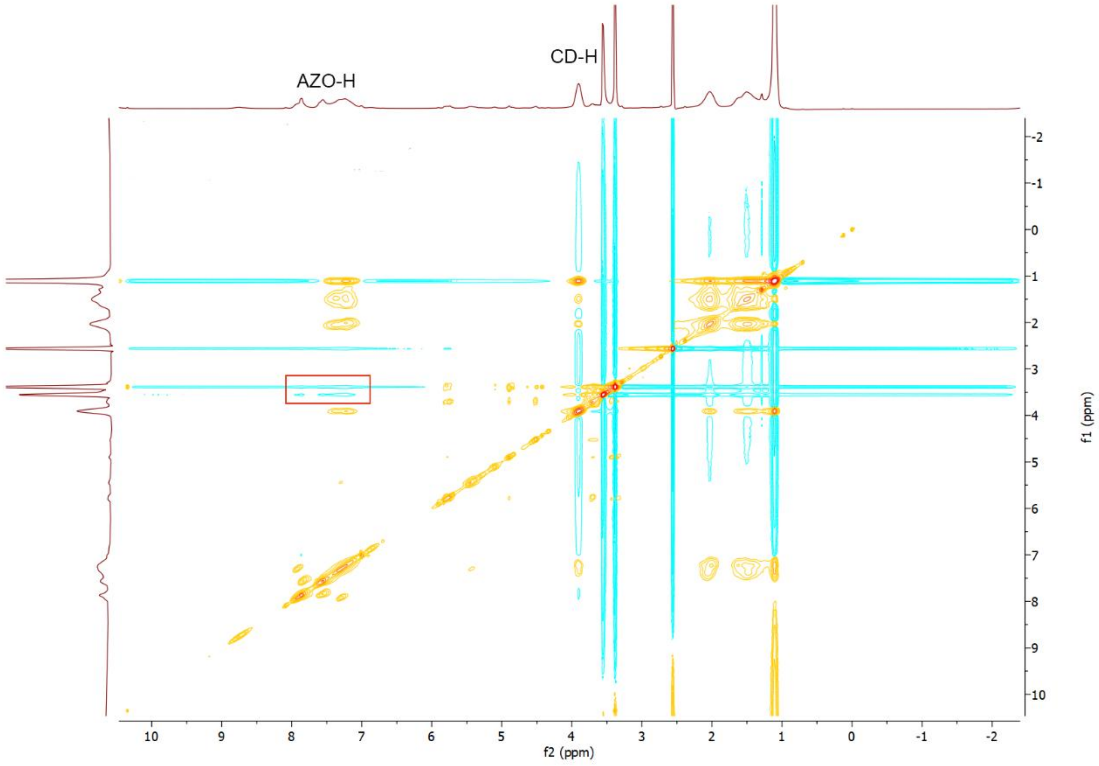

Figure 4.6 2D NOESY [1]H NMR spectra of *β*-CD-PNIPAAm@PEG-FS-AZO supramolecular micelles.

As shown in Figure 4.6, the host-guest complexation between *β*-CD and the azobenzene moiety has been demonstrated by 2D NOESY ^{1}H NMR. It is obviously that the proton signals of *β*-CD at 3.46-3.6 ppm are associated with the azobenzene proton signal at 7-8.01 ppm, producing some cross peaks (red boxes in the Figure). This indicated that *β*-CD can interact with azobenzene molecules to form a host-guest complexation system, and the azobenzene-containing PEG-FS-AZO was entrapped in the lumen of *β*-CD. The ^{1}H NMR also supported this outcome (Figure 4.5). Both azobenzene (7-8.01 ppm) and cyclodextrin protons (3.46-3.6 ppm) are visible. Therefore, the *β*-CD-PNIPAAm@PEG-FS-AZO supramolecular was obtained.

Azobenzene-containing supramolecules display a photosensitivity. Further research on the supramolecular polymer solution's light response was conducted using a UV-Vis spectrophotometer. The UV-Vis spectra of the guest polymer PEG-FS-AZO dispersed in DMF are shown in Figure 5.7 under UV (365 nm) and visible light (450 nm) irradiation at different times. The π-π* transition of trans-azobenzene and the π-π* transition of cis-azobenzene are considered to be responsible for the characteristic absorption peaks at 350 and 440 nm, respectively. Apparently, the absorbance of azobenzene at 350 nm decreased significantly with increasing UV irradiation time, while the absorbance at 440 nm increased slightly, indicating that azobenzene changes from trans to cis conformation under UV irradiation. In contrast, the absorbance of azobenzene at 350 nm increased rapidly with increasing visible light time, indicating that azobenzene reversibly shifts from the cis- to the trans- configuration under visible light irradiation. As shown in Figure 4.7 (a, b), the absorbance of PEG-FS-AZO at 350 nm rapidly increased to its original intensity in just 10 seconds under visible light irradiation, demonstrating the extremely quick photo-responsive cis-trans conversion. Consequently, under alternating UV and visible light irradiation, supramolecular self-assemblies containing azobenzene units may be able to reversibly self-assemble/dissociate as a result of the trans-cis and cis-trans isomerization transitions.

Based on this, the host-guest supramolecule's isomerization transition was also studied using the change in absorbance, as illustrated in Figure 4.7 (c, d). The supramolecule's absorbance at 350 nm considerably decreased when the UV exposure duration was extended, and the polymer's azobenzene unit switched from *trans*- to *cis*-. And after only 10 seconds of visible light irradiation, the absorbance of the supramolecule at 350 nm has been enhanced to the original intensity, which means the azobenzene unit switches from *cis*- to *trans*-. Therefore, the produced *β*-CD-PNIPAAm@PEG-FS-AZO complex is photo-responsive since the cis-trans isomerization process of the azobenzene unit can be switched repeatedly under alternating UV and visible light irradiation.

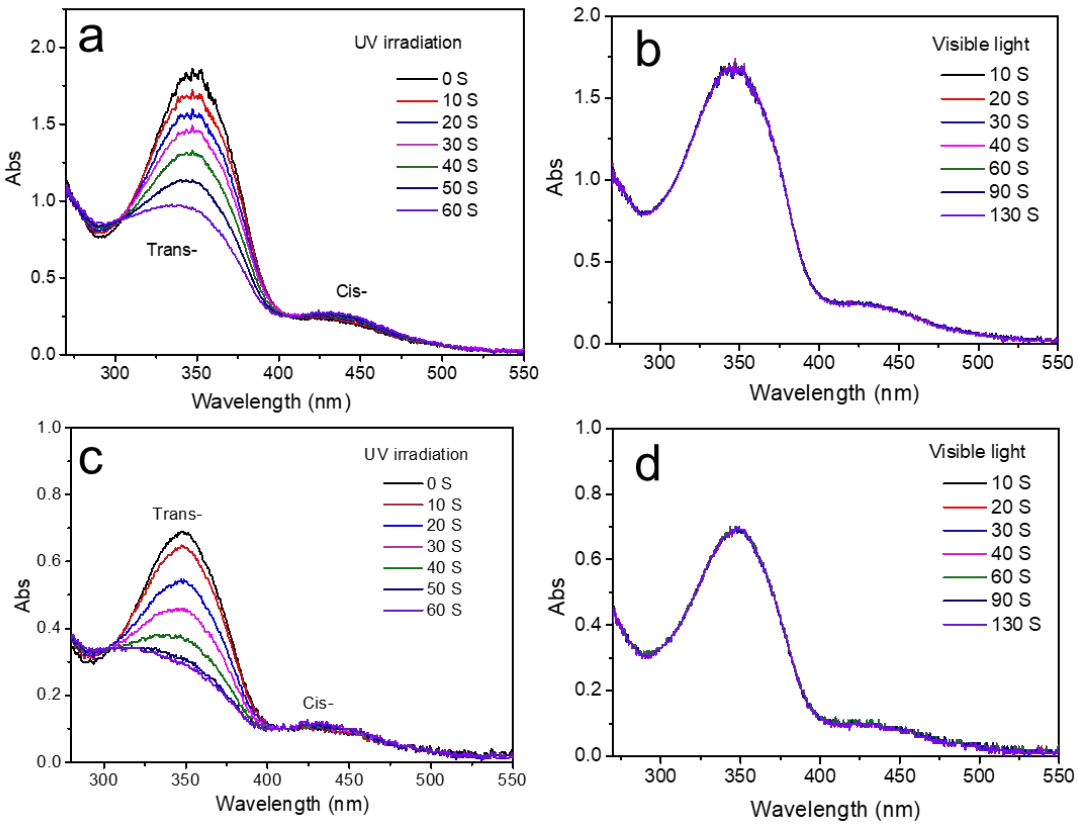

Figure 4.7 UV-Vis spectra of (a and b) PEG-FS-AZO (0.2 mg/mL) and (c and d) supramolecular (0.1 mg/mL) under (a and c) 365 nm UV and (b and d) 450 nm visible irradiation.

Thermally induced hydrophilic-hydrophobic transition based on PNIPAAm in

aqueous solution was studied utilizing self-assembled host-guest complex. The low critical solution temperature (LCST) of *β*-CD-PNIPAAm and host-guest complex was determined by turbidity measurements using UV-visible spectrophotometry. The transmittance vs temperature for *β*-CD-PNIPAAm and host-guest complex is plotted in Figure 4.8. Both polymers showed a clear thermally induced phase transition. The 50% transmittance points of the *β*-CD-PNIPAAm and host-guest complex were at 39.6 ℃ and 40.2 ℃, respectively. The higher LCST value of *β*-CD-PNIPAAm compared to the pure PNIPAAm polymer (~ 32 ℃) should be attributed to the presence of the hydrophilic *β*-CD terminal fraction. The complex also exhibits similar temperature phase transition properties, with a slightly higher LCST temperature compared to *β*-CD-PNIPAAm. This may be due to the presence of the hydrophilic macromolecule PEG. As a result, the produced complex exhibits a reversible temperature phase behavior, switching from hydrophilic to hydrophobic with increasing temperature leading to the dissociation of the complex.

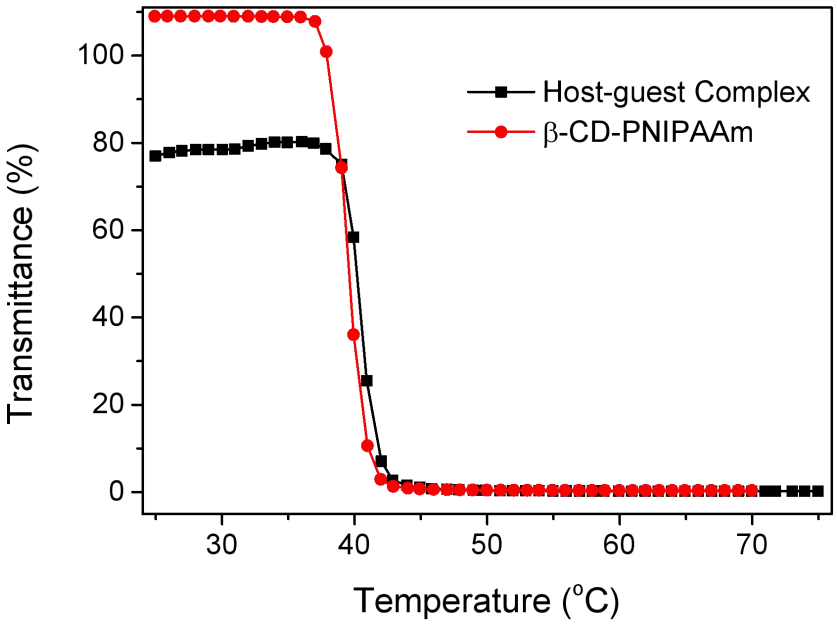

Figure 4.8 Transmittance as a function of temperature for an aqueous solution of *β*-CD-PNIPAAm and host-guest complex.

The O_2 responsiveness of the host-guest complex was studied by UV-visible spectrophotometry to investigate the change in hydrophilicity before and after the exposure to oxygen. As can be seen in Figure 5.9, the transmittance of the complex increased from 90% to 100% at room temperature after the injection of oxygen, indicating an increase in the hydrophilicity of the complex. The 50% transmittance points were 45.9 ℃ and 46.7 ℃ before and after oxygen injection, respectively. FS becomes more soluble, increasing the hydrophilicity of the complex, as a result of the interaction between the fluorine atoms and the dissolved O_2 molecules in solution. It means ΔT induced by oxygen was 0.8 ℃. ΔT is not large probably due to the fact that there are too many FS repeating units, or the hydrophobicity of FS is too strong. It is evident from the above that the host-guest complex is O_2-responsive, which is achieved by the oxygen-induced hydrophilic/hydrophobic conversion of the guest polymer, thus controlling the self-assembly/dissociation of the complex.

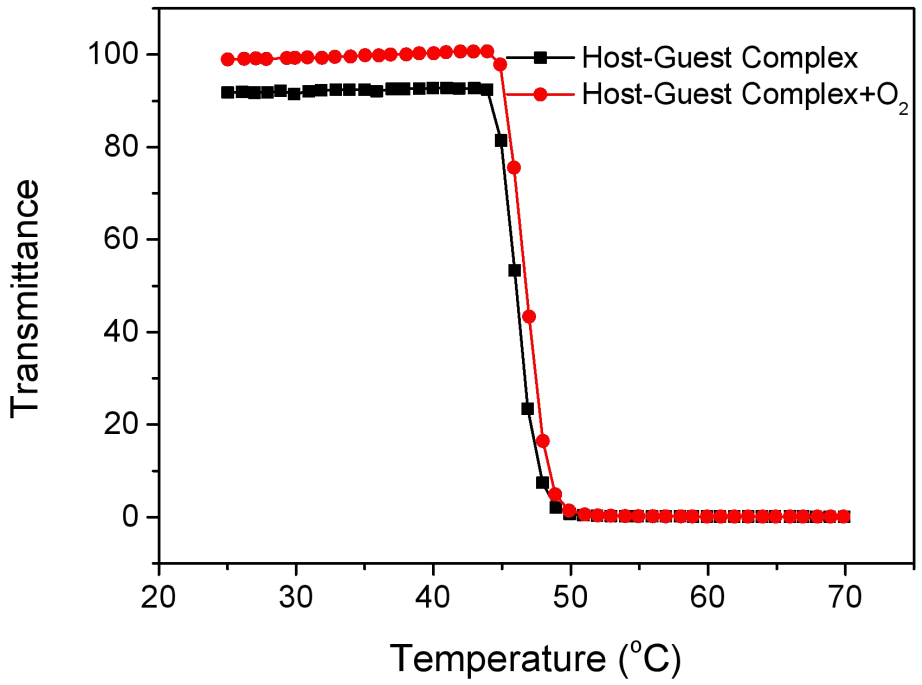

Figure 4.9 Transmittance as a function of temperature for an aqueous solution of host-guest complex and host-guest complex after exposure to O_2.

4.3 Conclusion

In summary, well-defined β-CD-terminated PNIPAAm (β-CD-PNIPAAm) was synthesized by a combination of atom transfer radical polymerization (ATRP) and click reaction. In addition, PEG-FS-AZO with azobenzene capped end groups was synthesized by ATRP and click reaction using PEG initiator and FS monomer. Subsequently, a novel β-CD-PNIPAAm@PEG-FS-AZO complex was designed and synthesized by host-guest interactions between β-CD and azobenzene, which was confirmed by FT-IR, (2D NOESY)^{1}H NMR, etc. The obtained complexes are triple responsive to light, oxygen and temperature. It undergoes reversible self-assembly and dissociation under alternating UV and visible light irradiation, oxygen influx/removal, and temperature increase/decrease. Therefore, this strategy holds promise for future use as a controlled drug delivery system.

5 Conclusion and Outlook

In this thesis, three different responsive materials were successfully prepared based on the temperature responsive polymer PNIPAAm.

First, the novel light-driven purification hydrogel (PNIPAAm-PVA-PDA) was successfully fabricated. It is achieved by incorporating PVA into a conventional PNIPAAm network to obtain a PVA/PNIPAAm semi-IPN hydrogel and then depositing PDA on it. Subsequently, a hydrogel (micro-PNIPAAm-GO) similar to the one above was prepared. This hydrogel is based on the photothermal material graphene oxide and the temperature responsive polymer PNIPAAm. Due to the presence of GO, this hydrogel has a unique three-dimensional network structure, which is shown in the SEM. The composition of the hydrogels was confirmed by FT-IR and LCST was confirmed by DSC. Under NIR irradiation with a wavelength of 850 nm, the hydrogels' surface temperature can increase to LCST, and changed from hydrophilic to hydrophobic while releasing pure water. Both the de-swelling and re-swelling kinetic curves of the hydrogels showed the good reusability. Oil-water mixtures, dye-contaminated water and heavy metal-contaminated water have been used to test the purification capacity of hydrogels. Both hydrogels have better adsorption for Pb^{2+} compared to Pd^{2+}. PNIPAAm-PVA-PDA hydrogel has higher adsorption for Pd^{2+} compared to micro-PNIPAAn-GO hydrogel, while micro-PNIPAAm-GO hydrogel has higher adsorption for Pb^{2+} than PNIPAAm-PVA-PDA hydrogel. All the generated water has very low concentration of heavy metal ions, especially the Pb^{2+} concentration is already below the minimum detection range of the instrument. Compared to the earlier evaporation-cleaning hydrogels, this novel method for purifying existing wastewater has the advantages of being more practical, quicker, and more potent.

Afterwards, β-CD-PNIPAAm@PEG-FS-AZO complex was designed and synthesized by host-guest interaction between β-CD and azobenzene and confirmed by FT-IR, (2D

NOESY) ^{1}H NMR, etc. The host polymer in the complex, β-CD-PNIPAM, was synthesized by atom transfer radical polymerization (ATRP) and click reaction. The guest polymer PEG-FS-AZO was synthesized by ATRP and click reaction using a PEG initiator and FS monomer. The obtained complex showed a triple response to light, oxygen and temperature and then the responsiveness was further investigated by UV-visible spectrophotometry. This work provides a new method for the synthesis of multi-responsive polymers, and this method is expected to be used in the future as a controlled drug delivery system.

In a summary, this thesis provides a variety of synthetic methods for the preparation of novel dual or multi-responsive polymers, and they are briefly explored and investigated.

6. Experimental section

6.1 Materials

Dopamine hydrochloride, *N*-isopropylacrylamide (NIPAAm) were purchased from TCI and employed without further purification. Amino-2-(hydroxymethyl)-1,3-propanediol (tris-base), *N,N′*-methylenebisacrylamide (MBA), PVA (average mol. wt. 89,000–98,000, 99% hydrolyzed), ammonium persulfate (APS), potassium persulfate (KPS, $K_2S_2O_8$), *N,N,N′,N′*-tetramethyl-ethylenediamine (TEMED), sodium dodecyl sulfate (SDS), hydrochloric acid (HCl)(37%), graphite powder, Yeast, Palladium (II) acetate ($Pd(OAc)_2$), Rhodamine 6G (R6G) and sulfuric acid(H_2SO_4), sodium nitrate($NaNO_3$), potassium permanganate($KMnO_4$), hydrogen peroxide(H_2O_2) are commercially available from Sigma–Aldrich and employed without further purification. Lead (II) acetate trihydrate (Pb $(CH_3CO_2)_2 \cdot 3H_2O$) was purchased from VWR and employed without further purification.

β-Cyclodextrin (*β*-CD, 99%), 2-Bromoisobutyryl bromide (BIBB, 98%), tris(2-(dimethylamino)ethyl)amine (Me_6TREN, > 98%), cuprous bromide (CuBr, 98%), 4-(phenyldiazenyl) phenol (Azo, 98%), potassium carbonate (K_2CO_3), triethylamine (TEA, 99%), monomethoxy poly ethylene glycol (MPEG; M_n = 3000), sodium azide (NaN_3; 99%), *N,N,N,N′,N′*-pentamethyldiethylenetriamine (PMDETA; 97%), 1,1,4,7,10,10-hexamethyltriethylenetetramine (HMTETA; 97%), 2,3,4,5,6-pentafluorostyrene (FS, 99%) were purchased from Sigma- Aldrich and used without further purification.

6.2 The characterization techniques

6.2.1 Nuclear Magnetic Resonance Spectroscopy (NMR)

Nuclear magnetic resonance (NMR) spectroscopy is a technique used in analytical chemistry for research and quality control to determine sample content, purity and molecular structure. It is based on the study of the interaction of radiofrequency electromagnetic radiation with the molecular nuclei of a sample coming from a strong magnetic field. In a standard NMR test, the sample to be tested is placed in a magnetic field and then excited with an RF pulse that causes the nuclei of the sample to resonate with the magnetic field, causing the nuclei to flip to a higher energy arrangement. When the nuclei return to their original state, a time-domain RF signal called the free induction decay (FID) signal is emitted. The FID signal is converted to a frequency domain signal through a Fourier transform to obtain a nuclear magnetic resonance spectrogram. Attributed to the intramolecular magnetic field, the resonant frequencies of the molecular atoms are variable and therefore represent the individual functional groups of the molecule and their electronic structure.

In this thesis, all ^{1}H NMR and ^{19}F NMR spectroscopy were performed at 298 K using Bruker Ascend 400 spectrometer (^{1}H NMR 400 MHz, ^{19}F NMR 376 MHz). The NOESY ^{1}H NMR was measured using a Bruker Ascend 600 spectrometer.

6.2.2 Gel Permeation Chromatography (GPC)

Gel permeation chromatography (GPC) is a size-exclusion chromatography method commonly used for polymer analysis. It is based on the separation of polymers according to their size (i.e., hydrodynamic volume) by using a column filled with porous beads. During a typical GPC measurement, molecules pass through the column by an elution rinse. Smaller analytes enter most of the pores before passing further through and therefore require more time for elution. In contrast, larger size

analytes will elute directly from the column, thereby reducing elution time. The molecular weight and dispersion can be obtained by comparing the retention time of the analytes with the calibration curve of the polymer standard.

6.2.3 Fourier-transformation Infrared Spectroscopy (FT-IR)

In chapter 3, hydrogels swelled to equilibrium at room temperature were freeze-dried to completely remove any water. After drying, the FTIR spectra of the dried-hydrogel was conducted by the attenuated total reflectance infrared spectroscopy (ATR-IR, Smart iTR) unit on a Bruker VERTEX 80 V FT-IR spectrometer in the range of 600–4000 cm^{-1} at ambient temperature.

6.2.4 Scanning Electron Microscopy (SEM)

The scanning electron microscope (SEM) is one of the most commonly used electron microscopes to study the surface morphology and composition of a sample. Typically, for a SEM measurement, an electron beam is emitted from the thermal ion of an electron gun and accelerated by an applied voltage of up to 30 kV. The electron beam is then focused through a combination of lenses to a spot of approximately 0.4 nm to 5 nm in diameter. The electron beam is shot into the sample surface after passing through a scanning coil. As a result of the electron-sample interaction, secondary electrons (low energy), backscattered electrons (high energy) and characteristic X-rays are produced. These signals can be collected by various detectors. Backscatter detectors collect backscattered electrons from electrons reflected from the sample surface and deeper and provide images that convey information about the sample composition as well as the sample's morphology, crystallography and magnetic field. The secondary electron detector collects secondary electrons produced by the interaction of the primary beam with the sample and further integrates them into an image of the surface topography on the screen. The X-ray detector collects X-rays generated by the absorbed electrons. Due to the element-specific emission of the

X-rays, the elemental composition of the sample can then be obtained.

In chapter 3, the morphologies of the hydrogels were characterized by scanning electron microscope (SEM, LEO 1530 Gemini with Schottky field emitter).

6.2.5 Differential scanning calorimetry (DSC)

Differential scanning calorimetry is a thermal analysis technique that measures the heating rate versus temperature required to bring the sample to the same temperature as the reference with the help of a compensator. The basic principle is that as the sample undergoes phase changes, glass transition and chemical reactions, it absorbs and releases heat, and the compensator measures how the heat flow can be increased or decreased to keep the sample and reference at the same temperature.

In chapter 3, the Lower critical solution temperature (LCST) behavior of the hydrogels was determined using a Differential scanning calorimeter (DSC, DSC Q200 TA Instruments). Before DSC measurement, the samples were equilibrated in deionized water at room temperature, and excess surface water should be removed with filter paper. The thermal analysis was performed at a heating rate of 5 °C/min from 0 to 50 ℃ under a dry N_2 atmosphere.

6.2.6 Optical Microscopy

The optical images of emulsions and eluates were recorded from Keyence biorevo microscope.

6.2.7 Contact Angle (WCA)

In chapter 3, Water contact angle was measured on the KRÜSS model DSA25S Drop Shape Analyzer.

6.2.8 Ultraviolet-visible (UV-vis) Spectrophotometer

UV-Visible spectrophotometer is an analytical instrument based on the principle of UV-Visible spectrophotometry, which uses the radiation absorption of material molecules in the UV-Visible spectral region to perform analysis. It is mainly composed of light source, monochromator, absorption cell, detector and signal processor and other components.

In chapter 3, the UV-vis spectra were measured on an Ocean optics spectrometer at ambient temperature.

In chapter 4, the UV-vis spectra were measured on a Perkin Elmer Lambda 35 UV-vis spectrometer with Peltier system.

6.2.9 Inductively Coupled Plasma Optical Emission Spectrometry (ICP-OES)

Inductively coupled plasma and optical emission spectrometry (ICP-OES) is ais a potent, adaptable, and sophisticated analytical method for the quick and sensitive identification of elements in various materials. It is based on the spontaneous emission of photons produced by ions or atoms that are excited by a radio frequency discharge. In the specific operation, the sample is first introduced into an inductively coupled argon plasma, where it is atomized and ionized and eventually excited. When the electrons return from the excited energy level to a lower energy level, the ions and atoms emit photons, which are referred to as ion or atomic emission. The emitted photons are then collected into a detector using an Eicher or Rolland ring optic, at which point the different emission wavelengths are separated from each other. The element concentration is later determined by measuring the intensity of the emission signal at the respective wavelength by the detector, as the intensity of the emission signal is proportional to the concentration of the element in the plasma.[211]

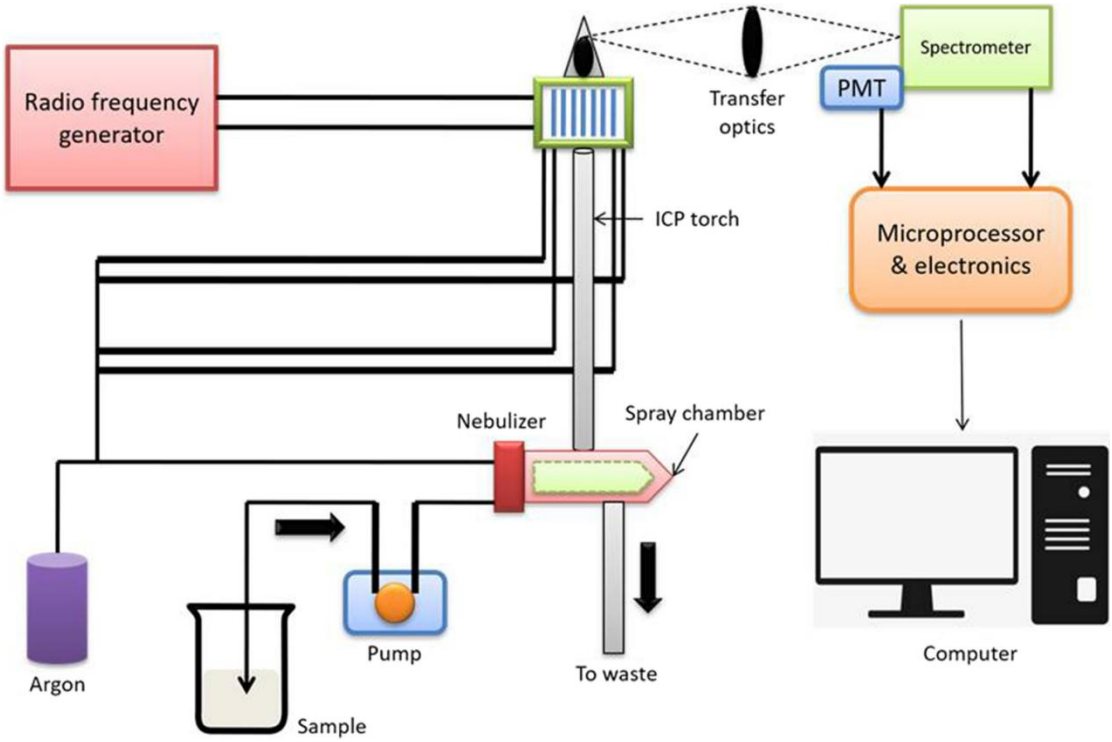

Figure 6.2.1 Instrumentation of ICP-OES. Reprinted with permission from Ref.[211], copyright (2022) Springer Nature.

The heavy metal ion solutions in Chapters 3 were measured on an iCAP 7600 DUO, Thermo-Fisher-Scientific. The aqueous solution of palladium ions was added with 5% hydrogen chloride before the measurement.

6.3 Experimental Procedures

6.3.1 Synthesis of Graphene oxide (GO)

Graphene oxide (GO) was prepared from graphite by the Hummers method. [212] The concentrated H_2SO_4 (69 mL) was added to a mixture of graphite (3.0 g) and $NaNO_3$ (1.5 g), and the mixture was cooled to 0 °C. $KMnO_4$ (9.0 g) was added slowly in portions to keep the reaction temperature below 20 °C. The reaction was warmed to 35 °C and stirred for 30 min, at which time water (138 mL) was added slowly, producing a large exotherm to 98 °C. External heating was introduced to maintain the reaction temperature at 98 °C for 15 min, then the heat was removed and the reaction

was cooled using a water bath for 10 min. Additional water (420 mL) and 30% H_2O_2 (3 mL) were added, producing another exotherm. After air cooling, the mixture was purified as described for the GO above (sifting, filtration, multiple washings, centrifugations and decanting, vacuum drying) to give a black solid.

6.3.2 Synthesis of Mono(6-O-(p-tolylsulfonyl))-*β*-cyclodextrin (*β*-CD-OTs)

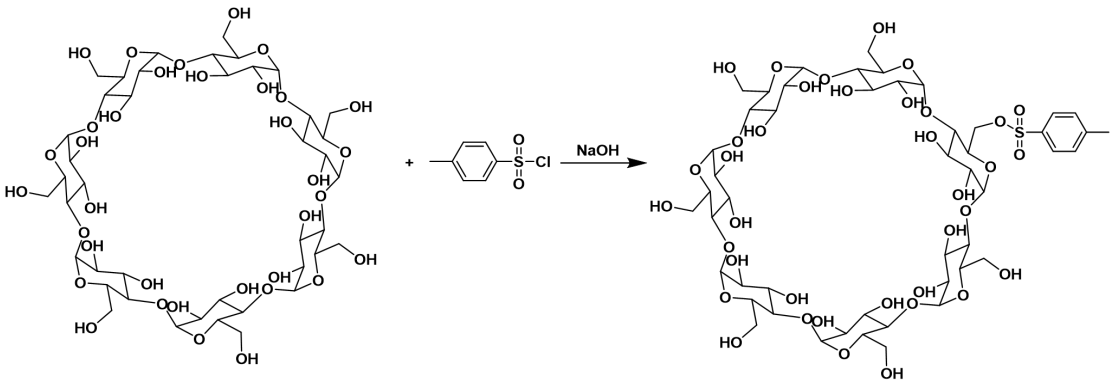

Scheme 6.3.1 The synthesis route of Mono(6-O-(p-tolylsulfonyl))-*β*-cyclodextrin (β-CD-OTs).

β-CD (17.0 g, 15.0 mmol) was dissolved in 200mL aqueous solution of sodium hydroxide (0.4 M) and cooled down to 0 ℃. Subsequently, *p*-toluenesulfonyl chloride (12.0 g, 63 mmol) was added to the solution in small portions over 5 min while vigorously stirring. The resultant suspension was promptly filtered out after being agitated for further 30 min below 5 ℃. The filtrate was neutralized with hydrochloric acid and stirred for 1 h. The resultant precipitate was filtered off, washed three times with water and dried overnight at 60 ℃. The product was kept in a desiccator with phosphorus pentoxide to further dry it off (5.07 g, yield 26%).

^{1}H NMR (DMSO-d_6, δ in ppm): 2.43 (3H, -CH_3); 3.17-3.74 (42H, repeat units from *β*-CD);4.40-4.61 (6H, -OH); 4.74-4.9 (7H, -OH); 5.61-5.86 (7H, -OH); 7.43 (d, 2H,

Ar-H); 7.75 (d, 2H, Ar-H).

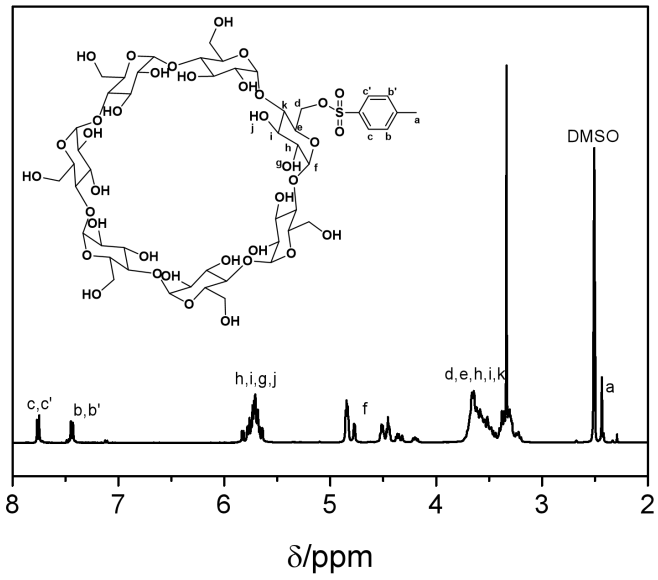

Figure 6.3.1 ^{1}H NMR spectra (400 MHz) of Mono(6-O-(p-tolylsulfonyl))-*β*-cyclodextrin (*β*-CD-OTs) DMSO-d_6.

6.3.3 Synthesis of Mono(6-azido-6-desoxy)-*β*-cyclodextrin (*β*-CD-N_3)

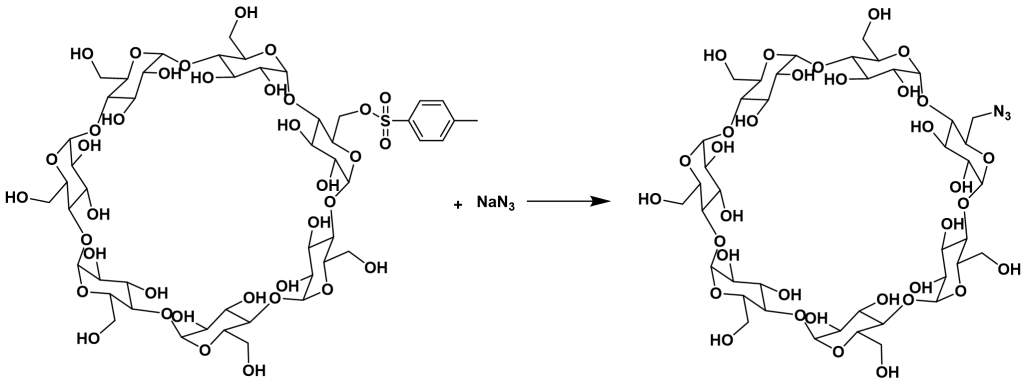

Scheme 6.3.2 The synthesis route of Mono(6-azido-6-desoxy)-*β*-cyclodextrin (*β*-CD-N_3).

Mono(6-O-(p-tolylsulfonyl))-*β*-cyclodextrin (2.6 g, 2 mmol) was suspended in 50 mL of water and heated to 80 °C. Afterwards, 0.65 g (10 mmol) of sodium azide was

added to the suspension and the mixture was stirred for 4 h until it became transparent. The solution was precipitated in 200 mL of acetone and then filtered off to obtain the crude product. A white powder was obtained after recrystallization from water/acetone (1.04 g, 45%).

^{1}H NMR (DMSO-d_6, δ in ppm): 3.33 (14H, H-a); 3.5-3.74 (28H, repeat units from *β*-CD); 4.44-4.56 (6H, from *β*-CD); 4.83 (d, 6H, from *β*-CD); 4.9 (d, 1H, H-c); 5.6-5.81 (14H, -OH).

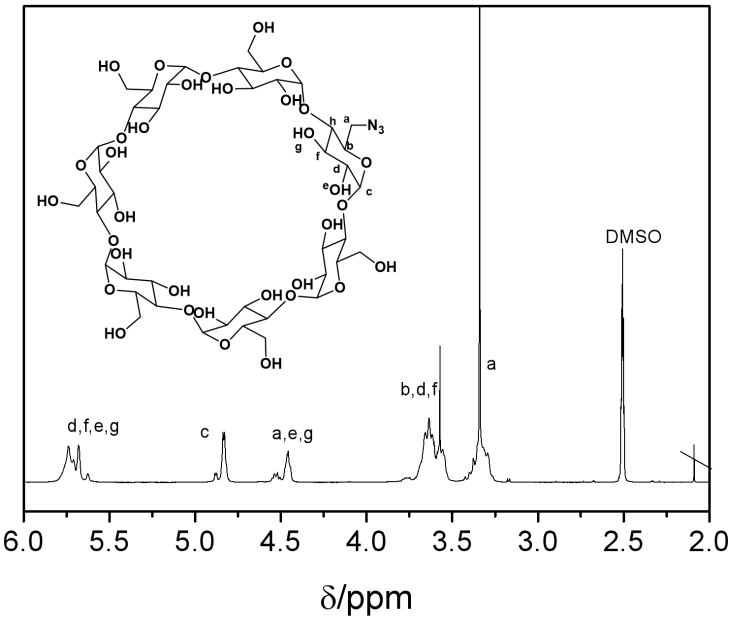

Figure 6.3.2 ^{1}H NMR spectra (400 MHz) of Mono(6-azido-6-desoxy)-*β*-cyclodextrin (*β*-CD-N_3) DMSO-d_6.

6.3.4 Synthesis of prop-2-yn-1-yl 2-bromo-2-methylpropanoate (PBM)

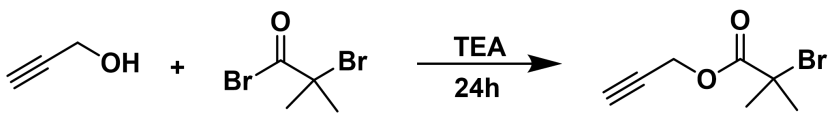

Scheme 6.3.3 The synthesis route of prop-2-yn-1-yl 2-bromo-2-methylpropanoate (PBM).

Propargyl alcohol (1.088 g, 19.4 mmol) and triethylamine (2.064 g, 20.4 mmol) were first dissolved in diethyl ether (50 mL). Then α-bromoisobutyryl bromide (4.692 g, 20.4 mmol) was dropwise added into the above solution at 0 °C. After addition, the reaction mixture was stirred at room temperature for 24 h. The resulting mixture was washed with water and brine for three times and the organic phase was dried over sodium sulfate anhydrous (Na_2SO_4). The obtained solution was concentrated and the crude product was purified via silica chromatography column (Hexane/ethyl acetate = 10:1) to give the product as a colorless liquid (4.51 g, yield 90%).

^{1}H NMR ($CDCl_3$, δ in ppm): 4.7 (d, 2H, H-2), 2.51 (t, 1H, H-1), 1.88 (s, 3H, H-3, 4).

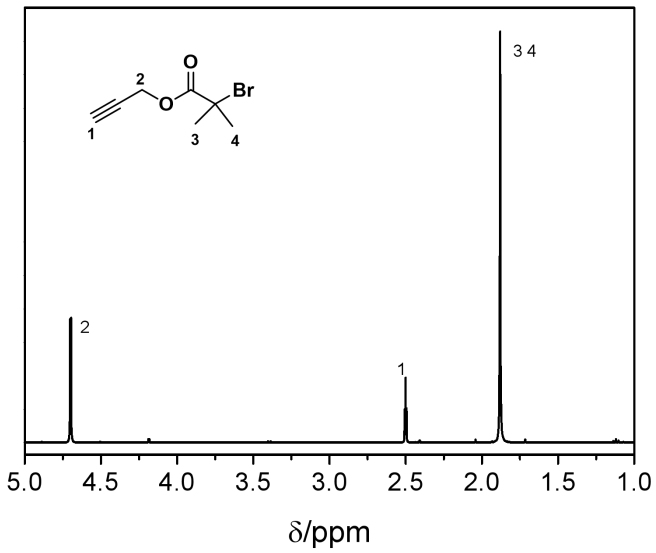

Figure 6.3.3 ^{1}H NMR spectra (400 MHz) of prop-2-yn-1-yl 2-bromo-2-methylpropanoate (PBM) $CDCl_3$.

6.3.5 Synthesis of *β*-CD-PBM

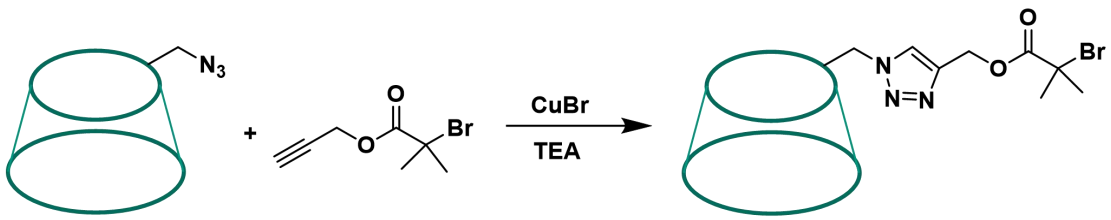

Scheme 6.3.4 The synthesis route of *β*-CD-PBM.

2-Bromoisobutyryl propargyl ester (0.2 g, 0.98 mmol) and copper(I) bromide (31.6 mg, 0.22 mmol) were added to a solution of mono(6-azido-6-desoxy)-*β*-cyclodextrin (0.6 g, 0.52 mmol) (ratio alkyne/azide =1.9: 1) in 30 mL DMF in the presence of nitrogen. Afterwards, Triethylamine (202.4 mg, 2.0 mmol) was added and the mixture was allowed to stir under nitrogen atmosphere for 14 h at room temperature. For working up, the mixture was poured into 200 mL of toluene. Then, 100 mL of n-hexane was added, leading to precipitation of the product. The yellowish solid was isolated by filtration and washed several times with diethyl ether (561 mg, yield 80%).

^{1}H NMR (DMSO-d_6, δ in ppm): 1.89 (s, 6H, H-i), 3.08 and 2.88 (m, 2H, H-f′), 3.16−3.46 (H-b, d, b′, d′), 3.46−3.83 (23H, H-c, e, f, c′), 4.00 (t, 1H, H-e′), 4.37−4.58 (6H, CH_2−O*H*), 4.85 (m, 2H, H-f′), 5.02 and 4.69−4.94 (7H, H-a, a′), 5.22 (s, 2H, H-h), 5.54−5.96 (14H, CH−O*H*), 8.12 (s, 1H, H-g).

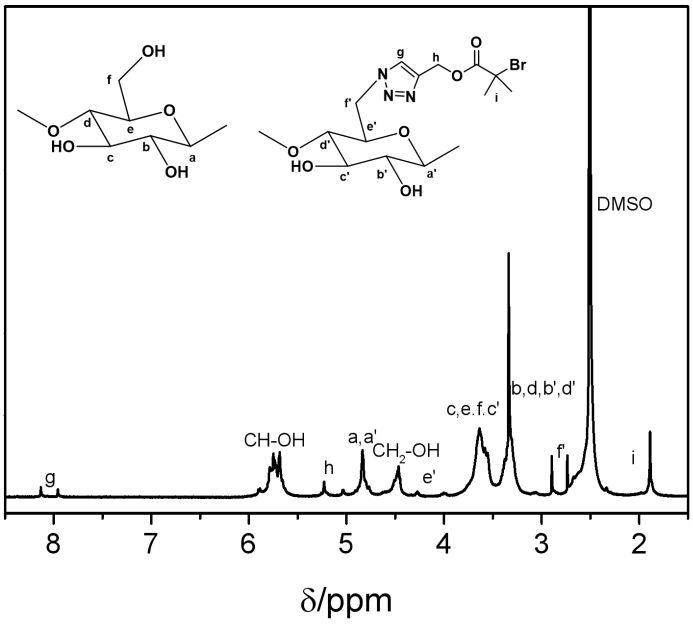

Figure 6.3.4 ^{1}H NMR spectra (400 MHz) of *β*-CD-PBM DMSO-d_6.

6.3.6 Synthesis of *β*-CD-PNIPAAm

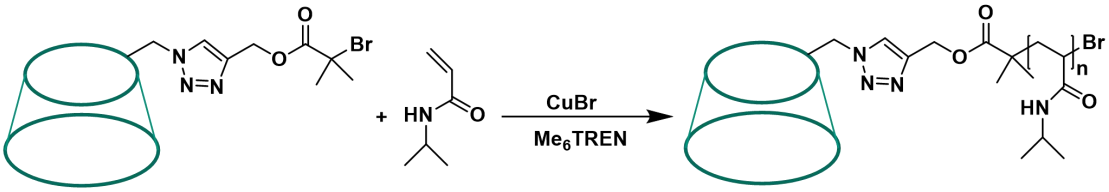

Scheme 6.3.5 The synthesis route of *β*-CD-PNIPAAm.

β-CD-PBM (0.1 g, 0.074 mmol), NIPAAm (0.282 g, 2.5 mmol) and Me_6TREN (0.017 mL, 0.074 mmol) were dissolved in 2 mL mixture of water/DMF (0.1:1.9) in the Schlenk flask. Through four consecutive "freeze-pump-thaw cycles," the solution was degassed. CuBr (7.3 mg, 0.0051 mmol) was then added to the mixture as a catalyst. The liquid was allowed to defrost after another "freeze-pump-thaw cycle" in order to start the room temperature ATRP. The polymerization was stopped after an hour by exposing to air. The mixture was precipitated into an excess of diethyl ether. For the purpose of removing the copper catalysts and small molecule *β*-CD derivatives, the

crude product was dissolved in deionized water and dialyzed against deionized water for two days. Finally, a white powder (120 mg) was obtained by freeze-drying.

^{1}H NMR (DMSO-d_6, δ in ppm): 1.00 (H-n), 1.1−1.66 (H-j), 2.16−1.7 (H-k), 3.03 and 2.85 (H-f′), 3.37−3.65 (H-c, e, f, c′), 3.65−3.89 (H-m), 3.98 (H-e′), 4.3−4.5 (CH_2-O*H*), 4.65−4.82 (H-a, a′), 5.0 (H-h), 5.53−5.84 (CH-O*H*), 6.84−7.5 (H-l), 7.96 (H-g).

GPC: $M_{n,\,GPC}$ = 4.32 ×10^3 g mol^{-1}, M_w/M_n = 1.34.

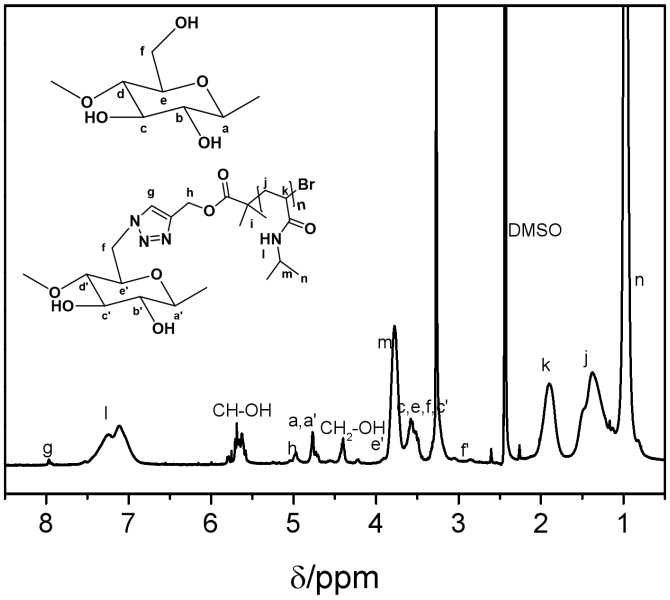

Figure 6.3.5 ^{1}H NMR spectra of *β*-CD-PNIPAAm recorded in DMSO-d_6.

6.3.7 Synthesis of poly (ethylene glycol) methyl ether 2-bromoisobutyrate (PEG-Br) macroinitiator

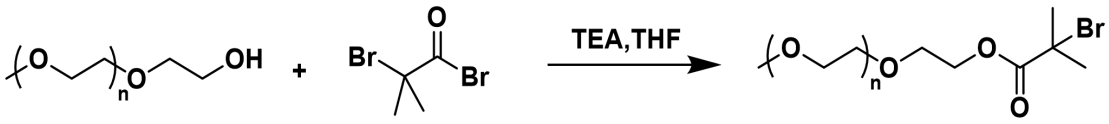

Scheme 6.3.6 The synthesis route of poly (ethylene glycol) methyl ether 2-bromoisobutyrate

(PEG-Br) macroinitiator.

PEG (3 g, 1 mmol) was dissolved in 50 mL of dry THF in the round flask. Trimethylamine (151 mg, 1.5 mmol) was then added into the flask and the mixture was put into an ice bath. Afterwards, the excess BiBB (276 mg, 1.2 mmol) dissolved in 15 mL of dry THF was added dropwise to the solution over 30 min. The reaction was kept overnight at room temperature after stirring for 2 h in the ice bath. The residual THF was extracted from the mixture using rotatory evaporation after it had been filtered. The crude product was dissolved in DCM and washed three times with saturated $NaHCO_3$ and DI water, respectively. The organic phase was collected and dried with anhydrous Na_2SO_4. The concentrated organic phase was precipitated into cold diethyl ether and dissolved in THF for three cycles after the Na_2SO_4 was removed. After drying in the vacuum oven at 30 ℃ for 30 hours, the final product was obtained as a white solid (2.36 g, yield 75%).

^{1}H NMR (400 MHz, δ in ppm): 1.87 (s, 6H, H-6, 7), 3.31 (s, 3H, H-1), 3.58 (H-2, 3), 3.67 (H-4), 4.25 (H-5).

GPC: $M_{n,\,GPC}$ = 3.024 ×10^3 g mol^{-1}, M_w/M_n = 1.02.

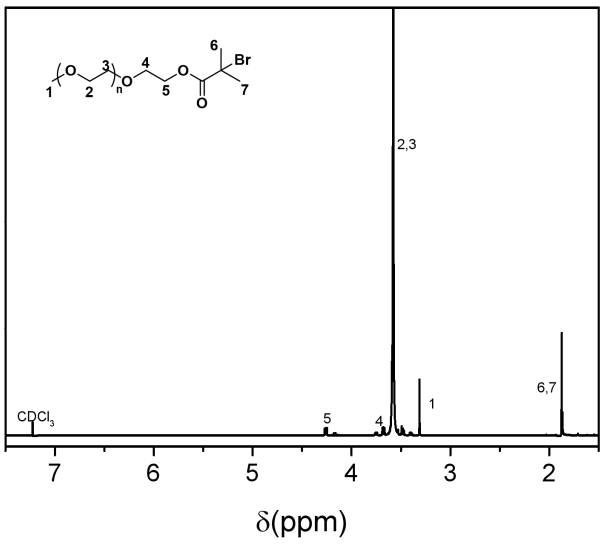

Figure 6.3.6 ^{1}H NMR spectra (400 MHz) of poly (ethylene glycol) methyl ether 2-bromoisobutyrate (PEG-Br) macroinitiator $CDCl_3$.

6.3.8 Synthesis of poly((ethylene glycol)methyl ether)-block-Poly(2,3,4,5,6-pentafluorostyrene) (PEG-FS-Br)

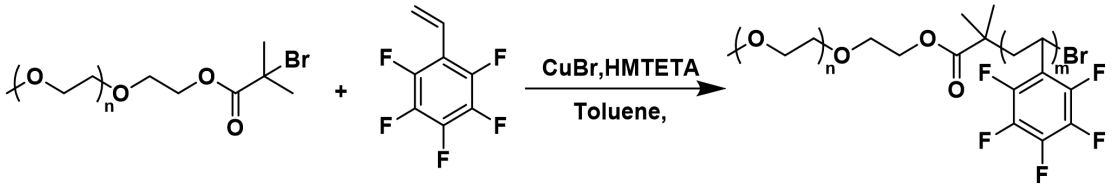

Scheme 6.3.7 The synthesis route of poly((ethylene glycol)methyl ether)-block-Poly(2,3,4,5,6-pentafluorostyrene) (PEG-FS-Br).

The typical ATRP procedure for the synthesis of PEG-FS-Br was as follows. PEG-Br macro-initiator (1.57 g, 0.5 mmol), FS (4.85 g, 25 mmol), HMTETA (115 mg, 0.5 mmol) and anhydrous toluene (2 mL) were added into Schlenk flask and stirred to make a clear solution. Three freeze-pump-thaw nitrogen cycles were performed to remove the oxygen inside. CuBr (71.7 mg, 0.5 mmol) was then added to the flask, followed by another freeze-pump-thaw cycle to remove oxygen in the mixture. The flask was sealed under N_2 atmosphere and kept in the oil bath at 60 ℃.

The reaction was quenched with liquid nitrogen, and then the mixture was diluted by THF and passed through a short neutral Al_2O_3 remove the copper catalyst. The final product was purified by precipitating into cold hexane and dissolving in THF for three times (3.5 g).

^{1}H NMR (400 MHz, δ in ppm): 1.65 (s, 6H, H-6), 1.75-2.07 (H-7), 2.16-2.46 (H-8), 3.31 (s, H-1), 3.58 (H-2, 3, 4, 5).

^{19}F NMR (376 MHz, δ in ppm): -137.8 (F-2), -148.2 (F-1), -160.2 (F-3).

GPC: $M_{n,\,GPC}$ = 1.256 ×10^4 g mol^{-1}, M_w/M_n = 1.05.

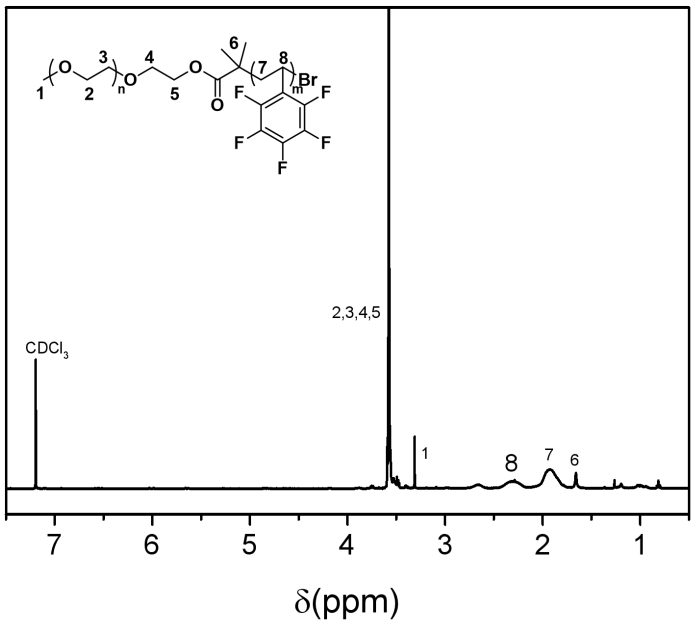

Figure 6.3.7 ^{1}H NMR spectra (400 MHz) of poly((ethylene glycol)methyl ether)-block-Poly(2,3,4,5,6-pentafluorostyrene) (PEG-FS-Br) $CDCl_3$.

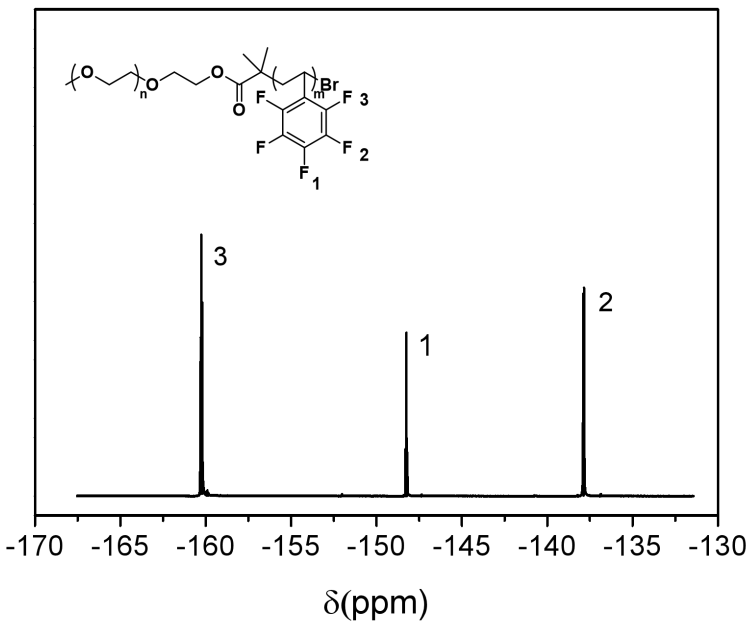

Figure 6.3.8 ^{19}F NMR spectra (376 MHz) of poly((ethylene glycol)methyl ether)-block-

Poly(2,3,4,5,6-pentafluorostyrene) (PEG-FS-Br) $CDCl_3$.

6.3.9 Synthesis of PEG-FS-N_3

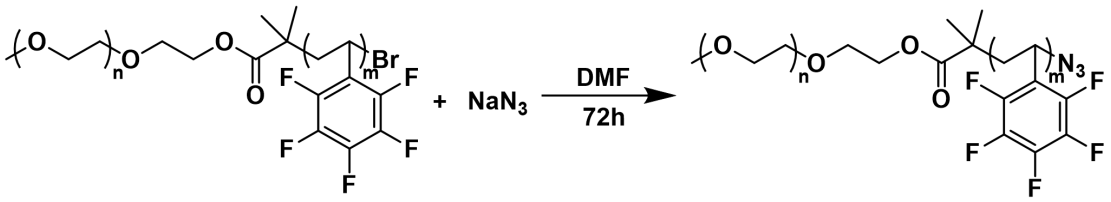

Scheme 6.3.8 The synthesis route of PEG-FS-Br-N_3.

PEG-FS-Br (500 mg, 0.04 mmol) was dissolved in DMF (10 mL) to form a solution. NaN_3 (13 mg, 0.2 mmol) was added and then heated to 80 °C for 10 hours. The mixture was dissolved in deionized water and dialyzed against deionized water for 3 days. Finally, a solid product (336 mg) was obtained by freeze-drying.

^{1}H NMR (400 MHz, δ in ppm): 1.65 (s, 6H, H-6), 1.73-2.1 (H-7), 2.18-2.44 (H-8), 3.3 (s, H-1), 3.58 (H-2, 3, 4, 5).

GPC: $M_{n,\,GPC} = 1.12 \times 10^4$ g mol^{-1}, $M_w/M_n = 1.09$.

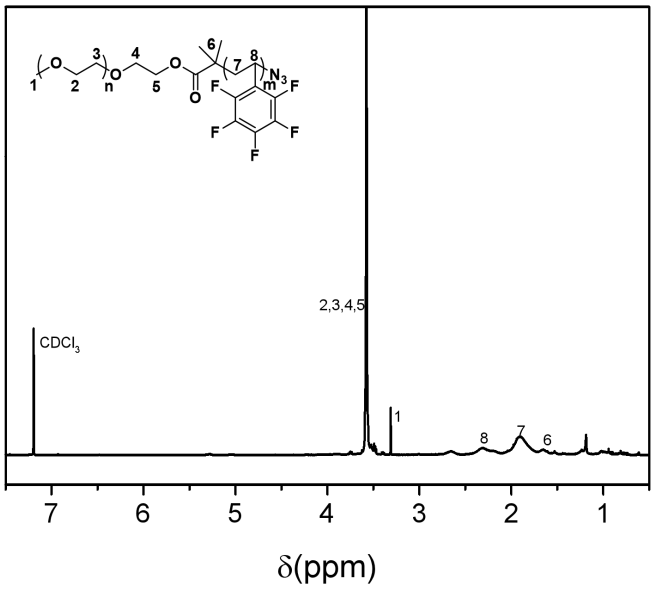

Figure 6.3.9 ^{1}H NMR spectra (400 MHz) of PEG-FS-N_3 $CDCl_3$.

6.3.10 Synthesis of 1-phenyl-2-(4-(prop-2-ynyloxy) phenyl) diazene

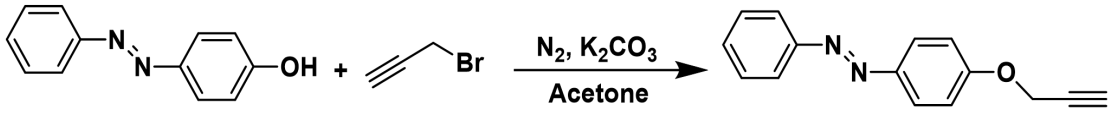

Scheme 6.3.9 The synthesis route of 1-phenyl-2-(4-(prop-2-ynyloxy)phenyl)diazene.

4-(phenyldiazenyl) phenol (5.94 g, 30 mmol) and K_2CO_3 (20.7 g, 150 mmol) were dissolved in anhydrous acetone (100 mL) and stirred at room temperature for 30 min under nitrogen atmosphere. Afterwards, Propargyl bromide (80% w/w in toluene, 17.85 g, 150 mmol) was added and the mixture was stirred at room temperature for 24 h. The solvent was removed by evaporation under vacuum. The product was obtained by purifying the crude product using column chromatography (ether/hexane: 1:1) (6.37 g, yield 90%).

^{1}H NMR (400 MHz, δ in ppm): 7.87 (d, 2H, H-3), 7.81 (d, 2H, H-4), 7.42 (2H, H-5), 7.36 (1H, H-1), 7.03 (2H, H-2), 4.7 (2H, CH_2), 2.48 (1H, C≡C*H*).

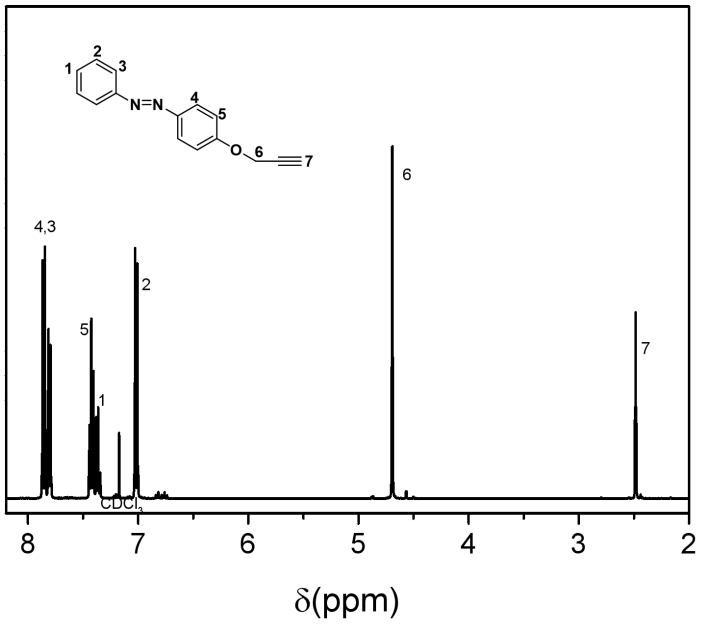

Figure 6.3.10 ^{1}H NMR spectra (400 MHz) of 1-phenyl-2-(4-(prop-2-ynyloxy)phenyl)diazene $CDCl_3$.

6.3.11 Synthesis of PEG-FS-AZO

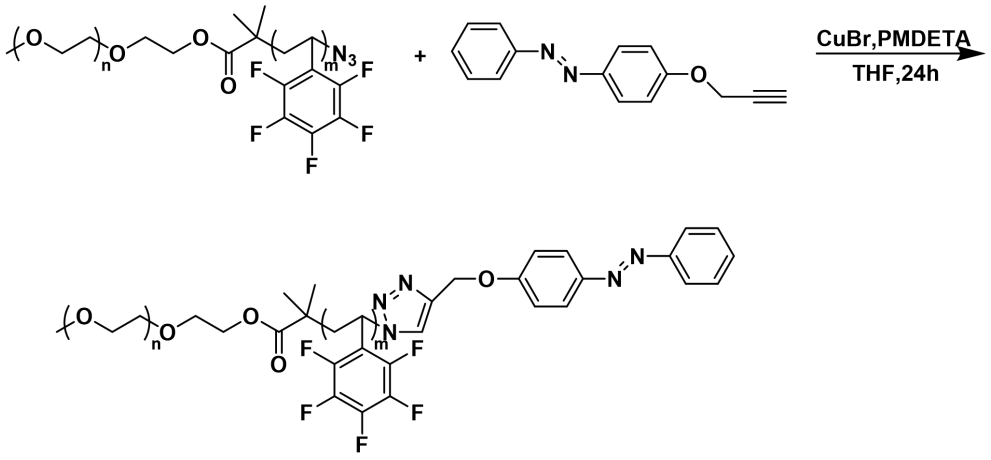

Scheme 6.3.10 The synthesis route of PEG-FS-AZO.

PEG-FS-N_3 (840 mg, 0.075 mmol), 1-phenyl-2-(4-(prop-2-ynyloxy)phenyl)diazene

(35.4 mg, 0.15 mmol), and CuBr (13 mg, 0.09 mmol) were added to a Schlenk flask. PMDETA (16.9 mg, 0.098 mmol) and DMF (5 mL) were added to the mixture under nitrogen atmosphere after one freeze-pump-thaw cycle. The mixture was stirred for 24 hours at room temperature after the flask was degassed for three freeze-pump-thaw cycles. The reaction mixture was then allowed to pass through a basic alumina column. Afterwards, the filtrate was concentrated using a rotary evaporator, precipitated in cold n-hexane and dried in a vacuum oven to obtain the final product as a yellow solid (600 mg).

^{1}H NMR (400 MHz, δ in ppm): 1.56 (s, 6H, H-6), 1.81-2.19 (H-7), 3.3 (3H, H-1), 3.42-3.65 (H-2, 3, 4, 5), 5.28 (s, 2H, H-9), 7.05 (H-10), 7.28-7.5 (3H, H-13, 14), 7.67-7.9 (4H, H-11,12).

GPC: $M_{n,\,GPC}$ = 1.28 ×10^4 g mol^{-1}, M_w/M_n = 1.18

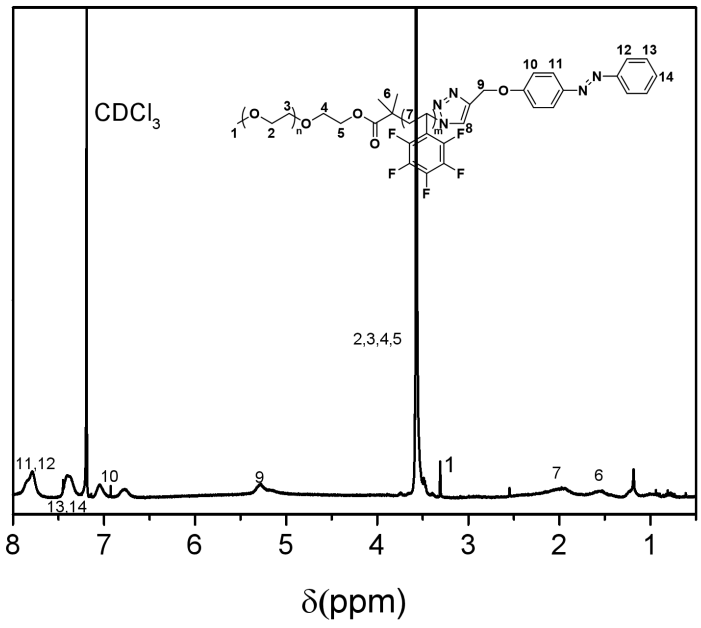

Figure 6.3.11 ^{1}H NMR spectra (400 MHz) of PEG-FS-AZO $CDCl_3$.

6.4 Fabrication Procedures

6.4.1 Preparation of the PNIPAAm-PVA-PDA hydrogel

The preparation of the hydrogel is followed the reported previously.[191,213] Specifically, 8 wt.% NIPAAm aqueous solution, 4 wt.% PVA aqueous solution and 10 wt.% APS aqueous solution were firstly prepared. Then NIPAAm (1 mL), MBA (3.2 mg) and PVA (1 mL) solutions were mixed together. Subsequently, APS (as an initiator, 25 μL) and TEMED (as an accelerator, 30 μL) were added to the mixture. The polymerization and cross-linking were carried out at 5 °C in the fridge for 24 h to obtain the target hydrogel. The obtained hydrogel was taken out and washed in distilled water for 4 days to remove unreacted monomers and other impurities. The water was changed every six hours. For dopamine functionalization on the hydrogel surface, 12.1 g of tris-base and 3 mL HCl were dissolved in 100 mL of water to form 1 M tris-HCl buffer solution. Then dopamine hydrochloride was dissolved in 1 mM tris-HCl buffer solution to obtain dopamine tris-buffer solution (2 mg/mL). The above hydrogel was immersed into 200 mL of dopamine tris-HCl buffer solution. Fresh dopamine tris-buffer was replaced every 6 hours until a dark hydrogel was formed.[206]

6.4.2 Preparation of the micro-PNIPAAm-GO hydrogel

The preparation of the hydrogel followed the reported previously.[214] Specifically, 4.8 mg of KPS initiator was mixed with 4 mL of aqueous solution containing 90 mg of NIPAAm monomer, 5 mg Bis and 21.6 mg SDS at 65 °C for 40 min under magnetic stirring. The PNIPAAm microgels were formed until the transparent solution changed to opaque. Next, the opaque mixture was put in an ice-water bath. 10 mg of GO was added to 1mL of deionized water and sonicated for 1 hour to obtain a black homogeneous solution. Then 0.56 g of NIPAAm and the GO solution were added in the above microgels, followed by addition of 40 μL of TEMED accelerator. The above mixture was sealed at 5 °C overnight, forming a black gel (i.e.,

micro-PNIPAAm-GO hydrogel).

6.4.3 Preparation of *β*-CD-PNIPAAm@PEG-FS-AZO

β-CD-PNIPAAm@PEG-FS-AZO supramolecular assemblies were prepared by a host-guest inclusion complexation interaction between *β*-CD and azobenzene at molar ratio of 1:1 through a dialysis technique. 4.32 mg of *β*-CD-PNIPAAm (0.001 mmol) and 12.83 mg of PEG-FS-AZO (0.001 mmol) were separately dissolved in 2 mL DMF and then stirred for 30 min. Then, the PEG-FS-AZO solution was added dropwise to the *β*-CD-PNIPAAm solution and the stirred for 2 h. Under vigorous stirring, deionized water was added dropwise to the mixed solution until the solution became turbid to induce the formation of supramolecular micelles. After stirring overnight, the mixture was dialyzed at room temperature for 3 days to completely remove DMF.

6.4.4 Photothermal performance test

In chapter 3, the photothermal performance was tested by exposing the hydrogel to near-infrared light (850nm, 9W) and detecting the surface temperature change with increasing irradiation time.

6.4.5 Swelling ratio measurement

In chapter 3, the hydrogels were incubated in water at a temperature ranging from 25 to 45 °C in order to determine the equilibrium swelling ratio (SR). The hydrogels were then removed from water, and their weight was calculated using the weight method after all the surface water had been wiped off using wet filter paper. The swelling ratio (SR) of the hydrogels was established as $SR = W_s/W_d$, where W_d is the weight of the hydrogel after freeze drying and W_s is the weight of the hydrogel in water at a specific temperature.

6.4.6 De-swelling kinetics measurement

In chapter 3, the de-swelling kinetics of hydrogels were carried out in deionized water at 50 °C. The hydrogels were first equilibrated in deionized water at room temperature. In order to measure the hydrogels' weight over time, the swollen hydrogels were then immersed into deionized water at 50 °C. Water retention (WR) is defined as follows:

$$WR\ (\%) = 100 \times (W_{t50} - W_d)/(W_0 - W_d)$$

W_0 is the weight of the hydrogel reaching equilibrium swelling at room temperature, W_d is the weight of the hydrogel after freeze drying, and W_{t50} is the weight of the hydrogel at a given time during de-swelling process.

6.4.7 Re-swelling kinetics measurement

In chapter 3, the re-swelling kinetics of hydrogels were carried out in deionized water at room temperature. The above deswelling hydrogels were immersed into deionized water at room temperature. In order to measure the hydrogels' weight over time, the hydrogels were removed from the water and their weights were determined after wiping excess water from the surface with wet filter paper. The re-swelling ratio (rSR) is defined as follows:

$$rSR(\%) = 100 \times (W_{t25} - W_d)/\ (W_0 - W_d),$$

W_0 is the weight of the hydrogel reaching equilibrium swelling at room temperature, W_d is the weight of the hydrogel after freeze drying, and W_{t25} is the weight of the hydrogel at a given time during re-swelling process.

6.4.8 Water Collection from Contaminated Water

In chapter 3, oil-, heavy metals-, microbe-, and dye-contaminated water were used to assess the hydrogel's purifying capacity.

To prepare organic oil-wastewater, hexane, cyclohexane and petroleum ether were respectively mixed with 0.5 mg/L SDS aqueous solution at a mass ratio of 1:99 by ultrasonication for 30 min forming oil-in-water emulsion. The clear water collection process was carried out by immersing the deswelling hydrogels in the prepared emulsion for 24 h, then the swollen hydrogels were taken out and irradiated it with near-infrared light (wavelength 850 nm) to generate clear water.[206] The obtained water was tested by microscopy to see if it contained oil-in-water droplets, thereby proving the ability of the hydrogel to purify oil-waste.

Rhodamine 6G (R6G) was selected as representative model contaminants to test photo-driven water of the hydrogels. The clear water collection process was carried out by immersing the deswelling hydrogels in 20 mL of 0.005 mg/mL R6G aqueous solution for 24 h at room temperature, then the swollen hydrogels were taken out and irradiated it with near-infrared light (wavelength 850 nm) for another 24 h to generate clear water. The original dye solution before and after the adsorption and the generated water were collected and detected by UV-Vis to see the existence of the dye absorption peak. After light-driven water release, the dye was removed from the hydrogels employing the mixture of ethanol and water as a desorption agent. The clean hydrogels were then dried in air or in the oven and employed for the next dye adsorption cycle to study the recyclability of the hydrogels. A total of ten cycles were performed.

Two heavy metals (Palladium (II) acetate (Pd $(OAc)_2$), Lead (II) acetate trihydrate (Pb $(CH_3CO_2)_2 \cdot 3H_2O$)) were selected as representative model contaminants to study the adsorption behaviors of heavy metal ions. The clear water collection process was carried out by immersing the deswelling hydrogels in 20 mL prepared solution containing 0.0001 M Pb^{2+} or Pd^{2+} for 24 h, then the swollen hydrogels were taken out and irradiated it with near-infrared light (wavelength 850 nm) to generate clear water. The purify heavy metal waste ability of the hydrogels was demonstrated by detecting the metal ion concentration of the original heavy metal solutions before and after the

purification and the generated water by Inductively coupled plasma - optical emission spectrometry (ICP-OES, iCAP 7600 DUO, Thermo-Fisher-Scientific).

To test the rejection capability of microbes, the hydrogels were placed into 0.1wt % yeast solution for 24 h, then the swollen hydrogels were taken out and irradiated with near-infrared light (wavelength 850 nm) to generate clear water. The ability of the hydrogels to purify microorganisms was demonstrated by using a microscope to test whether the obtained water contained yeast cells.

References

(1) Staudinger, H. Über Polymerisation. *Berichte der Dtsch. Chem. Gesellschaft (A B Ser.* **1920**, *53* (6), 1073–1085.

(2) Moon, R. J.; Martini, A.; Nairn, J.; Simonsen, J.; Youngblood, J. Cellulose Nanomaterials Review: Structure, Properties and Nanocomposites. *Chem. Soc. Rev.* **2011**, *40* (7), 3941–3994.

(3) Edgar, K. J.; Buchanan, C. M.; Debenham, J. S.; Rundquist, P. A.; Seiler, B. D.; Shelton, M. C.; Tindall, D. Advances in Cellulose Ester Performance and Application. *Prog. Polym. Sci.* **2001**, *26* (9), 1605–1688.

(4) Liu, H.; Xie, F.; Yu, L.; Chen, L.; Li, L. Thermal Processing of Starch-Based Polymers. *Prog. Polym. Sci.* **2009**, *34* (12), 1348–1368.

(5) Ibrahim, A.; Dahlan, M. Thermoplastic Natural Rubber Blends. *Prog. Polym. Sci.* **1998**, *23* (4), 665–706.

(6) Flory, P. J.; Volkenstein, M. Statistical Mechanics of Chain Molecules. Wiley Online Library 1969.

(7) Flory, P. J. Thermodynamics of High Polymer Solutions. *J. Chem. Phys.* **1942**, *10* (1), 51–61.

(8) Fox Jr, T. G.; Flory, P. J. Second-Order Transition Temperatures and Related Properties of Polystyrene. I. Influence of Molecular Weight. *J. Appl. Phys.* **1950**, *21* (6), 581–591.

(9) Stuart, M. A. C.; Huck, W. T. S.; Genzer, J.; Müller, M.; Ober, C.; Stamm, M.; Sukhorukov, G. B.; Szleifer, I.; Tsukruk, V. V; Urban, M.; others. Emerging Applications of Stimuli-Responsive Polymer Materials. *Nat. Mater.* **2010**, *9* (2), 101–113.

(10) Liu, F.; Urban, M. W. Recent Advances and Challenges in Designing Stimuli-Responsive Polymers. *Prog. Polym. Sci.* **2010**, *35* (1–2), 3–23.

(11) Grzelczak, M.; Liz-Marzán, L. M.; Klajn, R. Stimuli-Responsive Self-Assembly of Nanoparticles. *Chem. Soc. Rev.* **2019**, *48* (5), 1342–1361.

(12) Lu, C.; Urban, M. W. Stimuli-Responsive Polymer Nano-Science: Shape Anisotropy, Responsiveness, Applications. *Prog. Polym. Sci.* **2018**, *78*, 24–46.

(13) Thambi, T.; Lee, D. S. Stimuli-Responsive Polymersomes for Cancer Therapy. *Stimuli responsive Polym. nanocarriers drug Deliv. Appl.* **2019**, 413–438.

(14) Jahid, M. A.; Hu, J.; Zhuo, H. Stimuli-Responsive Polymers in Coating and Laminating for Functional Textile. In *Smart Textile Coatings and Laminates*; Elsevier, 2019; pp 155–173.

(15) Zhao, T.; Wang, P.; Li, Q.; Al-Khalaf, A. A.; Hozzein, W. N.; Zhang, F.; Li, X.; Zhao, D. Near-Infrared Triggered Decomposition of Nanocapsules with High Tumor Accumulation and Stimuli Responsive Fast Elimination. *Angew. Chemie Int. Ed.* **2018**, *57* (10), 2611–2615.

(16) Cobo, I.; Li, M.; Sumerlin, B. S.; Perrier, S. Smart Hybrid Materials by Conjugation of Responsive Polymers to Biomacromolecules. *Nat. Mater.* **2015**, *14* (2), 143–159.

(17) Stayton, P. S.; Shimoboji, T.; Long, C.; Chilkoti, A.; Ghen, G.; Harris, J. M.; Hoffman, A. S. Control of Protein--Ligand Recognition Using a Stimuli-Responsive Polymer. *Nature* **1995**, *378* (6556), 472–474.

(18) Motornov, M.; Roiter, Y.; Tokarev, I.; Minko, S. Stimuli-Responsive Nanoparticles, Nanogels and Capsules for Integrated Multifunctional Intelligent Systems. *Prog. Polym. Sci.* **2010**, *35* (1–2), 174–211.

(19) Chen, J.-K.; Chang, C.-J. Fabrications and Applications of Stimulus-Responsive Polymer Films and Patterns on Surfaces: A Review. *Materials (Basel).* **2014**, *7* (2), 805–875.

(20) Karban, R. Plant Behaviour and Communication. *Ecol. Lett.* **2008**, *11* (7), 727–739.

(21) Roy, D.; Cambre, J. N.; Sumerlin, B. S. Future Perspectives and Recent Advances in Stimuli-Responsive Materials. *Prog. Polym. Sci.* **2010**, *35* (1–2), 278–301.

(22) Gil, E. S.; Hudson, S. M. Stimuli-Reponsive Polymers and Their Bioconjugates. *Prog. Polym. Sci.* **2004**, *29* (12), 1173–1222.

(23) Dai, S.; Ravi, P.; Tam, K. C. PH-Responsive Polymers: Synthesis, Properties and Applications. *Soft Matter* **2008**, *4* (3), 435–449.

(24) Murthy, N.; Campbell, J.; Fausto, N.; Hoffman, A. S.; Stayton, P. S. Bioinspired PH-Responsive Polymers for the Intracellular Delivery of Biomolecular Drugs. *Bioconjug. Chem.* **2003**, *14* (2), 412–419.

(25) Magnusson, J. P.; Khan, A.; Pasparakis, G.; Saeed, A. O.; Wang, W.; Alexander, C. Ion-Sensitive "Isothermal" Responsive Polymers Prepared in Water. *J. Am. Chem. Soc.* **2008**, *130* (33), 10852–10853.

(26) Lvov, Y.; Antipov, A. A.; Mamedov, A.; Möhwald, H.; Sukhorukov, G. B. Urease Encapsulation in Nanoorganized Microshells. *Nano Lett.* **2001**, *1* (3), 125–128.

(27) Han, D.; Tong, X.; Boissiere, O.; Zhao, Y. General Strategy for Making CO2-Switchable Polymers. *ACS Macro Lett.* **2012**, *1* (1), 57–61.

(28) Akhoury, A.; Bromberg, L.; Hatton, T. A. Redox-Responsive Gels with Tunable Hydrophobicity for Controlled Solubilization and Release of Organics. *ACS Appl. Mater. \& interfaces* **2011**, *3* (4), 1167–1174.

(29) Yan, Q.; Yuan, J.; Cai, Z.; Xin, Y.; Kang, Y.; Yin, Y. Voltage-Responsive Vesicles Based on Orthogonal Assembly of Two Homopolymers. *J. Am. Chem. Soc.* **2010**, *132* (27), 9268–9270.

(30) Dimitrov, I.; Trzebicka, B.; Müller, A. H. E.; Dworak, A.; Tsvetanov, C. B. Thermosensitive Water-Soluble Copolymers with Doubly Responsive Reversibly Interacting Entities. *Prog. Polym. Sci.* **2007**, *32* (11), 1275–1343.

(31) Schild, H. G. Poly (N-Isopropylacrylamide): Experiment, Theory and Application. *Prog. Polym. Sci.* **1992**, *17* (2), 163–249.

(32) Zhao, Y. Photocontrollable Block Copolymer Micelles: What Can We Control? *J. Mater. Chem.* **2009**, *19* (28), 4887–4895.

(33) Ercole, F.; Davis, T. P.; Evans, R. A. Photo-Responsive Systems and Biomaterials: Photochromic Polymers, Light-Triggered Self-Assembly, Surface Modification, Fluorescence Modulation and Beyond. *Polym. Chem.* **2010**, *1* (1), 37–54.

(34) Schumers, J.-M.; Fustin, C.-A.; Gohy, J.-F. Light-Responsive Block Copolymers. *Macromol. Rapid Commun.* **2010**, *31* (18), 1588–1607.

(35) Weder, C. Polymers React to Stress. *Nature* **2009**, *459* (7243), 45–46.

(36) Konda, S. S. M.; Brantley, J. N.; Bielawski, C. W.; Makarov, D. E. Chemical Reactions Modulated by Mechanical Stress: Extended Bell Theory. *J. Chem. Phys.* **2011**, *135* (16), 164103.

(37) Brantley, J. N.; Wiggins, K. M.; Bielawski, C. W. Unclicking the Click: Mechanically Facilitated 1, 3-Dipolar Cycloreversions. *Science (80-.).* **2011**, *333* (6049), 1606–1609.

(38) Jochum, F. D.; Theato, P. Temperature-and Light-Responsive Smart Polymer Materials. *Chem. Soc. Rev.* **2013**, *42* (17), 7468–7483.

(39) Liu, F.; Urban, M. W. Recent Advances and Challenges in Designing Stimuli-Responsive Polymers. *Prog. Polym. Sci.* **2010**, *35* (1–2), 3–23.

(40) Schattling, P.; Jochum, F. D.; Theato, P. Multi-Stimuli Responsive Polymers--the All-in-One Talents. *Polym. Chem.* **2014**, *5* (1), 25–36.

(41) Jeong, B.; Gutowska, A. Lessons from Nature: Stimuli-Responsive Polymers and Their Biomedical Applications. *Trends Biotechnol.* **2002**, *20* (7), 305–311.

(42) Bajpai, A. K.; Shukla, S. K.; Bhanu, S.; Kankane, S. Responsive Polymers in Controlled Drug Delivery. *Prog. Polym. Sci.* **2008**, *33* (11), 1088–1118.

(43) Delcea, M.; Möhwald, H.; Skirtach, A. G. Stimuli-Responsive LbL Capsules and Nanoshells for Drug Delivery. *Adv. Drug Deliv. Rev.* **2011**, *63* (9), 730–747.

(44) Cheng, Y.; He, C.; Xiao, C.; Ding, J.; Zhuang, X.; Chen, X. Versatile Synthesis of Temperature-Sensitive Polypeptides by Click Grafting of Oligo (Ethylene Glycol). *Polym. Chem.* **2011**, *2* (11), 2627–2634.

(45) Xu, J.; Luo, S.; Shi, W.; Liu, S. Two-Stage Collapse of Unimolecular Micelles with Double Thermoresponsive Coronas. *Langmuir* **2006**, *22* (3), 989–997.

(46) Okhapkin, I. M.; Makhaeva, E. E.; Khokhlov, A. R. Water Solutions of Amphiphilic Polymers: Nanostructure Formation and Possibilities for Catalysis. *Conform. Des. Seq. Copolym. I* **2006**, 177–210.

(47) Zhang, G.; Wu, C. Folding and Formation of Mesoglobules in Dilute Copolymer Solutions. *Conform. Des. Seq. Copolym. I* **2006**, 101–176.

(48) Bromberg, L. E.; Ron, E. S. Temperature-Responsive Gels and Thermogelling Polymer Matrices for Protein and Peptide Delivery. *Adv. Drug Deliv. Rev.* **1998**, *31* (3), 197–221.

(49) Roth, P. J.; Davis, T. P.; Lowe, A. B. Comparison between the LCST and UCST Transitions of Double Thermoresponsive Diblock Copolymers: Insights into the Behavior of POEGMA in Alcohols. *Macromolecules* **2012**, *45* (7), 3221–3230.

(50) Diehl, C.; Schlaad, H. Thermo-Responsive Polyoxazolines with Widely Tuneable LCST. *Macromol. Biosci.* **2009**, *9* (2), 157–161.

(51) Yao, Z. L.; Tam, K. C. Temperature Induced Micellization and Aggregation of Biocompatible Poly (Oligo (Ethylene Glycol) Methyl Ether Methacrylate) Block Copolymer Analogs in Aqueous Solutions. *Polymer (Guildf).* **2012**, *53* (16), 3446–3453.

(52) Strandman, S.; Zhu, X. X. Thermo-Responsive Block Copolymers with Multiple Phase Transition Temperatures in Aqueous Solutions. *Prog. Polym. Sci.* **2015**, *42*, 154–176.

(53) Scarpa, J. S.; Mueller, D. D.; Klotz, I. M. Slow Hydrogen-Deuterium Exchange in a Non-. Alpha.-Helical Polyamide. *J. Am. Chem. Soc.* **1967**, *89* (24), 6024–6030.

(54) Hourdet, D.; L'alloret, F.; Audebert, R. Reversible Thermothickening of Aqueous Polymer Solutions. *Polymer (Guildf).* **1994**, *35* (12), 2624–2630.

(55) Chow, T. S. Miscible Blends and Block Copolymers. Crystallization, Melting, and Interaction. *Macromolecules* **1990**, *23* (1), 333–337.

(56) las Heras Alarcón, C.; Pennadam, S.; Alexander, C. Stimuli Responsive Polymers for Biomedical Applications. *Chem. Soc. Rev.* **2005**, *34* (3), 276–285.

(57) Idziak, I.; Avoce, D.; Lessard, D.; Gravel, D.; Zhu, X. X. Thermosensitivity of Aqueous Solutions of Poly (N, N-Diethylacrylamide). *Macromolecules* **1999**, *32* (4), 1260–1263.

(58) Han, S.; Hagiwara, M.; Ishizone, T. Synthesis of Thermally Sensitive Water-Soluble Polymethacrylates by Living Anionic Polymerizations of Oligo (Ethylene Glycol) Methyl Ether Methacrylates. *Macromolecules* **2003**, *36* (22), 8312–8319.

(59) Lutz, J.-F. Polymerization of Oligo (Ethylene Glycol)(Meth) Acrylates: Toward New Generations of Smart Biocompatible Materials. *J. Polym. Sci. Part A Polym. Chem.* **2008**, *46* (11), 3459–3470.

(60) Lau, A. C. W.; Wu, C. Thermally Sensitive and Biocompatible Poly (N-Vinylcaprolactam): Synthesis and Characterization of High Molar Mass Linear Chains. *Macromolecules* **1999**, *32* (3), 581–584.

(61) Suwa, K.; Wada, Y.; Kikunaga, Y.; Morishita, K.; Kishida, A.; Akashi, M. Synthesis and Functionalities of Poly (N-Vinylalkylamide). IV. Synthesis and Free Radical Polymerization of N-Vinylisobutyramide and Thermosensitive Properties of the Polymer. *J. Polym. Sci. Part A Polym. Chem.* **1997**, *35* (9), 1763–1768.

(62) Suwa, K.; Morishita, K.; Kishida, A.; Akashi, M. Synthesis and Functionalities of Poly (N-Vinylalkylamide). V. Control of a Lower Critical Solution Temperature of Poly (N-Vinylalkylamide). *J. Polym. Sci. Part A Polym. Chem.* **1997**, *35* (15), 3087–3094.

(63) Diab, C.; Akiyama, Y.; Kataoka, K.; Winnik, F. M. Microcalorimetric Study of the Temperature-Induced Phase Separation in Aqueous Solutions of Poly (2-Isopropyl-2-Oxazolines). *Macromolecules* **2004**, *37* (7), 2556–2562.

(64) Glatzel, S.; Badi, N.; Päch, M.; Laschewsky, A.; Lutz, J.-F. Well-Defined Synthetic Polymers with a Protein-like Gelation Behavior in Water. *Chem. Commun.* **2010**, *46* (25), 4517–4519.

(65) Seuring, J.; Bayer, F. M.; Huber, K.; Agarwal, S. Upper Critical Solution Temperature of Poly (N-Acryloyl Glycinamide) in Water: A Concealed Property. *Macromolecules* **2012**, *45* (1), 374–384.

(66) Seuring, J.; Agarwal, S. First Example of a Universal and Cost-Effective Approach: Polymers with Tunable Upper Critical Solution Temperature in

Water and Electrolyte Solution. *Macromolecules* **2012**, *45* (9), 3910–3918.

(67) Glatzel, S.; Laschewsky, A.; Lutz, J.-F. Well-Defined Uncharged Polymers with a Sharp UCST in Water and in Physiological Milieu. *Macromolecules* **2011**, *44* (2), 413–415.

(68) Chung, J. E.; Yokoyama, M.; Aoyagi, T.; Sakurai, Y.; Okano, T. Effect of Molecular Architecture of Hydrophobically Modified Poly (N-Isopropylacrylamide) on the Formation of Thermoresponsive Core-Shell Micellar Drug Carriers. *J. Control. Release* **1998**, *53* (1–3), 119–130.

(69) Kujawa, P.; Winnik, F. M. Volumetric Studies of Aqueous Polymer Solutions Using Pressure Perturbation Calorimetry: A New Look at the Temperature-Induced Phase Transition of Poly (N-Isopropylacrylamide) in Water and D2O. *Macromolecules* **2001**, *34* (12), 4130–4135.

(70) Hoogenboom, R.; Thijs, H. M. L.; Jochems, M. J. H. C.; van Lankvelt, B. M.; Fijten, M. W. M.; Schubert, U. S. Tuning the LCST of Poly (2-Oxazoline) s by Varying Composition and Molecular Weight: Alternatives to Poly (N-Isopropylacrylamide)? *Chem. Commun.* **2008**, No. 44, 5758–5760.

(71) Zhang, W.; Shi, L.; Wu, K.; An, Y. Thermoresponsive Micellization of Poly (Ethylene Glycol)-b-Poly (N-Isopropylacrylamide) in Water. *Macromolecules* **2005**, *38* (13), 5743–5747.

(72) Ksendzov, E. A.; Nikishau, P. A.; Zurina, I. M.; Presniakova, V. S.; Timashev, P.; Rochev, Y. A.; Kotova, S.; Kostjuk, S. V. Graft Copolymers of N-Isopropylacrylamide with Poly (d, l-Lactide) or Poly (ε-Caprolactone) Macromonomers: A Promising Class of Thermoresponsive Polymers with a Tunable LCST. *ACS Appl. Polym. Mater.* **2022**, *4* (2), 1344–1357.

(73) Winnik, F. M.; Ringsdorf, H.; Venzmer, J. Methanol-Water as a Co-Nonsolvent System for Poly (N-Isopropylacrylamide). *Macromolecules* **1990**, *23* (8), 2415–2416.

(74) Schild, H. G.; Muthukumar, M.; Tirrell, D. A. Cononsolvency in Mixed Aqueous Solutions of Poly (N-Isopropylacrylamide). *Macromolecules* **1991**, *24*

(4), 948–952.

(75) Winnik, F. M.; Ottaviani, M. F.; Bossmann, S. H.; Garcia-Garibay, M.; Turro, N. J. Consolvency of Poly (N-Isopropylacrylamide) in Mixed Water-Methanol Solutions: A Look at Spin-Labeled Polymers. *Macromolecules* **1992**, *25* (22), 6007–6017.

(76) Asano, M.; Winnik, F. M.; Yamashita, T.; Horie, K. Fluorescence Studies of Dansyl-Labeled Poly (N-Isopropylacrylamide) Gels and Polymers in Mixed Water/Methanol Solutions. *Macromolecules* **1995**, *28* (17), 5861–5866.

(77) Mukae, K.; Sakurai, M.; Sawamura, S.; Makino, K.; Kim, S. W.; Ueda, I.; Shirahama, K. Swelling of Poly (N-Isopropylacrylamide) Gels in Water-Alcohol (C1-C4) Mixed Solvents. *J. Phys. Chem.* **1993**, *97* (3), 737–741.

(78) Otake, K.; Inomata, H.; Konno, M.; Saito, S. Thermal Analysis of the Volume Phase Transition with N-Isopropylacrylamide Gels. *Macromolecules* **1990**, *23* (1), 283–289.

(79) Zhu, P. W.; Napper, D. H. Coil-to-Globule Type Transitions and Swelling of Poly (N-Isopropylacrylamide) and Poly (Acrylamide) at Latex Interfaces in Alcohol--Water Mixtures. *J. Colloid Interface Sci.* **1996**, *177* (2), 343–352.

(80) Zhang, G.; Wu, C. The Water/Methanol Complexation Induced Reentrant Coil-to-Globule-to-Coil Transition of Individual Homopolymer Chains in Extremely Dilute Solution. *J. Am. Chem. Soc.* **2001**, *123* (7), 1376–1380.

(81) Liu, G.; Zhang, G. Reentrant Behavior of Poly (N-Isopropylacrylamide) Brushes in Water- Methanol Mixtures Investigated with a Quartz Crystal Microbalance. *Langmuir* **2005**, *21* (5), 2086–2090.

(82) Katayama, S.; Hirokawa, Y.; Tanaka, T. Reentrant Phase Transition in Acrylamide-Derivative Copolymer Gels. *Macromolecules* **1984**, *17* (12), 2641–2643.

(83) Yamauchi, H.; Maeda, Y. LCST and UCST Behavior of Poly (N-Isopropylacrylamide) in DMSO/Water Mixed Solvents Studied by IR and Micro-Raman Spectroscopy. *J. Phys. Chem. B* **2007**, *111* (45), 12964–12968.

(84) Wolf, B. A.; Willms, M. M. Measured and Calculated Solubility of Polymers in Mixed Solvents: Co-Nonsolvency. *Die Makromol. Chemie Macromol. Chem. Phys.* **1978**, *179* (9), 2265–2277.

(85) Amiya, T.; Hirokawa, Y.; Hirose, Y.; Li, Y.; Tanaka, T. Reentrant Phase Transition of N-Isopropylacrylamide Gels in Mixed Solvents. *J. Chem. Phys.* **1987**, *86* (4), 2375–2379.

(86) Hirotsu, S. Phase Transition of a Polymer Gel in Pure and Mixed Solvent Media. *J. Phys. Soc. Japan* **1987**, *56* (1), 233–242.

(87) Hirotsu, S. Critical Points of the Volume Phase Transition in N-Isopropylacrylamide Gels. *J. Chem. Phys.* **1988**, *88* (1), 427–431.

(88) Liu, C.; Wang, Y.; Wang, S.; Xu, P.; Liu, R.; Han, D.; Wei, Y. A Star-Shaped Copolymer with Tetra-Hydroxy-Phenylporphyrin Core and Four PNIPAM-b-PMAGA Arms for Targeted Photodynamic Therapy. *Polymers (Basel).* **2023**, *15* (3), 509.

(89) Xu, X.; Guillomaitre, N.; Christie, K. S. S.; Bay, R. K.; Bizmark, N.; Datta, S. S.; Ren, Z. J.; Priestley, R. D. Quick-Release Antifouling Hydrogels for Solar-Driven Water Purification. *ACS Cent. Sci.* **2023**.

(90) Blasco, E.; del Barrio, J.; Piñol, M.; Oriol, L.; Berges, C.; Sánchez, C.; Alcalá, R. Azobenzene-Containing Linear--Dendritic Block Copolymers Prepared by Sequential ATRP and Click Chemistry. *Polymer (Guildf).* **2012**, *53* (21), 4604–4613.

(91) Yanai, N.; Uemura, T.; Inoue, M.; Matsuda, R.; Fukushima, T.; Tsujimoto, M.; Isoda, S.; Kitagawa, S. Guest-to-Host Transmission of Structural Changes for Stimuli-Responsive Adsorption Property. *J. Am. Chem. Soc.* **2012**, *134* (10), 4501–4504.

(92) Zhu, Z.; Sukhishvili, S. A. Layer-by-Layer Films of Stimuli-Responsive Block Copolymer Micelles. *J. Mater. Chem.* **2012**, *22* (16), 7667–7671.

(93) Chen, C.-J.; Jin, Q.; Liu, G.-Y.; Li, D.-D.; Wang, J.-L.; Ji, J. Reversibly Light-Responsive Micelles Constructed via a Simple Modification of Hyperbranched Polymers with Chromophores. *Polymer (Guildf).* **2012**, *53* (17),

3695–3703.

(94) Feng, K.; Xie, N.; Chen, B.; Zhang, L.-P.; Tung, C.-H.; Wu, L.-Z. Reversible Light-Triggered Transition of Amphiphilic Random Copolymers. *Macromolecules* **2012**, *45* (13), 5596–5603.

(95) Doron, A.; Portnoy, M.; Lion-Dagan, M.; Katz, E.; Willner, I. Amperometric Transduction and Amplification of Optical Signals Recorded by a Phenoxynaphthacenequinone Monolayer Electrode: Photochemical and PH-Gated Electron Transfer. *J. Am. Chem. Soc.* **1996**, *118* (37), 8937–8944.

(96) Ipe, B. I.; Mahima, S.; Thomas, K. G. Light-Induced Modulation of Self-Assembly on Spiropyran-Capped Gold Nanoparticles: A Potential System for the Controlled Release of Amino Acid Derivatives. *J. Am. Chem. Soc.* **2003**, *125* (24), 7174–7175.

(97) Huang, C.-Q.; Wang, Y.; Hong, C.-Y.; Pan, C.-Y. Spiropyran-Based Polymeric Vesicles: Preparation and Photochromic Properties. *Macromol. Rapid Commun.* **2011**, *32* (15), 1174–1179.

(98) Pennakalathil, J.; Hong, J.-D. Self-Standing Polyelectrolyte Multilayer Films Based on Light-Triggered Disassembly of a Sacrificial Layer. *ACS Nano* **2011**, *5* (11), 9232–9237.

(99) Shi, D.; Matsusaki, M.; Akashi, M. Photo-Tunable Protein Release from Biodegradable Nanoparticles Composed of Cinnamic Acid Derivatives. *J. Control. release* **2011**, *149* (2), 182–189.

(100) Garle, A.; Kong, S.; Ojha, U.; Budhlall, B. M. Thermoresponsive Semicrystalline Poly (ε-Caprolactone) Networks: Exploiting Cross-Linking with Cinnamoyl Moieties to Design Polymers with Tunable Shape Memory. *ACS Appl. Mater. \& interfaces* **2012**, *4* (2), 645–657.

(101) Bian, Q.; Xiao, Y.; Zhou, C.; Lang, M. Synthesis, Self-Assembly, and PH-Responsive Behavior of (Photo-Crosslinked) Star Amphiphilic Triblock Copolymer. *J. Colloid Interface Sci.* **2013**, *392*, 141–150.

(102) Roy, P. S.; Mention, M. M.; Patti, A. F.; Garnier, G.; Allais, F.; Saito, K. Photo-Responsive Lignin Fragment-Based Polymers as Switchable Adhesives.

Polym. Chem. **2023**.

(103) Ribas-Arino, J.; Shiga, M.; Marx, D. Understanding Covalent Mechanochemistry. *Angew. Chemie Int. Ed.* **2009**, *48* (23), 4190–4193.

(104) Rapoport, N. Y.; Kennedy, A. M.; Shea, J. E.; Scaife, C. L.; Nam, K.-H. Controlled and Targeted Tumor Chemotherapy by Ultrasound-Activated Nanoemulsions/Microbubbles. *J. Control. Release* **2009**, *138* (3), 268–276.

(105) Wang, C.-H.; Kang, S.-T.; Lee, Y.-H.; Luo, Y.-L.; Huang, Y.-F.; Yeh, C.-K. Aptamer-Conjugated and Drug-Loaded Acoustic Droplets for Ultrasound Theranosis. *Biomaterials* **2012**, *33* (6), 1939–1947.

(106) Klajn, R. Spiropyran-Based Dynamic Materials. *Chem. Soc. Rev.* **2014**, *43* (1), 148–184.

(107) Kim, D. W.; Medvedev, G. A.; Caruthers, J. M.; Jo, J. Y.; Won, Y.-Y.; Kim, J. Enhancement of Mechano-Sensitivity for Spiropyran-Linked Poly (Dimethylsiloxane) via Solvent Swelling. *Macromolecules* **2020**, *53* (18), 7954–7961.

(108) Baughman, R. H. Conducting Polymer Artificial Muscles. *Synth. Met.* **1996**, *78* (3), 339–353.

(109) Jensen, M.; Hansen, P. B.; Murdan, S.; Frokjaer, S.; Florence, A. T. Loading into and Electro-Stimulated Release of Peptides and Proteins from Chondroitin 4-Sulphate Hydrogels. *Eur. J. Pharm. Sci.* **2002**, *15* (2), 139–148.

(110) Ramanathan, S.; Block, L. H. The Use of Chitosan Gels as Matrices for Electrically-Modulated Drug Delivery. *J. Control. release* **2001**, *70* (1–2), 109–123.

(111) Tanaka, T.; Nishio, I.; Sun, S.-T.; Ueno-Nishio, S. Collapse of Gels in an Electric Field. *Science (80-.).* **1982**, *218* (4571), 467–469.

(112) Smela, E. Conjugated Polymer Actuators for Biomedical Applications. *Adv. Mater.* **2003**, *15* (6), 481–494.

(113) Nasari, M.; Semnani, D.; Amanpour, S. Manufacturing and Characterizing of the Poly (ε-Caprolactone)/Poly (N-Vinyl-2-Pyrrolidone) Core-Shell Nanofibers Loaded by Multi-Walled Carbon Nanotubes Coated by

Polypyrrole via Vapor Phase and Chemical Method and Its Application as an Electr. *Int. J. Polym. Mater. Polym. Biomater.* **2022**, 1–12.

(114) Yuan, F.; Dellian, M.; Fukumura, D.; Leunig, M.; Berk, D. A.; Torchilin, V. P.; Jain, R. K. Vascular Permeability in a Human Tumor Xenograft: Molecular Size Dependence and Cutoff Size. *Cancer Res.* **1995**, *55* (17), 3752–3756.

(115) Kataoka, K.; Harada, A.; Nagasaki, Y. Block Copolymer Micelles for Drug Delivery: Design, Characterization and Biological Significance. *Adv. Drug Deliv. Rev.* **2012**, *64*, 37–48.

(116) Krämer, M.; Stumbé, J.-F.; Türk, H.; Krause, S.; Komp, A.; Delineau, L.; Prokhorova, S.; Kautz, H.; Haag, R. PH-Responsive Molecular Nanocarriers Based on Dendritic Core-Shell Architectures. *Angew. Chemie Int. Ed.* **2002**, *41* (22), 4252–4256.

(117) Kocak, G.; Tuncer, C.; Bütün, V. PH-Responsive Polymers. *Polym. Chem.* **2017**, *8* (1), 144–176.

(118) Ofridam, F.; Tarhini, M.; Lebaz, N.; Gagnière, É.; Mangin, D.; Elaissari, A. PH-Sensitive Polymers: Classification and Some Fine Potential Applications. *Polym. Adv. Technol.* **2021**, *32* (4), 1455–1484.

(119) Zhang, J.; Gu, Y.; Jiang, J.; Zheng, R. PH-Responsive Liquid Marbles Based on Dihydroxystearic Acid. *Langmuir* **2022**, *38* (18), 5702–5707.

(120) Motornov, M.; Sheparovych, R.; Katz, E.; Minko, S. Chemical Gating with Nanostructured Responsive Polymer Brushes: Mixed Brush versus Homopolymer Brush. *ACS Nano* **2008**, *2* (1), 41–52.

(121) Fielding, L. A.; Edmondson, S.; Armes, S. P. Synthesis of PH-Responsive Tertiary Amine Methacrylate Polymer Brushes and Their Response to Acidic Vapour. *J. Mater. Chem.* **2011**, *21* (32), 11773–11780.

(122) Abousalman-Rezvani, Z.; Eskandari, P.; Roghani-Mamaqani, H.; Mardani, H.; Salami-Kalajahi, M. Grafting Light-, Temperature, and CO2-Responsive Copolymers from Cellulose Nanocrystals by Atom Transfer Radical Polymerization for Adsorption of Nitrate Ions. *Polymer (Guildf).* **2019**, *182*, 121830.

(123) Zhang, D.; Fan, Y.; Chen, H.; Trépout, S.; Li, M.-H. CO2-Activated Reversible Transition between Polymersomes and Micelles with AIE Fluorescence. *Angew. Chemie Int. Ed.* **2019**, *58* (30), 10260–10265.

(124) Chen, L.; Liu, R.; Yan, Q. Polymer Meets Frustrated Lewis Pair: Second-Generation CO2-Responsive Nanosystem for Sustainable CO2 Conversion. *Angew. Chemie* **2018**, *130* (30), 9480–9484.

(125) Hu, L.; Zhang, Q.; Li, X.; Serpe, M. J. Stimuli-Responsive Polymers for Sensing and Actuation. *Mater. Horizons* **2019**, *6* (9), 1774–1793.

(126) Zhang, Q.; Lei, L.; Zhu, S. Gas-Responsive Polymers. ACS Publications 2017.

(127) Guo, Z.; Feng, Y.; Wang, Y.; Wang, J.; Wu, Y.; Zhang, Y. A Novel Smart Polymer Responsive to CO 2. *Chem. Commun.* **2011**, *47* (33), 9348–9350.

(128) Yan, Q.; Zhou, R.; Fu, C.; Zhang, H.; Yin, Y.; Yuan, J. CO2-Responsive Polymeric Vesicles That Breathe. *Angew. Chemie Int. Ed.* **2011**, *50* (21), 4923–4927.

(129) Lin, S.; Theato, P. CO2-Responsive Polymers. *Macromol. Rapid Commun.* **2013**, *34* (14), 1118–1133.

(130) Al Akoumy, C.; Augé, A.; Ma, D.; Zhao, Y. Yolk--Shell Nanoparticles with CO2-Responsive Outer Shells for Gas-Controlled Catalysis. *ACS Appl. Nano Mater.* **2022**, *5* (12), 18237–18246.

(131) Lei, L.; Zhang, Q.; Shi, S.; Zhu, S. Oxygen and Carbon Dioxide Dual Gas-Switchable Thermoresponsive Homopolymers. *ACS Macro Lett.* **2016**, *5* (7), 828–832.

(132) Lei, L.; Zhang, Q.; Shi, S.; Zhu, S. Oxygen-Switchable Thermo-Responsive Random Copolymers. *Polym. Chem.* **2016**, *7* (34), 5456–5462.

(133) Lei, L.; Zhang, Q.; Shi, S.; Zhu, S. Oxygen and Carbon Dioxide Dual Gas-Responsive and Switchable Microgels Prepared from Emulsion Copolymerization of Fluoro-and Amino-Containing Monomers. *Langmuir* **2015**, *31* (7), 2196–2201.

(134) Zhang, Q.; Zhu, S. Oxygen and Carbon Dioxide Dual Responsive Nanoaggregates of Fluoro-and Amino-Containing Copolymer. *ACS Macro Lett.*

2014, *3* (8), 743–746.

(135) Zhang, Q.; Zhu, S. Oxygen--Nitrogen Switchable Copolymers of 2, 2, 2-Trifluoroethyl Methacrylate and N, N-Dimethylaminoethyl Methacrylate. *Macromol. Rapid Commun.* **2014**, *35* (19), 1692–1696.

(136) Choi, J. Y.; Kim, J. Y.; Moon, H. J.; Park, M. H.; Jeong, B. CO2-and O2-Sensitive Fluorophenyl End-Capped Poly (Ethylene Glycol). *Macromol. Rapid Commun.* **2014**, *35* (1), 66–70.

(137) Zhang, X.; Wang, J.; Zhou, S.; Sun, S.; Wang, X.; Guo, S.; Zhao, F. Dual Gas-Responsive Fluorescent Diblock Copolymer Synthesized via RAFT Polymerization. *J. Fluoresc.* **2022**, *32* (2), 435–442.

(138) Mintz, J.; Vedenko, A.; Rosete, O.; Shah, K.; Goldstein, G.; Hare, J. M.; Ramasamy, R.; Arora, H. Current Advances of Nitric Oxide in Cancer and Anticancer Therapeutics. *Vaccines* **2021**, *9* (2), 94.

(139) Hu, J.; Whittaker, M. R.; Duong, H.; Li, Y.; Boyer, C.; Davis, T. P. Biomimetic Polymers Responsive to a Biological Signaling Molecule: Nitric Oxide Triggered Reversible Self-Assembly of Single Macromolecular Chains into Nanoparticles. *Angew. Chemie Int. Ed.* **2014**, *53* (30), 7779–7784.

(140) Zhu, M.; Wu, Y.; Ge, C.; Ling, Y.; Tang, H. SO2-Induced Solution Phase Transition of Water-Soluble and $α$-Helical Polypeptides. *Macromolecules* **2016**, *49* (9), 3542–3549.

(141) Kathmann, E. E. L.; White, L. A.; McCormick, C. L. Water-Soluble Polymers. 73. Electrolyte-and PH-Responsive Zwitterionic Copolymers of 4-[(2-Acrylamido-2-Methylpropyl)-Dimethylammonio] Butanoate with 3-[(2-Acrylamido-2-Methyl-Propyl) Dimethylammonio] Propanesulfonate. *Macromolecules* **1997**, *30* (18), 5297–5304.

(142) Szczubiaka, K.; Jankowska, M.; Nowakowska, M. " Smart" Polymeric Nanospheres as New Materials for Possible Biomedical Applications. *J. Mater. Sci. Mater. Med.* **2003**, *14* (8), 699.

(143) Lallana, E.; Tirelli, N. Oxidation-Responsive Polymers: Which Groups to Use, How to Make Them, What to Expect from Them (Biomedical Applications).

Macromol. Chem. Phys. **2013**, *214* (2), 143–158.

(144) Song, C.-C.; Du, F.-S.; Li, Z.-C. Oxidation-Responsive Polymers for Biomedical Applications. *J. Mater. Chem. B* **2014**, *2* (22), 3413–3426.

(145) Jäger, E.; Höcherl, A.; Janoušková, O.; Jäger, A.; Hrub\`y, M.; Konefał Rafałand Netopilik, M.; Pánek, J.; Šlouf, M.; Ulbrich, K.; others. Fluorescent Boronate-Based Polymer Nanoparticles with Reactive Oxygen Species (ROS)-Triggered Cargo Release for Drug-Delivery Applications. *Nanoscale* **2016**, *8* (13), 6958–6963.

(146) Harini, K.; Pallavi, P.; Gowtham, P.; Girigoswami, K.; Girigoswami, A. Smart Polymer-Based Reduction Responsive Therapeutic Delivery to Cancer Cells. *Curr. Pharmacol. Reports* **2022**, *8* (3), 205–211.

(147) Monteiro, P. F.; Travanut, A.; Conte, C.; Alexander, C. Reduction-Responsive Polymers for Drug Delivery in Cancer Therapy—Is There Anything New to Discover? *Wiley Interdiscip. Rev. Nanomedicine Nanobiotechnology* **2021**, *13* (2), e1678.

(148) Sun, B.; Luo, C.; Zhang, X.; Guo, M.; Sun, M.; Yu, H.; Chen, Q.; Yang, W.; Wang, M.; Zuo, S.; others. Probing the Impact of Sulfur/Selenium/Carbon Linkages on Prodrug Nanoassemblies for Cancer Therapy. *Nat. Commun.* **2019**, *10* (1), 3211.

(149) Islam, M. R.; Lu, Z.; Li, X.; Sarker, A. K.; Hu, L.; Choi, P.; Li, X.; Hakobyan, N.; Serpe, M. J. Responsive Polymers for Analytical Applications: A Review. *Anal. Chim. Acta* **2013**, *789*, 17–32.

(150) Kumar, A.; Srivastava, A.; Galaev, I. Y.; Mattiasson, B. Smart Polymers: Physical Forms and Bioengineering Applications. *Prog. Polym. Sci.* **2007**, *32* (10), 1205–1237.

(151) Hu, J.; Zhang, G.; Liu, S. Enzyme-Responsive Polymeric Assemblies, Nanoparticles and Hydrogels. *Chem. Soc. Rev.* **2012**, *41* (18), 5933–5949.

(152) Zhang, J.; Jiang, X.; Wen, X.; Xu, Q.; Zeng, H.; Zhao, Y.; Liu, M.; Wang, Z.; Hu, X.; Wang, Y. Bio-Responsive Smart Polymers and Biomedical Applications. *J. Phys. Mater.* **2019**, *2* (3), 32004.

(153) Wang, X.; Sun, B.; Ye, Z.; Zhang, W.; Xu, W.; Gao, S.; Zhou, N.; Wu, F.; Shen, J. Enzyme-Responsive COF-Based Thiol-Targeting Nanoinhibitor for Curing Bacterial Infections. *ACS Appl. Mater. \& Interfaces* **2022**, *14* (34), 38483–38496.

(154) Wu, Q.; Wang, L.; Yu, H.; Wang, J.; Chen, Z. Organization of Glucose-Responsive Systems and Their Properties. *Chem. Rev.* **2011**, *111* (12), 7855–7875.

(155) Xu, Z.; Liu, G.; Li, Q.; Wu, J. A Novel Hydrogel with Glucose-Responsive Hyperglycemia Regulation and Antioxidant Activity for Enhanced Diabetic Wound Repair. *Nano Res.* **2022**, *15* (6), 5305–5315.

(156) Wichterle, O.; Lim, D. Hydrophilic Gels for Biological Use. *Nature* **1960**, *185* (4706), 117–118.

(157) Mahinroosta, M.; Farsangi, Z. J.; Allahverdi, A.; Shakoori, Z. Hydrogels as Intelligent Materials: A Brief Review of Synthesis, Properties and Applications. *Mater. Today Chem.* **2018**, *8*, 42–55.

(158) Gong, J. P.; Katsuyama, Y.; Kurokawa, T.; Osada, Y. Double-Network Hydrogels with Extremely High Mechanical Strength. *Adv. Mater.* **2003**, *15* (14), 1155–1158.

(159) Yun, J.; Jin, D.; Lee, Y.-S.; Kim, H.-I. Photocatalytic Treatment of Acidic Waste Water by Electrospun Composite Nanofibers of PH-Sensitive Hydrogel and TiO2. *Mater. Lett.* **2010**, *64* (22), 2431–2434.

(160) Peng, N.; Wang, Y.; Ye, Q.; Liang, L.; An, Y.; Li, Q.; Chang, C. Biocompatible Cellulose-Based Superabsorbent Hydrogels with Antimicrobial Activity. *Carbohydr. Polym.* **2016**, *137*, 59–64.

(161) Murakami, K.; Aoki, H.; Nakamura, S.; Nakamura, S.; Takikawa, M.; Hanzawa, M.; Kishimoto, S.; Hattori, H.; Tanaka, Y.; Kiyosawa, T.; others. Hydrogel Blends of Chitin/Chitosan, Fucoidan and Alginate as Healing-Impaired Wound Dressings. *Biomaterials* **2010**, *31* (1), 83–90.

(162) Shahbuddin, M.; Bullock, A. J.; MacNeil, S.; Rimmer, S. Glucomannan-Poly (N-Vinyl Pyrrolidinone) Bicomponent Hydrogels for Wound Healing. *J. Mater.*

Chem. B **2014**, *2* (6), 727–738.

(163) Koetting, M. C.; Peters, J. T.; Steichen, S. D.; Peppas, N. A. Stimulus-Responsive Hydrogels: Theory, Modern Advances, and Applications. *Mater. Sci. Eng. R Reports* **2015**, *93*, 1–49.

(164) Lim, H. L.; Hwang, Y.; Kar, M.; Varghese, S. Smart Hydrogels as Functional Biomimetic Systems. *Biomater. Sci.* **2014**, *2* (5), 603–618.

(165) Qiu, Y.; Park, K. Environment-Sensitive Hydrogels for Drug Delivery. *Adv. Drug Deliv. Rev.* **2001**, *53* (3), 321–339.

(166) Sponchioni, M.; Palmiero, U. C.; Moscatelli, D. Thermo-Responsive Polymers: Applications of Smart Materials in Drug Delivery and Tissue Engineering. *Mater. Sci. Eng. C* **2019**, *102*, 589–605.

(167) Becerra, N. Y.; López, B. L.; Restrepo, L. M. Thermosensitive Behavior in Cell Culture Media and Cytocompatibility of a Novel Copolymer: Poly (N-Isopropylacrylamide-Co-Butylacrylate). *J. Mater. Sci. Mater. Med.* **2013**, *24*, 1043–1052.

(168) Osman, A.; Oner, E. T.; Eroglu, M. S. Novel Levan and PNIPA Temperature Sensitive Hydrogels for 5-ASA Controlled Release. *Carbohydr. Polym.* **2017**, *165*, 61–70.

(169) Liu, F.; Seuring, J.; Agarwal, S. A Non-Ionic Thermophilic Hydrogel with Positive Thermosensitivity in Water and Electrolyte Solution. *Macromol. Chem. Phys.* **2014**, *215* (15), 1466–1472.

(170) Xu, X.-D.; Zhang, X.-Z.; Wang, B.; Cheng, S.-X.; Zhuo, R.-X.; Wang, Z.-C. Fabrication of a Novel Temperature Sensitive Poly (N-Isopropyl-3-Butenamide) Hydrogel. *Colloids Surfaces B Biointerfaces* **2007**, *59* (2), 158–163.

(171) Halperin, A.; Kröger, M.; Winnik, F. M. Poly (N-Isopropylacrylamide) Phase Diagrams: Fifty Years of Research. *Angew. Chemie Int. Ed.* **2015**, *54* (51), 15342–15367.

(172) Isikci Koca, E.; Bozdag, G.; Cayli, G.; Kazan, D.; Cakir Hatir, P. Thermoresponsive Hydrogels Based on Renewable Resources. *J. Appl. Polym. Sci.* **2020**, *137* (28), 48861.

(173) Liu, J.; Fan, X.; Tao, Y.; Deng, C.; Yu, K.; Zhang, W.; Deng, L.; Xiong, W. Two-Step Freezing Polymerization Method for Efficient Synthesis of High-Performance Stimuli-Responsive Hydrogels. *ACS omega* **2020**, *5* (11), 5921–5930.

(174) Liu, J.; Jiang, L.; He, S.; Zhang, J.; Shao, W. Recent Progress in PNIPAM-Based Multi-Responsive Actuators: A Mini-Review. *Chem. Eng. J.* **2022**, *433*, 133496.

(175) Vörösmarty, C. J.; Green, P.; Salisbury, J.; Lammers, R. B. *Global Water Resources: Vulnerability from Climate Change and Population Growth*.

(176) Rodgers, P.; Heath, J. *Nanoscience and Technology: A Collection of Reviews from Nature Journals*; World Scientific Publishing Co., 2009.

(177) Vörösmarty, C. J.; Mcintyre, P. B.; Gessner, M. O.; Dudgeon, D.; Prusevich, A.; Green, P.; Glidden, S.; Bunn, S. E.; Sullivan, C. A.; Liermann, C. R.; Davies, P. M. Global Threats to Human Water Security and River Biodiversity. **2010**.

(178) Fu, F.; Wang, Q. Removal of Heavy Metal Ions from Wastewaters: A Review. *J. Environ. Manage.* **2011**, *92* (3), 407–418.

(179) Fengler, C.; Arens, L.; Horn, H.; Wilhelm, M. Desalination of Seawater Using Cationic Poly (Acrylamide) Hydrogels and Mechanical Forces for Separation. *Macromol. Mater. Eng.* **2020**, *305* (10), 2000383.

(180) Sharma, K.; Kaith, B. S.; Kumar, V.; Kalia, S.; Kumar, V.; Swart, H. C. Water Retention and Dye Adsorption Behavior of Gg-Cl-Poly (Acrylic Acid-Aniline) Based Conductive Hydrogels. *Geoderma* **2014**, *232*, 45–55.

(181) Weerasundara, L.; Gabriele, B.; Figoli, A.; Ok, Y.-S.; Bundschuh, J. Hydrogels: Novel Materials for Contaminant Removal in Water—A Review. *Crit. Rev. Environ. Sci. Technol.* **2021**, *51* (17), 1970–2014.

(182) Maji, B.; Maiti, S. Chemical Modification of Xanthan Gum through Graft Copolymerization: Tailored Properties and Potential Applications in Drug Delivery and Wastewater Treatment. *Carbohydr. Polym.* **2021**, *251*, 117095.

(183) Zhao, F.; Zhou, X.; Liu, Y.; Shi, Y.; Dai, Y.; Yu, G. Super Moisture-Absorbent

Gels for All-Weather Atmospheric Water Harvesting. *Adv. Mater.* **2019**, *31* (10), 1806446.

(184) Zhang, P.; Liu, F.; Liao, Q.; Yao, H.; Geng, H.; Cheng, H.; Li, C.; Qu, L. A Microstructured Graphene/Poly (N-Isopropylacrylamide) Membrane for Intelligent Solar Water Evaporation. *Angew. Chemie Int. Ed.* **2018**, *57* (50), 16343–16347.

(185) Geng, H.; Xu, Q.; Wu, M.; Ma, H.; Zhang, P.; Gao, T.; Qu, L.; Ma, T.; Li, C. Plant Leaves Inspired Sunlight-Driven Purifier for High-Efficiency Clean Water Production. *Nat. Commun.* **2019**, *10* (1), 1512.

(186) Li, R.; Shi, Y.; Alsaedi, M.; Wu, M.; Shi, L.; Wang, P. Hybrid Hydrogel with High Water Vapor Harvesting Capacity for Deployable Solar-Driven Atmospheric Water Generator. *Environ. Sci. \& Technol.* **2018**, *52* (19), 11367–11377.

(187) Wei, T.; Huang, S.; Hu, Q.; Wang, J.; Huo, Z.; Zhu, T.; Wu, C.; Chen, H. Thermoresponsive Metalloprotein-Based Hybrid Hydrogels for the Reversible and Highly Selective Removal of Lead (II) from Water. *Polym. Chem.* **2022**, *13* (10), 1422–1428.

(188) Shojaeiarani, J.; Bajwa, D.; Shirzadifar, A. A Review on Cellulose Nanocrystals as Promising Biocompounds for the Synthesis of Nanocomposite Hydrogels. *Carbohydr. Polym.* **2019**, *216* (April), 247–259.

(189) Mohammadzadeh Pakdel, P.; Peighambardoust, S. J. A Review on Acrylic Based Hydrogels and Their Applications in Wastewater Treatment. *J. Environ. Manage.* **2018**, *217*, 123–143.

(190) Hassan, C. M.; Peppas, N. A. Structure and Applications of Poly(Vinyl Alcohol) Hydrogels Produced by Conventional Crosslinking or by Freezing/Thawing Methods. In *Advances in Polymer Science*; Springer, Berlin, Heidelberg, 2000; Vol. 153, pp 37–65.

(191) Zhang, J. T.; Bhat, R.; Jandt, K. D. Temperature-Sensitive PVA/PNIPAAm Semi-IPN Hydrogels with Enhanced Responsive Properties. *Acta Biomater.* **2009**, *5* (1), 488–497.

(192) Liebscher, J. Chemistry of Polydopamine – Scope, Variation, and Limitation. *European J. Org. Chem.* **2019**, *2019* (31–32), 4976–4994.

(193) Poinard, B.; Neo, S. Z. Y.; Yeo, E. L. L.; Heng, H. P. S.; Neoh, K. G.; Kah, J. C. Y. Polydopamine Nanoparticles Enhance Drug Release for Combined Photodynamic and Photothermal Therapy. *ACS Appl. Mater. Interfaces* **2018**, *10* (25), 21125–21136.

(194) Jiang, Q.; Gholami Derami, H.; Ghim, D.; Cao, S.; Jun, Y. S.; Singamaneni, S. Polydopamine-Filled Bacterial Nanocellulose as a Biodegradable Interfacial Photothermal Evaporator for Highly Efficient Solar Steam Generation. *J. Mater. Chem. A* **2017**, *5* (35), 18397–18402.

(195) Zhang, Y.; Yin, X.; Yu, B.; Wang, X.; Guo, Q.; Yang, J. Recyclable Polydopamine-Functionalized Sponge for High-Efficiency Clean Water Generation with Dual-Purpose Solar Evaporation and Contaminant Adsorption. *ACS Appl. Mater. Interfaces* **2019**, *11* (35), 32559–32568.

(196) Delparastan, P.; Malollari, K. G.; Lee, H.; Messersmith, P. B. Direct Evidence for the Polymeric Nature of Polydopamine. *Angew. Chemie* **2019**, *131* (4), 1089–1094.

(197) Ye, Q.; Zhou, F.; Liu, W. Bioinspired Catecholic Chemistry for Surface Modification. *Chem. Soc. Rev.* **2011**, *40* (7), 4244–4258.

(198) Ryu, J. H.; Messersmith, P. B.; Lee, H. Polydopamine Surface Chemistry: A Decade of Discovery. *ACS Appl. Mater. Interfaces* **2018**, *10* (9), 7523–7540.

(199) Kim, J.; Cote, L. J.; Kim, F.; Yuan, W.; Shull, K. R.; Huang, J. Graphene Oxide Sheets at Interfaces. *J. Am. Chem. Soc.* **2010**, *132* (23), 8180–8186.

(200) Yang, K.; Wang, J.; Chen, X.; Zhao, Q.; Ghaffar, A.; Chen, B. Application of Graphene-Based Materials in Water Purification: From the Nanoscale to Specific Devices. *Environ. Sci. Nano* **2018**, *5* (6), 1264–1297.

(201) Han, Y.; Xu, Z.; Gao, C. Ultrathin Graphene Nanofiltration Membrane for Water Purification. *Adv. Funct. Mater.* **2013**, *23* (29), 3693–3700.

(202) Robinson, J. T.; Tabakman, S. M.; Liang, Y.; Wang, H.; Sanchez Casalongue, H.; Vinh, D.; Dai, H. Ultrasmall Reduced Graphene Oxide with High

Near-Infrared Absorbance for Photothermal Therapy. *J. Am. Chem. Soc.* **2011**, *133* (17), 6825–6831.

(203) Zedan, A. F.; Moussa, S.; Terner, J.; Atkinson, G.; El-Shall, M. S. Ultrasmall Gold Nanoparticles Anchored to Graphene and Enhanced Photothermal Effects by Laser Irradiation of Gold Nanostructures in Graphene Oxide Solutions. *ACS Nano* **2013**, *7* (1), 627–636.

(204) Wu, M.-C.; Deokar, A. R.; Liao, J.-H.; Shih, P.-Y.; Ling, Y.-C. Graphene-Based Photothermal Agent for Rapid and Effective Killing of Bacteria. *ACS Nano* **2013**, *7* (2), 1281–1290.

(205) Guilherme, M. R.; Da Silva, R.; Rubira, A. F.; Geuskens, G.; Muniz, E. C. Thermo-Sensitive Hydrogels Membranes from PAAm Networks and Entangled PNIPAAm: Effect of Temperature, Cross-Linking and PNIPAAm Contents on the Water Uptake and Permeability. *React. Funct. Polym.* **2004**, *61* (2), 233–243.

(206) Xu, X.; Ozden, S.; Bizmark, N.; Arnold, C. B.; Datta, S. S.; Priestley, R. D. A Bioinspired Elastic Hydrogel for Solar-Driven Water Purification. *Adv. Mater.* **2021**, *33* (18).

(207) Xu, X.; Bai, B.; Wang, H.; Suo, Y. A Near-Infrared and Temperature-Responsive Pesticide Release Platform through Core-Shell Polydopamine@PNIPAm Nanocomposites. *ACS Appl. Mater. Interfaces* **2017**, *9* (7), 6424–6432.

(208) Li, J.; Zhou, Z.; Ma, L.; Chen, G.; Li, Q. Hierarchical Assembly of Amphiphilic POSS-Cyclodextrin Molecules and Azobenzene End-Capped Polymers. *Macromolecules* **2014**, *47* (16), 5739–5748.

(209) Chen, M.; Nielsen, S. R.; Uyar, T.; Zhang, S.; Zafar, A.; Dong, M.; Besenbacher, F. Electrospun UV-Responsive Supramolecular Nanofibers from a Cyclodextrin--Azobenzene Inclusion Complex. *J. Mater. Chem. C* **2013**, *1* (4), 850–855.

(210) Stadermann, J.; Komber, H.; Erber, M.; Däbritz, F.; Ritter, H.; Voit, B. Diblock Copolymer Formation via Self-Assembly of Cyclodextrin and Adamantyl

End-Functionalized Polymers. *Macromolecules* **2011**, *44* (9), 3250–3259.

(211) Khan, S. R.; Sharma, B.; Chawla, P. A.; Bhatia, R. Inductively Coupled Plasma Optical Emission Spectrometry (ICP-OES): A Powerful Analytical Technique for Elemental Analysis. *Food Anal. Methods* **2022**, 1–23.

(212) Marcano, D. C.; Kosynkin, D. V.; Berlin, J. M.; Sinitskii, A.; Sun, Z.; Slesarev, A.; Alemany, L. B.; Lu, W.; Tour, J. M. Improved Synthesis of Graphene Oxide. *ACS Nano* **2010**, *4* (8), 4806–4814.

(213) Zhang, J. T.; Cheng, S. X.; Zhuo, R. X. Poly(Vinyl Alcohol)/Poly(N-Isopropylacrylamide) Semi-Interpenetrating Polymer Network Hydrogels with Rapid Response to Temperature Changes. *Colloid Polym. Sci.* **2003**, *281* (6), 580–583.

(214) Xia, L. W.; Xie, R.; Ju, X. J.; Wang, W.; Chen, Q.; Chu, L. Y. Nano-Structured Smart Hydrogels with Rapid Response and High Elasticity. *Nat. Commun.* **2013**, *4*, 1–11.

Appendix

A.Abbreviations

PNIPAAm	Poly(*N*-isopropylacrylamide)
PVA	Poly(vinyl alcohol)
PDA	Polydopamine
GO	Graphene Oxide
β-CD	*β*-Cyclodextrin
TEMED	*N,N,N′,N′*-Tetramethylethylendiamin
MBA	*N,N′*-Methylenebisacrylamide
APS	Ammonium persulfate
R6G	Rhodamine 6G
SDS	Sodium dodecyl sulfate
KPS	Potassium persulfate
BIBB	2-Bromoisobutyryl Bromide
Me_6TREN	tris(2-(dimethylamino)ethyl)amine
CuBr	Copper(I) bromide
TEA	Triethylamine
PEG	Poly(ethylene glycol)
PMDETA	*N,N,N′,N″,N‴*-Pentamethyldiethylentriamin
HMTETA	1,1,4,7,10,10-Hexamethyltriethylentetramin
FS	2,3,4,5,6- Pentafluorostyrene

AZO	Azobenzene
$Pd(OAc)_2$	Palladium(II)-acetat
$Pb\ (CH_3CO_2)_2 \cdot 3H_2O$	Lead(II)-acetate Trihydrate
TsCl	*p*-Toluenesulfonyl chloride
PBM	Prop-2-yn-1-yl 2-bromo-2-methylpropanoate
LCST	Lower critical solution temperature
$CHCl_3$	Chloroform
DMSO	Dimethyl sulfoxide
DMF	*N,N*-dimethylformamide
THF	Tetrahydrofuran
DCM	Dichloromethane
DI water	Deionized water
HCl	Hydrochloric acid
H_2SO_4	Sulfuric acid
$NaNO_3$	Sodium nitrate
$KMnO_4$	Potassium permanganate
H_2O_2	Hydrogen peroxide
K_2CO_3	Potassium carbonate
$NaHCO_3$	Sodium bicarbonate
NaN_3	Sodium azide
Na_2SO_4	Sodium sulfate
Al_2O_3	Aluminium oxide

FT-IR	Fourier-transformation infrared spectroscopy
GPC	Gel permeation chromatography
SEM	Scanning electron microscopy
WCA	Water contact angle
UV-vis	Ultraviolet-visible
NMR	Nuclear Magnetic Resonance Spectroscopy
DSC	Differential scanning calorimetry
ICP-OES	Inductively Coupled Plasma Optical Emission Spectrometry
ATRP	Atom transfer radical polymerization
NOESY	Nuclear Overhauser effect spectroscopy
M_w	Weight-average molar mass
M_n	Number-average molar mass
NIR	Near Infrared
SR	Swelling ratio

B. Additional figures

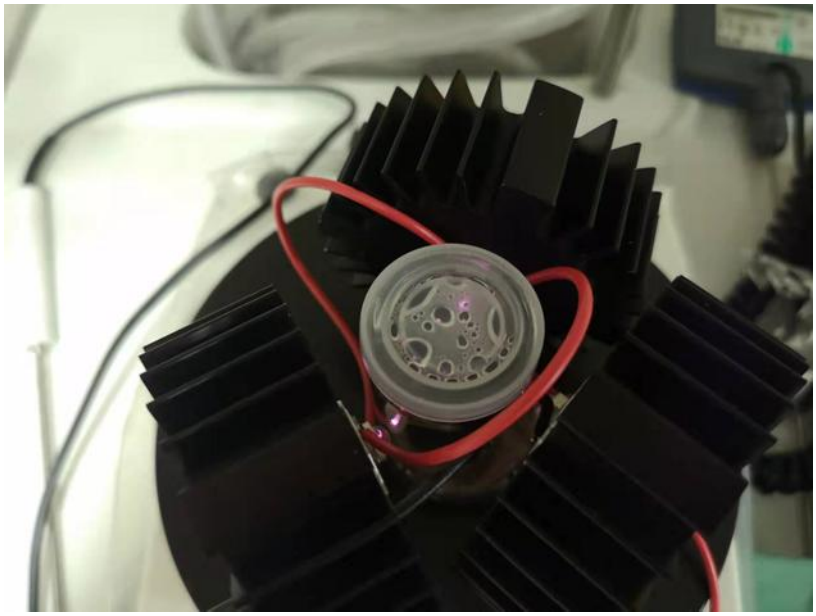

Figure B1 Hydrogels release water under 850nm near-infrared light.

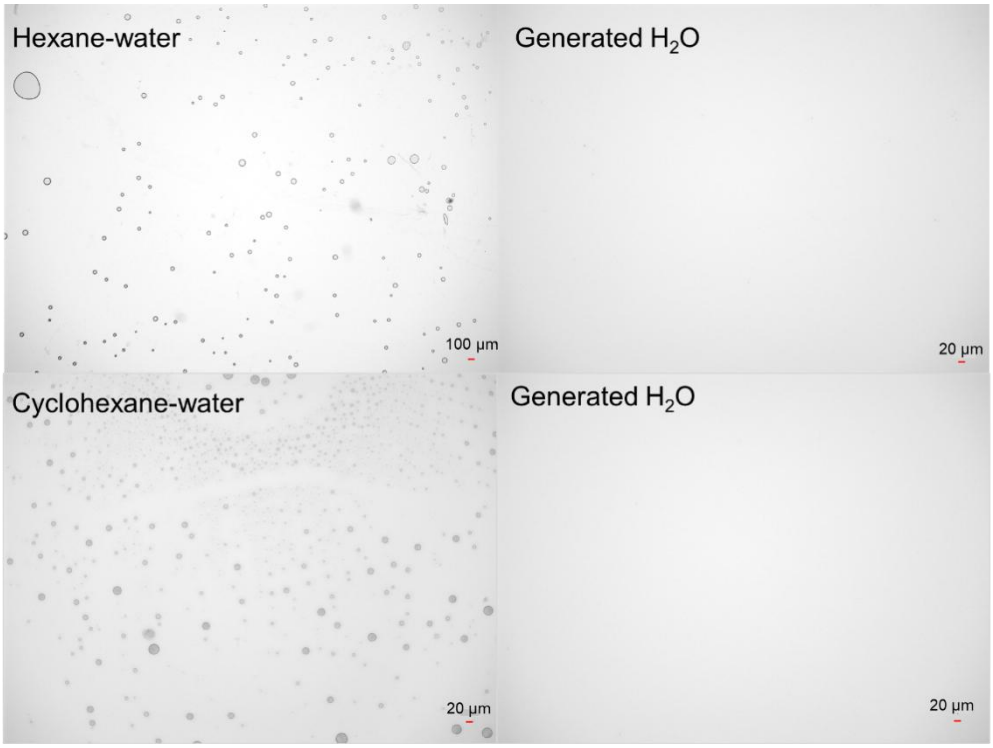

Figure B2 Microscopy photographs of SDS-stabilized hexane-in-water and cyclohexane-in-water emulsions before and after treatment with PNIPAAm-PVA-PDA hydrogel.

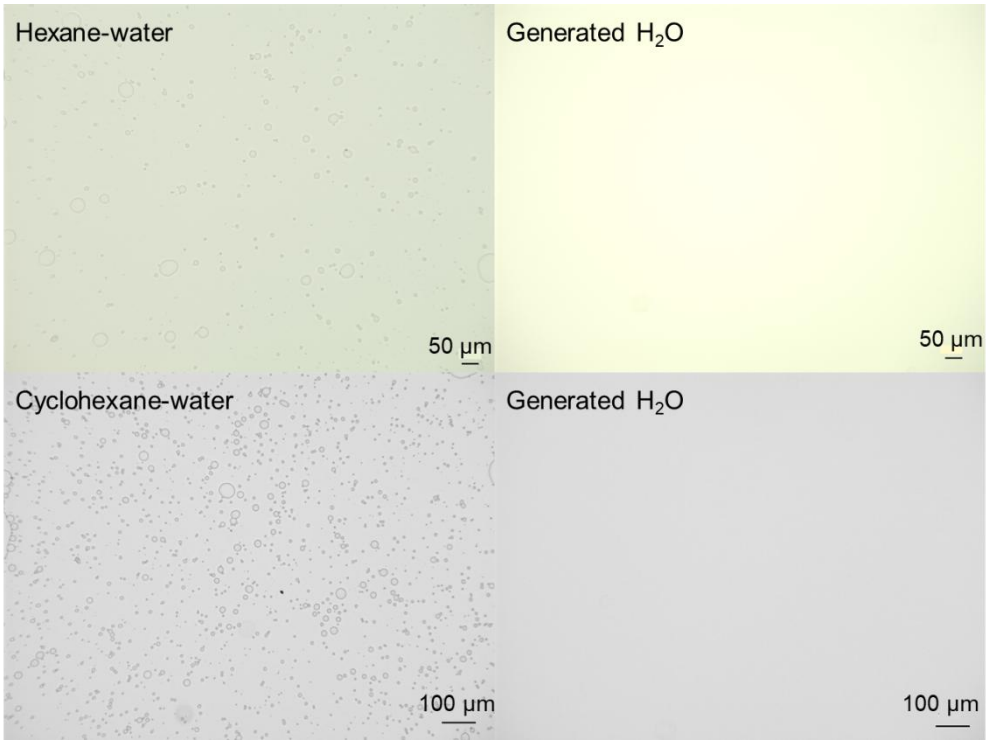

Figure B3 Microscopy photographs of SDS-stabilized hexane-in-water and cyclohexane-in-water emulsions before and after treatment with micro-PNIPAAm-GO hydrogel.

Acknowledgments

Unknowingly, my doctoral study is coming to an end. Looking back on the five years of study, I met many people who helped me, and I want to use this opportunity to thank them all for their assistance.

First and foremost, I would like to thank my supervisor, Prof. Patrick Théato, for providing me with the opportunity to join this nice research group working on this interesting and challenging topic. Thank you for your constant support of my research work, from the design of the experiments to the writing and revision of my thesis. Thank you very much for your understanding and help when my experiments failed one after another.

In addition, I would like to thank Prof. Pavel Levkin for accepting to be a co-reviewer of my thesis and for taking the time to review my thesis.

I would like to thank Dr. Dominik Voll for your tireless guidance in my research work, for your fruitful discussions with me, and for your help in my dissertation. I also want to thank Dr. Christian Schmitt for your help and support in my thesis.

I would like to thank Katharina Elies, our technician, who provided me with training on various lab testing instruments, your support in ordering everything I needed for my lab work, and your support in DSC and GPC measurements. I am also very grateful to Birgit Huber for helping me with the DSC measurements, which are very important for my experiments.

Special thanks to Mr. Volker Zibat, who helped me to carry out SEM measurements, an important characterization method in my research. I want to thank Dr. Thomas Bergfeldt for the help with my ICP-OES measurement, which is very important for my experimental results. I would like to thank Jovana Topalovska for your unselfish help and support with my water contact angle test.

I would like to thank Yunji for your help in the past four years, both in life and in experimental work. Special thanks to Johannes for always kindly helping me with sample characterization. I would like to thank Dr. Jingmei Yang, who accompanied me in the first year of my doctorate and gave me a lot of help. Thanks to krittin, my Thai intern. Thank you for your help with my experiments. I would like to thank Dr. Edgar Molle, Dr. Martin Gauthier-Jaques, Dr. Stefan Frech, Dr. Andreas Butzelaar and Victoria for their help with the NMR tests. I would like to thank Dr. Hongxin Zhang, Dr. Zengwen Li, Dr. Xiaohui Li, Dr. WenWen Xue and Dr. Xia Huang for your support in handling the daily laboratory work. It is a pleasure to discuss with you, which is also beneficial to my research work.

I also want to thank all my colleagues. I would like to thank Dr. Hatice Multu, Dr. Sergej Baraban, Dr. Yosuke Akae, Dr. Isabella Weiß, Dr. Marvin Subarew, Dr. Azra Kocaarslan, Dr. Miriam Khodeir, Meryem, Vaishali, Daniel, Alex, Cornelius, David, Sven, and Nico et al., thank you so much for your support and help, I appreciate working with all of you.

I sincerely thank the China Scholarship Council (CSC) for the scholarship for my doctoral research. I would also like to thank KHYS for the funding during the final stage of my doctoral studies.

I would also like to thank my beloved parents and brother for your support and understanding, and for patiently encouraging me throughout my studies.

Last but not least, I met numerous people throughout my PhD studies who are not mentioned above; I'd want to thank all of you for your time and for making my trip in Germany meaningful.